Modelling and Simulation of the Cargo Heating Procedures on Crude Oil Tankers

Angelos Pachis

Diploma Thesis

Faculty of Naval Architecture and Marine Engineering
National Technical University of Athens

Supervisor: Prof. Nikolaos P.Kyrtatos

Committee Member : Prof. S. Mavrakos

Committee Member : Prof. L. Kaiktsis

July 27, 2018

Acknowledgements

Abstract

The present diploma thesis focuses on modelling and simulating the cargo heating procedures taking place on a modern tanker vessel. A methodology for predicting cargo temperature inside the cargo tanks is proposed. Through thermal calculations, the model is able to predict cargo temperature at any moment throughout the journey and at different weather and/or loading conditions.

The implementation of the model was carried out in the programming environment Matlab. The present text covers the theoretical background of all the heat transfer phenomena occuring onboard, as well as a complete review of the calculation process the generated code follows. The cornerstone for the aforementioned thermal calculations was the trial and error method, which Matlab made feasible to deploy. Heat flow to and from the cargo tanks was modelled based on the existing analogy between thermal and electrical circuits. Finally, the developed model is validated based on data from two case studies of two sister vessels, provided by Thenamaris Inc., each representing a unique journey.

Validation of the developed model showed satisfactory agreement with the available data for both case studies. Error in temperature prediction was in most cases of the order of 1°C. Average cargo temperature trajectories correspond well to those included in the case studies, for the vast part of each journey. At the end of the present work, an attempt to suggest an optimum heating sequence for one of the study cases is exhibited.

The final product of this thesis can pose an indispensable tool in the hands of someone who would look to optimize, by minimizing fuel oil consumption, cargo heating through proper planning of cargo heating operations onboard.

Contents

Chapter 1

Introduction - Scope of thesis

In recent years the shipping industry suffered by the adverse international economic environment, the steep increase of fuel (bunker) prices and new regulations (i.e. Emission Control Areas [1]), which have dramatically altered the running cost / profit ratio for ship owners and operators. To address this situation, the marine industry focused on the implementation of various energy/cost saving practices (e.g. slow steaming, optimal routing etc). Moreover, ship energy and fuel cost savings can be attained if fleet managers and crew follow procedures aiming at efficient cargo heating practices and operations.

Today the oil trade is so vast and wide spread that an average oil tanker may be trading in the tropics one voyage and in Arctic conditions the next. It is therefore necessary that cargo heating systems are designed to cope with extreme conditions. Heavy petroleum fractions, such as fuel and crude oil become very thick and sluggish when their temperature drops. In order for these oils to be loaded, transported and discharged without delay, it is necessary to keep them at elevated temperatures. Steam is used to heat the oil in a ship's tank. The heating arrangements in the actual cargo tanks consist of a system of coils, which are spread over the bottom of the tank, at a distance of twenty to fifty centimeters from the bottom plating. Heavy fuel oils are generally required to be kept at a temperature ranging between 46°C and 58°C. Within this temperature range, they are easy to handle and do not allow excessive deposits of wax to form on cooling surfaces.

A 105000 dwt crude oil tanker sailing at ambient conditions of 5°C and a sea water temperature of 3°C, carrying IFO 380 in all tanks, will load the cargo at a temperature of 60°C, carry it at a temperature not less than 40°C and ensure it is discharged at 60°C. To heat the cargo from 40°C to 60°C in 4 days, cargo heating at this rate will burn almost 50 tons of fuel per day, which will cost the owner between US$ 30000 and US$ 50000, subject to the type of fuel used. During the same voyage, the main engine on board the ship, running at 70% MCR, will consume about 40 tons per day. In other words, the cost of heating is at least equal to, if not greater than, the cost of propulsion.

Hence it is evident that in search of the optimum heating procedure, a means to predict cargo temperature inside each one of the tanks, as well as the requested fuel oil consumption would be of vital significance. Although, similar papers or efforts towards that direction appear to scarce in literature. The present model is applied on the cargo heating systems of a modern AFRAMAX tanker. The calculated results have been validated against actual figures provided by vessel's operator for two different heating operations, with acceptable agreement.

Thus, the developed model constitutes a decision support tool, which can assist the ship operator to minimize the energy consumption during cargo heating by simulating the operation of existing heating equipment, in order to achieve the optimum heating schedule. The support of Thenamaris in the provision of data for the validation of the developed

model is acknowledged.

Thesis Structure

Firstly, the main modes of heat transfer phenomena that take place onboard a crude oil carrier ship are presented in Chapter 2. Also, in the final part of the aforementioned chapter, pressure drop for two-phase and single-phase flows is mentioned, to the extend of our study on steam condensation inside the ship's steam pipeline and heating coils. Chapter 3 includes the calculation process the developed model follows at Matlab environment, along with all the necessary assumptions made in order for the estimations to be feasible. Chapter 4 introduces the case studies used for the validation of this model, as well as results of the simulations in comparison to the given data. A brief suggestion for improving heating processes in case study No.1 is also proposed in this chapter, with relevant results stated at the end. Finally, Chapter 5 includes the conclusions and possible future work that can be done.

Chapter 2

Heat Transfer Calculations Through Various Surfaces

2.1 Introduction

In this chapter, we intend to review all heat transfer phenomena that occur along the various surfaces of a tanker's cargo tanks and result in heat transfer towards the environment. Then we will refer to the production of steam from marine boilers, the steam condensation procedure taking place inside the ship's pipelines. All heat transfer mechanisms will be examined under a steady-state condition assumption.

Whenever a temperature difference exists in a medium or between media, heat transfer must occur in pursuance of energy equilibrium. We refer to the different types of heat transfer processes as modes. When a temperature gradient exists in a stationary medium, which may be a solid or a fluid, we use the term *conduction* to refer to the transfer of energy, in the form of heat, from the more energetic to the less energetic particles of a substance due to interactions between the particles.

Convection is the mode of heat transfer between a solid surface and the adjacent liquid or gas that is in motion, and it involves the combined effects of conduction and fluid motion. Convection heat transfer may be classified according to the nature of flow. We speak of forced convection when flow is caused by external means, such as a fan, sea currents or winds. In contrast, for free (also called natural) convection, the flow is induced by buoyancy forces, which are due to density differences caused by temperature variations in the fluid. The third mode of heat transfer is termed *thermal radiation*, as all surfaces of finite temperature emit energy in the form of electromagnetic waves.

Heat is exchanged between the cargo and the environment by all surrounding surfaces, as illustrated in Figure 2.1. In order to acquire a precise estimation on the amount of energy exchanged, we had to study each surface seperately. Thus vessel's geometry was seperated into four different areas under investigation :

1. The side shell plating of the ship, which includes both freeboard and wetted surfaces,

2. The deck plating,

3. The bottom plating,

4. The longitudinal and transverse bulkheads between the cargo tanks.
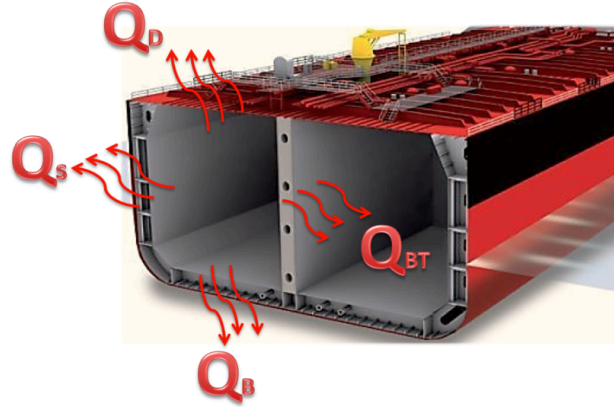
Figure 2.1: Heat flow through the surfaces of a tanker's cargo tank

2.2 Side Shell Plating Heat Transfer

2.2.1 Outside of side shell

Due to the fact that a loaded tanker has comparatively little freeboard, the temperature of seawater through which the vessel is passing is of major significance. Cold water washing around the ship's side and bottom rapidly reduces the temperature of the cargo and makes the task of heating it much harder. Warm seawater, however, has the reverse effect, and can be very useful in helping to maintain the temperature of the cargo with a minimum of steam.

Consider the flow illustrated in Fig.2.2. The total length of the plate is L and x-coordinate is measured along the plate surface from the leading edge, towards the direction of the flow. Fluid approaches the plate in the x-direction with uniform upstream velocity V and temperature T_∞. In the velocity boundary layer, the flow starts out as laminar, but as the plate is sufficiently long, the flow eventually becomes turbulent at a distance x_{cr} from the leading edge. Transition from laminar to turbulent flow is best characterized by the Reynolds number, a dimensionless quantity used in fluid mechanics in order to predict flow patterns.
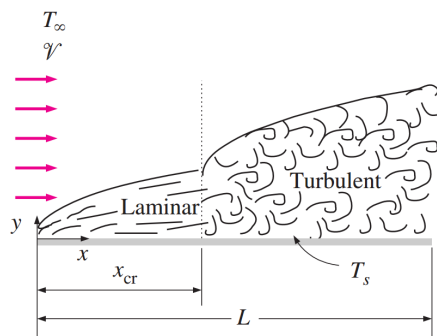
Figure 2.2: Flat plate in parallel flow

Reynolds number at a distance x from the leading edge of a flat plate is expressed as :

$$Re = \frac{\rho V x}{\mu} = \frac{V x}{\nu}$$

and transition from laminar to turbulent flow is usually considered to occur when Reynolds number surpasses a critical value of :

$$Re_{cr} = \frac{\rho V x_{cr}}{\mu} = 5 \times 10^5$$

For the wetted surface of the hull, we are aware that kinematic viscosity of sea water is a function of temperature, salinity and pressure at the reference depth, with temperature being the predominant factor. As a rule of thumb, viscosity decreases as fluid's temperature raises. It is not difficult to prove that flow around the hull, will constantly be turbulent. For temperatures ranging from $-10\,°C$ - $30\,°C$ the kinematic viscosity of seawater fluctuates between 2.72×10^{-6} and 8.36×10^{-7} respectively[1]. Considering the leading edge of the plate to coincide with the ship's bulb (located 16 m ahead of the fore bulkheads of No.1 cargo tanks), it was found that even for very low velocities, in the region of 0.1 m/s, the calculated Reynolds number always exceeds the critical value. Thus outside of the side shell and below sea level, heat transfer is always under the regime of forced convection under turbulent flow.

Similarly, the heat transfer mode at freeboard would predominantly be forced convection under turbulent flow, only this time the surrounding fluid is not seawater, but air. That's because, albeit the kinematic viscosity of atmospheric air is larger than that of seawater (increasing from 1.26×10^{-5} at $-10\,°C$, to 1.63×10^{-5} at $30\,°C$), for $x_{cr} = 16m$, the flow will be turbulent, as long as the relevant velocity between the ship and ambient air exceeds 0.51 m/s (≈ 1 knot). As the freeboard is under the regime of forced convection, the effects of radiation can easily be neglected. This assumption is based on experiments carried out by Cess [58], as well as on literature research, where for forced convection regimes, thermal radiation effects are considered negligible.

2.2.2   Inside of side shell

Inside the cargo tank, heat transfer occurs via means of natural-free convection. Free convection is generated by density differences inside the fluid, occurring due to temperature gradients. Fluid surrounding a heat source receives heat and by thermal expansion becomes less dense and rises. The surrounding cooler fluid then moves in to replace it. This cooler fluid is then heated and the process continues, forming a convection current; this procedure transfers heat energy from the bottom of the convection cell towards the top. The driving force for natural convection is buoyancy, a result of differences in fluid density, while resisting forces are considered to be of viscous nature. A rough approximation of the phenomenon taking place inside the cargo tank can be seen in Fig.2.3a, illustrating a Benard cell. Benard cells are convection cells of a regular pattern, developed when the fluid is heated from below in a plane horizontal layer during the so called Rayleigh - Benard convection. We note that fluid ascends in the geometrical center of the tank and descends across the wall boundaries.

This is almost the case inside a cargo tank, where heat sources (heating coils) are unevenly distributed. Cargo temperature inside the tank is not steady in it's whole, but it varies across the three dimensions. The core of the cargo at the centre of the tank is warmer than that at the sides, with temperature increasing as we move towards the bottom of the tank, where the heating coils are located and decreasing as we move towards the cargo's free surface. As the cargo gets warmer, a natural flow is created due to density gradients, with cargo raising upwards and flowing downwards in the vicinity of the tank's walls, especially to the one approximate to the seaside.

---

[1]Based to the correlations for the thermophysical properties of seawater attached to the Appendix of the present thesis

A more comprehensive illustration of what's happening inside the cargo tank with unevenly distributed heat sources was given by Pivac and Magazinovic [19], who conducted a numerical analysis of the heat transfer process at the heating coil surface. For steady - state conditions, a large central whirl is formed in the center of the tank, while the majority of small whirls at the edges are vanished, as shown in Fig.2.3b. This cargo circulation enhances heat flow as well as thermal distribution inside the tank.

(a) Rayleigh Benard Cell

(b) Cargo flow pattern
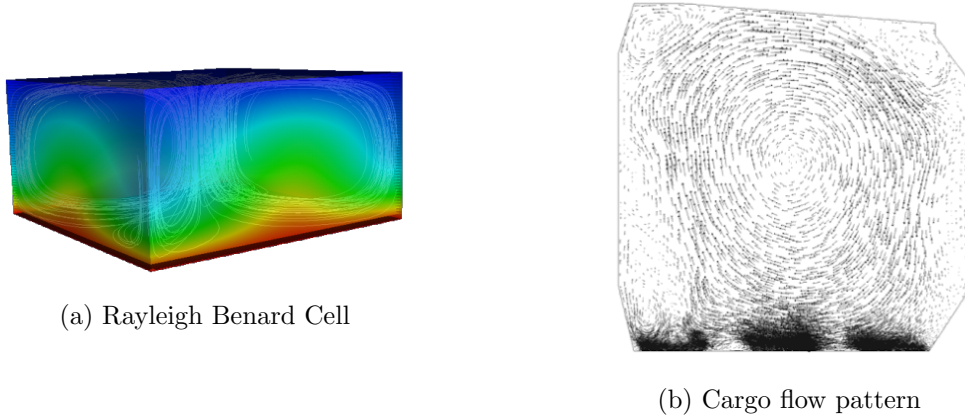
Figure 2.3: Flow representation inside a cargo tank

However, according to Mavrakos [6], the transition from the bulk cargo temperature to the wall's temperature, occurs in a quite thin layer. That is also confirmed experimentally by Saunders [7], who attached thermocouples 3, 6 and 12 inches away from the cargo tank's walls. Measurements from these thermocouples, confirmed that the largest temperature drop happens somewhere between the first thermocouple (3 in. away from the tank wall) and the wall itself, as all measured temperatures were compareable to the bulk cargo temperature. Finally, similar observations were also made by Akagi and Kato [66] from experiments on a tank heated from below, cooled at both sides and insulated from above, where in the layers near the tank walls and heating surface, temperature profile changes steeply. Thus, we can assume that cargo temperature varies significantly only in the vertical direction. Nowadays, it is a common practice in cargo temperature monitoring to measure temperatures at three different heights, and exporting a mean value for the total cargo temperature per tank.

As mentioned in the preceding section, flow regime in forced convection is governed by the dimensionless *Reynolds number*, which represents the ratio of inertial forces to viscous forces acting on the fluid. The flow regime in natural convection is governed by the dimensionless *Grashof number*, which represents the ratio of the buoyancy forces to the viscous forces acting on the fluid. For a vertical plate of a characteristic length L_c, the Grashof number over the entire plate is given by the equation :

$$Gr_L = \frac{g\beta(T_s - T_\infty)L_c^3}{\nu^2} \tag{2.1}$$

Another dimensionless number used to characterise flows during natural convection heat transfer is the Rayleigh number, which is the product of Grashof and Prandtl numbers:

$$Ra_L = Gr_L Pr = \frac{g\beta(T_s - T_\infty)L_c^3}{\nu^2}Pr \tag{2.2}$$

Natural convection heat transfer on a surface depends on the geometry of the surface as well as its orientation. It also depends on the variation of temperature on the surface

and the thermophysical properties of the fluid involved. Until lately, many textbooks recommended that transition to turbulence depends on the Rayleigh number and occurs at the critical value of about 10^9. Nevertheless, both publications of Popiel [51] and Bejan and Lage [52] reviewed a number of reports and concluded that the Grashof number is much more suitable for the critical similarity parameter, describing the transition from laminar to turbulent boundary layer on a vertical flat wall to take place at :

$$Gr_{cr} \approx 10^9$$

2.2.3 Double Hull Area

A double hull is a ship hull design and construction method where the bottom and sides of the ship have two complete layers of watertight hull surface: one outer layer forming the normal hull of the ship, and a second inner hull which is some distance inboard, typically by a few meters, which forms a redundant barrier to seawater in case the outer hull is damaged. The space between the two hulls is usually used for storage of ballast water in order to improve the stability and seakeeping capabilities of the vessel.

The side of the ballast tank adjacent to the cargo tank will most commonly have a higher temperature than the side adjacent to the sea, as the cargo inside the tank is heated. That temperature difference between the two hulls (normal & inner) is not negligible and can even rise to around $40\,°C$ or even more. In case the ship is fully loaded, thus ballast tanks will be free of seawater, air in the vicinity of the hot surface will increase in temperature, becoming less dense and will begin to raise from the bottom of the tank towards the top. Reaching the top, it will eventually touch the colder side shell and it will start cooling, similarly becoming denser and moving downwards. Hence the fluid motion is characterized by a recirculating or cellular flow for which fluid ascends along the hot wall and descends along the cold wall. Figure 2.4 taken by Cengel [3] illustrates such a recirculating flow, while the arrow points towards the direction of heat transfer.

Each enclosure is geometrically characterised from it's three dimensions:

- Height[H], measured vertically from the bottom of each tank (z-axis)

- Width[L], which is measured transversly (y-axis)

- Length[w], which is measured horizontally (x-axis, parralel to the C_L)
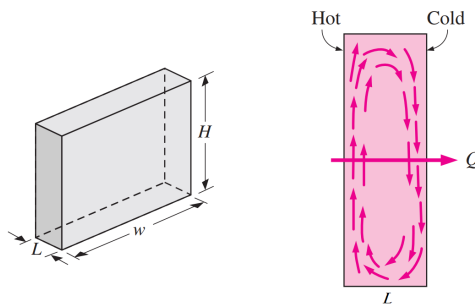
Figure 2.4: Natural convection inside vertical enclosure

The heat flux across the cavity depends more on the aspect ratio H/L rather than w/L, which can easily be neglected for large values of cavity's length (w). As mentioned by Altac and Ugurlubilek [22], the 3D effect of the boundary layer is not significant in the

average Nusselt at high Rayleigh (Ra) numbers. Thus the 3D effects can be considered negligible. For small Rayleigh numbers, $Ra_L \leq 10^3$, the buoyancy-driven flow is weak and, in the absence of radiation, heat transfer is primarily by conduction across the fluid. With increasing Rayleigh number, according to Gill's theory [13] the cellular flow intensifies and becomes concentrated in thin boundary layers adjoining the sidewalls. The core becomes nearly stagnant and vertically stratified. Additional cells can develop in the tank's corners and the sidewall boundary layers eventually undergo transition to turbulence.

Under the assumption that the horizontal walls are adiabatic, transition to turbulence occurs at a critical $Ra \approx 10^8$. However, Winters [15] studied the more realistic configuration of perfectly conducting horizontal walls that enhance the unsteadiness of the flow, obtaining a critical number of $Ra = 2 \times 10^6$, which was also confirmed later by Henkes [16].

Furthermore, according to Singh and Eames [54], a conducting side wall thermal boundary condition results in a linear temperature profile (LTP) in the walls. Hence, we would anticipate for the temperature profile inside the cargo tank to be also linear. Moreover, as we can see in Fig.2.5, the lower end of the frame is connected to the tank top by means of a hopper plating. As no data were found for enclosures that gradually change size in one of their dimensions, we will ignore the existence of the hopper plating and we will assume that the inner hull longitudinal bulkhead extends all the way to the tank top. In that way, both ballast and cargo tanks acquire a rectangular shape.
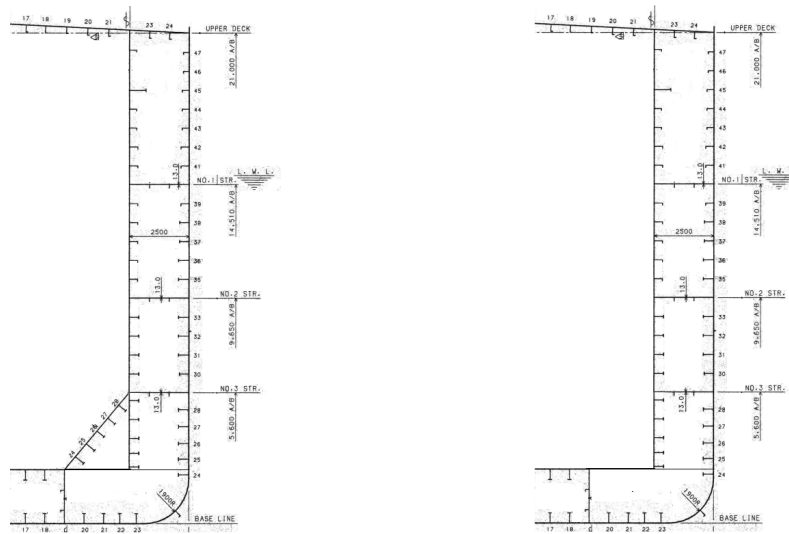
Figure 2.5: Ballast Tank Arrangement at Midship.

Regarding radiation, Sharma et al. [55] investigated conjugate turbulent natural convection with surface radiation in air filled rectangular enclosures proving that natural convection and thermal radiation are complementary to some extent. The effect of natural convection is slightly reduced by thermal radiation, as it modifies the wall temperature distribution which, in turn, affects natural convection. As a result, the convective contribution to heat transfer is reduced by 18-27%, which is principally compensated by the contribution of radiation.

Effects of structural elements on heat transfer augmentation

As we notice in Fig.2.5, all ballast tanks include longitudinal stiffeners which are attached both on the inner side of the outer shell plate and on the outer side of the inner hull plate. These stiffeneres have a vital role in enhancing the overall strength of the ship's hull in forces like torsion and longitudinal bending. Apart from that, they also play an important part in heat transfer. They conduct heat from the cargo tank wall and are exposed to the uprising flow of air in the ballast tank area mentioned before. Furthermore, an identical phenomenon occurs to the opposing side, as stiffeners subtract heat from the air flowing downwards and dump it to the surrounding fluid. Hence, heat transfer from the inner hull plate is made by conduction within the solid and by convection from the boundaries and vice versa for the outer shell plate. Additionally, the outer shell plate and the inner hull plate are directly connected via stringers and web frames, in that aspect heat transfer is also made via conduction through these structural elements.

2.3   Deck Heat Transfer

As mentioned in section 2.2.2, cargo temperature varies vertically, as measurements along the other two dimensions revealed temperature to be rather constant. Above the free surface of oil, a mixture of air, inert gas and hydrocarbon vapors is contained. Under normal conditions, it is not necessary to run the Inert Gas System during loaded voyage, as the level of oxygen inside the tanks should be well under the required levels of O_2 8% v/v, provided no ingress of air has occurred. To prevent that ingress of air, it is common to maintain a possitive pressure inside the ullage space and, in case of any leakage to compensate the loss by purging. Furthermore, air molecules come in touch with the free surface of crude oil, which is comparatively elevated in temperature. By ignoring cargo sloshing phenomena caused by the ship's pitching and rolling movements, we can consider this case equivalent to air trapped inside a horizontal three dimensional rectangular enclosure heated from below and cooled from above.

As we refer once again to natural convection, the determining factor for the nature of flow is the Rayleigh number. According to Incropera [2] and Cengel [3], in Rayleigh numbers less than the critical value of $Ra_{L,c} = 1708$, buoyancy forces cannot overcome the resistance imposed by viscous forces and there is no advection within the cavity. Hence heat transfer from the bottom to the top surface occurs by conduction and radiation. Since conditions correspond to one-dimensional conduction through a plane fluid layer, the convection coefficient is $h = k/L$ and $Nu_L = 1$. However, for $Ra_L > 1708$, conditions are thermally unstable and there is advection within the cavity in terms of a cellular structure. For Rayleigh numbers in the range $1708 \leq Ra_L \leq 5 \times 10^4$, fluid motion consists of regularly spaced roll cells (Figure 2.6 a), while for larger Rayleigh numbers, the cells break down and the fluid motion evolves through many different patterns before eventually becoming turbulent.

On deck, heat transfer coefficient is highly connected to the prevailing weather conditions, which can vary drastically over each day. For example, under unfavorable weather conditions, the waves and ship motions can become so large that water flows onto the deck of a ship. This problem is known as 'shipping of water', 'deck wetness' or 'green water loading'[1], and results to an increase of the overall heat transfer coefficient. On the other hand, during a dry sunny day, the overall heat transfer coefficient can even become negative, meaning that heat energy flows towards the cargo tank rather than from it, due

---

[1]The term 'green water' is used to distinguish between the spray (small amounts of water and foam) flying around and the real solid seawater on the deck.
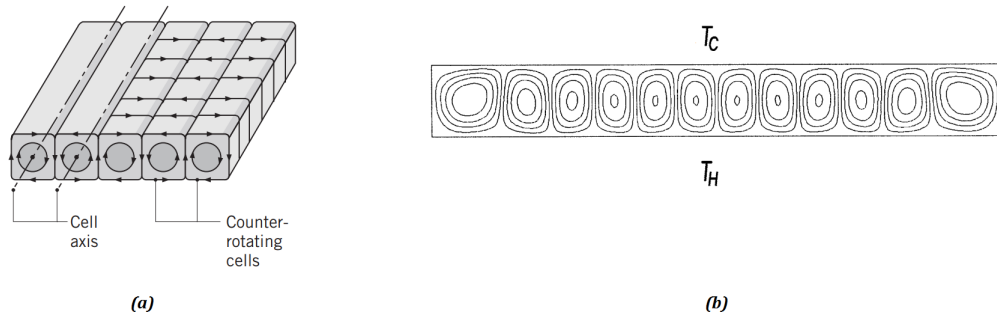
Figure 2.6: Longitudinal roll cells characteristic of advection in a horizontal fluid layer heated from below

to solar radiation. A precise calculation would only be possible if we had access to accurate data of sunlight duration, frequency of deck wetness etc. As this kind of data would hardly be applicable, we will consider that air transfers heat solely under the regime of forced convection, in a similar manner as outside of the side shell (mentioned in Section 2.2.1)

2.4   Bottom

Externally of the bottom plating, the heat transfer regime is identical with that of section 2.2.1, so forced convection in turbulent flow occurs. Inside the cargo tank, above the tank top and below the heating coils, a very viscous, almost solid, layer of oil tends to form. Most crude oils have a propensity to separate into heavier and lighter hydrocarbons before refining. Such problem is often exacerbated by cool temperatures and by the static condition of fluid during storage. The heavy ends of crude oil that are separated and deposited onto the bottoms of storage tanks/vessels, are known as sludge. Sludge is a combination of heavier fractions of hydrocarbons, sediment, paraffin accompanying with increased density and viscosity and decreased fluidity.
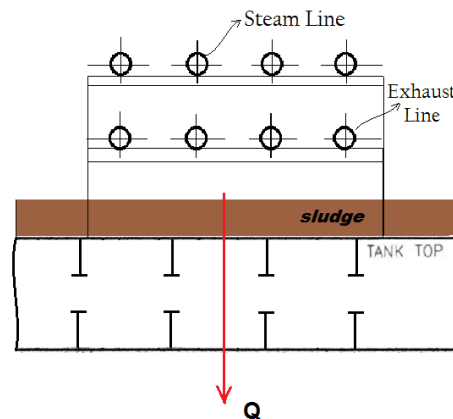
Figure 2.7: Heat Transfer Towards the ships bottom

An extensive amount of sludge is also formed during the loading procedures, when the bottom of the tank has approximately the same temperature with that of sea. Once oil

is pumped into the tank, it solidifies rapidly, as in most cases the pour point [2] of crude oil is well above the existing temperatures inside the tank. This initial formation of semi-solid layer however, contributes to the insulation of the tank, as it behaves similarly to a protective coating between the cold tank top surface and the hot incoming oil, restricting the further formation of oil sludge.

The layer's thickness is interchangeably connected to the crude oil's viscosity, and is a determining factor to the total heat transfer coefficient. Mavrakos [6], using specific experimental data from a 50,000 DWT single hull tanker, assumed that the thickness of the viscous oil layer would be equal to 9cm. Monteiro et al. [32], on their experimental investigation of a 19,625 m^3 crude oil insulated storage tank, assumed the layer's thickness to be equal to 10cm.

Furthermore, as heat is conducted from the tank top plating, it must find its way across the double bottom area. This is the case of a horizontal cavity heated from above and cooled from below, where heat transfer from the top to the bottom surface is exclusively by conduction ($Nu_L = 1$), irrespective of the value of Ra_L. The extended surfaces (longitudinal stiffeners) attached to both areas of the horizontal cavity serve no purpose in the augmentation of heat transfer, apart from increasing the total surface area. However heat transfer is enhanced by radiation.

2.5 Between Tanks

Heat is also exchanged between adjacent cargo tanks, when the secluded cargoes have different temperatures. This case is similar to that of the inside of side shell plating, as mentioned in page 13, and heat transfer in both tanks is carried out by the mode of natural convection. Similar to chapter 2.2.2, the flow regime is again governed by the Grashof number, which determines whether the flow is laminar or turbulent. To depict the situation properly, lets assume that two adjacent tanks have different temperatures, $T_{\infty A}$ and $T_{\infty B}$, where $T_{\infty A} > T_{\infty B}$ (Fig. 2.8).

Heat will begin to transfer from tank A towards tank B, in order to achieve equilibrium. Because of that, cargo in the vicinity of the seperating bulkhead will have a lower temperature compared to that at the center of the tank $T_{\infty A}$, thus cargo density will increase locally and it will begin to move towards the bottom of the tank. In tank B, the exact opposite phenomenon occurs, as cargo in the vicinity of the bulkhead will have a higher temperature than the bulk mass of cargo at the center of the tank, as it is heated by the cargo of tank A. Hence it will start to move upwards. The correlations addressed in earlier chapters are independent of the flow's direction over a plate and can be used whether the fluid is cooled or heated by the wall.

2.6 Boiler Specification and Operation

Many tanker ships are not equipped with steam heating coils, as they are designed for short voyages and travel in areas with relevantly high temperatures. It is possible for the cargo to be loaded at a high temperature and the heat losses throughout the voyage to be trivial, thus the use of steam heating coils to be deemed unnecessary. Nonetheless, for voyages of longer duration, the oil inside the cargo tanks must be kept at relatively low viscosity, in order to make the discharge processes faster and reduce the amount of cargo remaining on board (ROB), which later has to be cleaned by crude oil washing.

---

[2]Pour point is defined as the temperature at which a fluid ceases to pour. For example, a Vacuum Gas Oil (VGO) with Api Gravity equal to 23.6, has a pour point of 108 °F ≈ 42 °C.
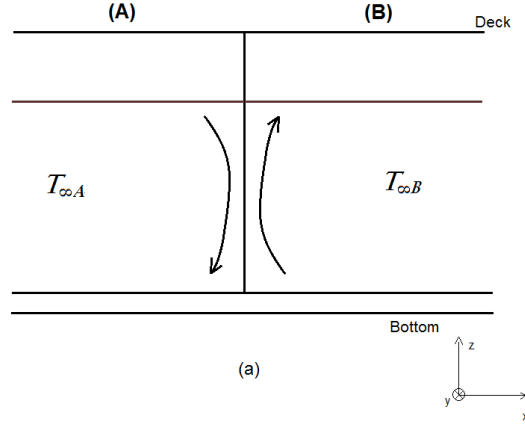
Figure 2.8: Fluid motion inside tanks A and B

To achieve that, modern crude oil carriers are equipped with two auxiliary marine boilers, which provide enough steam to cover cargo heating needs, as well as run various ship's machinery and services. Marine boilers can operate independently or in collaboration in a Master/Slave Boiler arrangement. When demands for steam are high, the second boiler is automatically fired, in order to cover the gaps in steam production, and shuts down when steam demands drop. Furthermore, boilers can produce steam of two different pressures, the lower of which is used for engine room amenities (i.e. in fuel oil heaters for the main engine and generator engines etc.). The higher pressure mode is solely used to run the cargo oil pumps during loading and discharging procedures. For operations carried out on deck which demand the use of steam, such as cargo heating or tank cleaning, steam pressure is reduced to a more safe region, commonly by an automatic pressure reducing valve using a PI controller, just before exiting the engine room.

2.7 Flow Over Steam Pipelines and Heating Coils

2.7.1 Steam Pipeline

Steam is piped from the boilers along the length of the vessel's deck to the various tanks via a carbon steel pipeline. Generally, the main steam and condensate pipes are secured by vertical or horizontal girders exactly below the foot treads of the catwalk, while the pipe branches leading to the steam entrance of each tank are completely exposed to weather and wind gusts. As steam condenses inside a pipeline, it emits its latent energy and is converted to condesate. While wind flows above the pipeline, it transfers heat from the surface of the pipeline towards the environment. As flow over the pipeline is induced by an external factor, we refer to the mode of forced convection. The characteristic length used to define Reynolds number is the cylinder's outside diameter, hence :

$$Re_D = \frac{\rho V D}{\mu} = \frac{V D}{\nu}$$

The critical Reynolds number for that kind of flow is considered to be $Re_{D_{cr}} \approx 2 \times 10^5$. If $Re_D \leq 2 \times 10^5$, the boundary layer remains laminar, otherwise boundary layer transition occurs.

Heat radiation is another factor which contributes to heat transfer from the pipeline. However, the effect of radiation will generally be negligible for turbulent forced convection

over flat plates or circular cylinders [58]. In addition to this, in case the pipeline is insulated, then radiation can surely be ignored, as the temperature of the pipeline's surface is greatly reduced. On the other hand, as the ship operates at environments where humidity is high, insulation tends to absorb moisture causing unfavorable conditions for the viability of the pipeline. Nowadays, many shipowners decide to remove insulation, as the costs of repairing the pipeline every now and then were considered to be higher compared to what you would pay in order to compensate for the added heat losses from steam. If that is the case, temperature at the outside diameter of the pipeline is expected to be comparable to that of saturated steam flowing inside the pipe leading to larger temperature differences between the pipeline's surface and the environment. Consequently, heat losses from heat radiation are considered too great to be neglected. Solar radiation is a factor which can add heat to the pipeline and reduce the amount of energy lost towards the environment. However it varies greatly in respect of cloud coverage, atmospheric conditions and the relevant position of the sun compared to the vessel.

2.7.2   Heating Coils

In each cargo tank, there are four heating coils installed that run down the aft bulkhead and proceed along the tank at about 0.5 m from the tank's bottom. The pattern that each heating coil follows inside the tank varies for each cargo tank, as there are some that extend along the whole length of the tank and others that remain closer to the aft bulkhead. Steam flows through the coils and is simultaneously condensed, emitting the latent heat which is used to heat the cargo. Subject to the orientation of each heating coil compared to the plane defined by the ship's bottom, a heating coil can either by vertical or horizontal. Vertical heating coils are those running down and up the aft bulkhead of the cargo tank, while horizontal are those that run across the tank bottom. In both cases, the heat transfer mechanism developed externally is considered to be natural convection, although each orieantation develops a completely different thermal boundary layer.

Each heating coil inside a cargo tank extends at two layers. The upper layer is considered the steam feed line, which provides steam in the tank, and the bottom layer is the condensate-return line or exhaust, which is meant to return the condensate back to the top of the tank. Steam is circulated from the upper to the bottom layer via 180° bend. The condensate line is located 0.3 m below the steam line and just 0.2 m above the tank top. Hence we can understand that the boundary layers originating from each layer will interact. However in the present work, the interaction between the two lines is disregarded, and all calculation are made as if each line's thermal boundary layer develops independently and does not affect the other.

Vertical Cylinders

In vertical tubes, the laminar boundary layer begins to form from the bottom of the cylinder, as shown in Fig. 2.9, around its circumference and gradually increases in thickness. When reaching a critical value of δ, the boundary layer becomes unstable and very susceptible even to small disturbances. These disturbances are growing in size as they move towards the upper part of the cylinder, transforming periodically into large scale vortices that collide and merge, finally taking a form of chaotic fluctuations, typical for turbulent flow.

A vertical cylinder can be classified as short or long based on equation [12] :

$$\frac{D}{H} \leq \frac{35}{Gr_H^{0.25}}, \ \ Pr \leq 1 \tag{2.3}$$
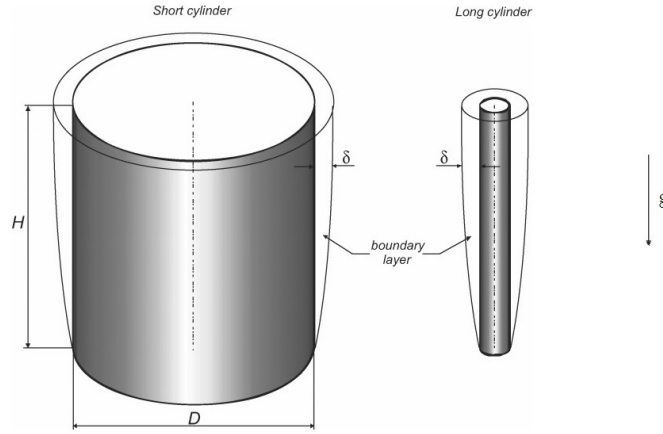
Figure 2.9: Free convection boundary layers on the lateral surface of a vertical cylinder(Popiel, 2008).

while for fluids with Prandtl number greater than unity, the condition under which the correlation for flat plate is applicable [28] is

$$\frac{D}{H} > Ra_H^{-0.25}, \;\; Pr > 1 \tag{2.4}$$

where Gr_H, Ra_H is the Grashof and Rayleigh numbers acquired based on the cylinder's height H. Condition of Eq. 2.4, is referred to as the thick cylinder limit. If D/H is greater than $Ra_H^{-0.25}$, the boundary layer thickness will not be comparable to the radius of the cylinder, and the effect of surface curvature can be neglected. For long or slender cylinders Eq. 2.3 is valid and the transversal curvature effect cannot be neglected. Transverse curvature influences boundary layer development and leads to increased rates of heat transfer. In flows around short cylinders, the curvature effect can be ignored and then the natural convection flow is the same with that of a vertical plate. In this case, Nusselt number can be calculated with the correlations developed by vertical plates (Bejan, 2003) [28].

Horizontal Cylinders

In horizontal tubes, the boundary layer develops along the curved surface, begining from the bottom portion of the tube and increasing in thickness along the circumference, forming a rising plume at the top, as shown in Fig.2.10. As gravity acts perpendicularly to the flow direction, under laminar flow regime, boundary layer formed around the tube is symmetric in respect to the tubes centroid.

It can be seen that the local Nusselt number is highest at the bottom where the boundary layer is thinnest. As the angle θ increases, the thickness of the boundary layer increases and the local Nusselt number decreases monotonically. Although an integral solution can yield results all the way to the top where $\theta = 180°$ and $Nu_\theta = 1$, the result beyond $\theta = 165°$ is no longer applicable because boundary layer separation occurred and plume flow takes place. At Rayleigh numbers sufficiently large $(Ra_D \geq 10^9)$, this decay of the local Nusselt number would be disrupted, in order to permit transition to turbulence within the boundary layer.
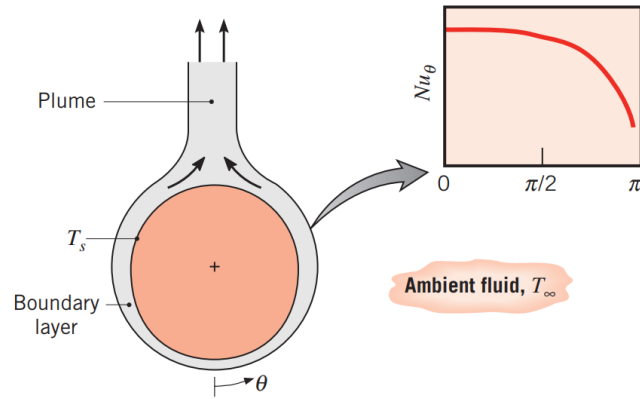
Figure 2.10: Boundary layer development and Nusselt number distribution on a heated horizontal cylinder (Bergman et al.,2011).

Annotations

In this chapter, we considered heat to transfer from the heating coils under the mode of natural convection. Numerical analysis conducted by Pivac and Magazinovic [19], of the heat transfer process at the heating coil surface has revealed that the heat transfer coefficient is significantly higher than the value following the ordinary natural convection theory. That difference was attributed mostly to the influence of oil viscosity change close to the heating coil surface.

Furthermore, in reality heat transfer does not occur under the mode of natural convection, as ship motions such as heaving, pitching, rolling and surging result in cargo sloshing inside the tank. As cargo movement is imposed by an external factor, forced convection should also contribute to heat transfer from the heating coils. Heat transfer coefficients encountered in forced convection are typically much higher than those encountered in natural convection because of the higher fluid velocities. As a result, natural convection is usually ignored, although we recognize that natural convection always accompanies forced convection. The error involved in ignoring natural convection is negligible at high velocities, but may be considerable at low velocities associated with forced convection.

Therefore, it is desirable to have a criterion to assess the relative magnitude of natural convection in the presence of forced convection. For a given fluid, it is observed that the parameter Gr/Re^2 represents the importance of natural convection relative to forced convection. This is not surprising, since the convection heat transfer coefficient is a strong function of the Reynolds number Re in forced convection and the Grashof number Gr in natural convection. Natural convection is negligible when $Gr/Re^2 < 0.1$, forced convection is negligible when $Gr/Re^2 > 10$, and neither is negligible when $0.1 < Gr/Re^2 < 10$. In order to define Reynolds number, we should somehow calculate the relevant velocity at which the cargo moves in respect to the oscillating ship. As that wasn't possible, in the present thesis, we assumed that heat transfer above the heating coils is totally due to natural convection.

2.8 Oscillation effects on the heat transfer rate

Numerical analyses carried out by Akagi and Kato [66] for high viscosity fluid in a rectangular tank with rolling motion, showed that rolling ship movements tend to decrease the heat transfer coefficient from the heating coils. That is because the secluded fluid is

accompanied by a strong viscosity dependence on temperature; due to rolling motion, the cooler fluid with higher viscosity near the side wall of the tank flows down to the heating surface, preventing heat transfer to the fluid and decreasing its mean temperature inside the tank. That problem would be more severe to heating coils located in the vicinity of the side walls.

Also, in their analysis, Akagi and Kato concluded that the heat transfer rate towards the tank walls is likewise reduced. That was considered to be due to the fact that the cooled fluid with higher viscosity, running down the cargo tanks sidewall, becomes thicker and thicker at the tank walls, preventing heat transfer from the fluid to the tank walls. However, these adversary effects combined, resulted in slight decrease of the mean temperature inside the tank.

2.9 Flow Inside Pipelines

2.9.1 Two-Phase Flow

Two-phase flow refers to the interactive flow of two distinct phases with common interfaces in a channel, with the most common being that of a liquid-vapor (gas) flow. Each regime in liquid-vapor (gas) two-phase flow has a characteristic flow behavior that can substantially affect both pressure drop and heat transfer. Also, in the case of a single-component two phase flow, such as forced convective condensation, continuous mass transfer occurs between the vapor and the liquid phases. Because of that, the interfacial configurations in two-phase flow are also very complicated and can vary over a wide range. The interfacial distribution in the liquid-vapor(gas) flow can be classified into a number of categories known as flow patterns or flow regimes.

Vertical tubes

Although downward two-phase flow condensation finds applications in many areas, it has received very little attention from investigators, and so there is very little flow pattern data for this case. The regimes for vertical downward two phase flow are similar to those shown in Fig.2.11, except that the downward-acting shear force and gravitational force eliminate the churn flow regime [29].
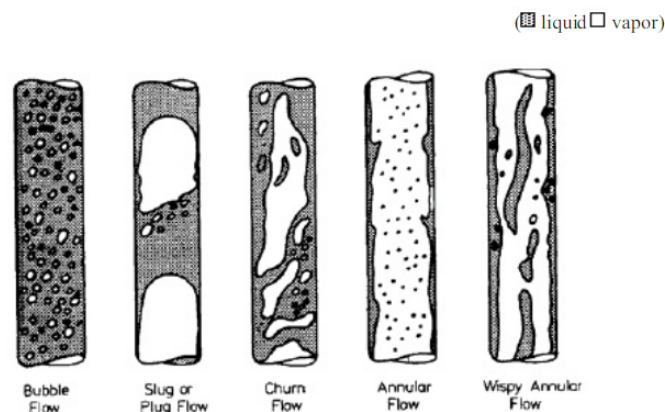
Figure 2.11: Flow regimes in vertical upward cocurrent two-phase flow (Hewitt, 1998).

However, the limited research indicates that the annular flow regime is dominant in vertical downward flow, as the annular liquid film forms on the inner surface of the tube,

as gravity acts parallel to the flow direction. Also, two phase flow in a vertical tube tends to be more symmetric, since gravity acts equally in the circumferential direction.

Horizontal Tubes

Horizontal two-phase flow exhibits flow patterns different from those in vertical two-phase flow, because gravity acts perpendicularly to the flow direction. In addition, two-phase flow in horizontal tubes is more complex than vertical two-phase flow, because the flow is usually not axisymmetric, due to the effect of gravity. The flow patterns encountered in horizontal two-phase flow are illustrated below (Hewitt,1998 [**?**];Thome,2004 [30])

(a) Bubbly Flow   (d) Wavy Flow

(b) Plug Flow   (e) Slug Flow

(c) Stratified Flow   (f) Annular flow

(■ liquid, □ vapor)
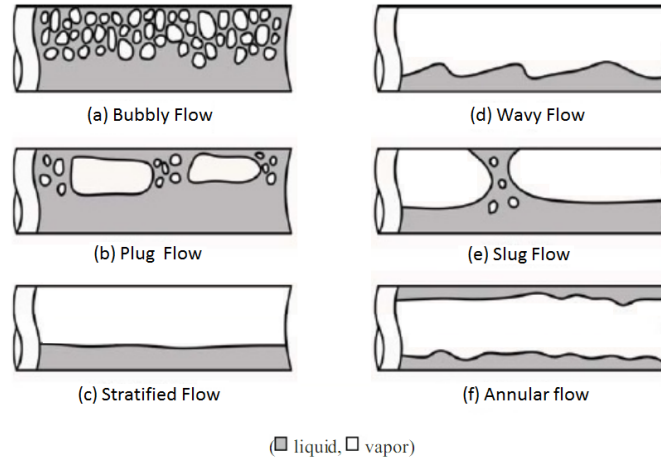
Figure 2.12: Flow regimes in horizontal two-phase flow (Hewitt, 1998)

When condensation occurs in a horizontal tube, different flow regimes are observed at different positions along its length. Depending on the mass flow rate of steam, two possible sequences of flow regime are possible (Hewitt,1998).

| Vapor | Annular | Slug | Plug | Bubbly | Liquid |

(a) Higher mass flow rate

| Vapor | Annular | Wavy | Stratified |

(b) Lower mass flow rate
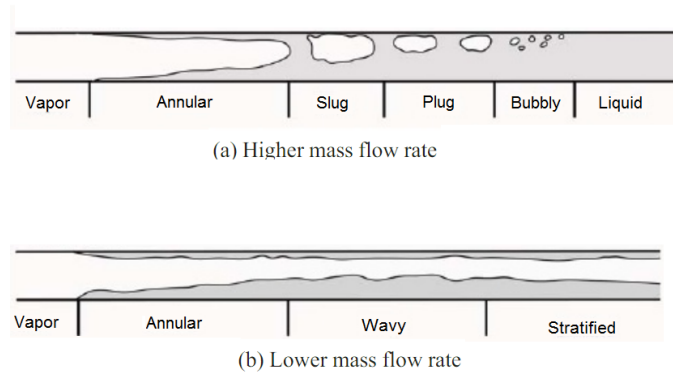
Figure 2.13: Flow patterns for condensation inside horizontal tubes (Thome, 2004)

As the steam progressively cools, condensation starts to occur on the inner wall of the tube. The flow pattern at the beginning of condensation is annular, because the velocity of the vapor is much higher than that of the condensate. The dominant force in the annular regime is shear stress at the liquid-vapor interface, with gravity playing a less important role. These shear stresses will pull the liquid at the interface along since the vapor velocity at the interface must drop to the value of the liquid velocity. This additional force will increase the average velocity of the liquid and thus decrease the film thickness. This, in

turn, will decrease the thermal resistance of the liquid film and thus increase heat transfer. As condensation continues, the velocity of the vapor phase decreases and the dominant force shifts from shear force at the interface to gravitational force. Liquid accumulates at the bottom of the tube, while condensation takes place mainly at the top portion of the tube where the liquid film is thin. As the vapor condenses downstream, the flow pattern changes to slug, plug and bubbly flows before the completion of condensation.

The flow regime for lower mass flow rates also begins with annular flow at the commencement of condensation. As condensation continues, the condensate at the top portion of the tube flows to the bottom portion due to gravitational force while the liquid pool is propelled down the length of the tube by shear forces imparted by the flowing vapor. Since mass flow rate is not high enough to produce slug or plug flow, two phase flow in the horizontal tube enters a stratified flow regime where liquid flows in the bottom portion of the tube and vapor flows in the top portion. Unlike the case of high mass flow rate, the vapor at lower flow rate never completely condenses.

It should be pointed out that different flow maps were developed by various investigators, aiming to predict two-phase flow patterns, based on generalised flow parameters for liquid and vapor flow. However the accuracy of each flow map is debated as most of them were obtained for adiabatic two phase flow; if we use these flow maps to determine the flow patterns for forced condensation inside a tube, for which external cooling takes place, results cannot be deemed reliable. A flow map for condensation in a horizontal tube was suggested by Tandon et al. (1982) [64] and is shown in Fig.2.14, illustrating that the most frequently occurring flow regimes for condensation in a horizontal tube are the annular-dispersed flow and the stratified flow.
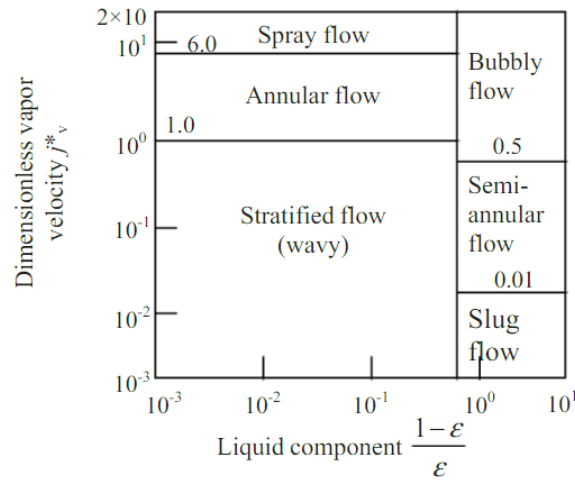
Figure 2.14: Flow pattern map for condensation in a horizontal tube (Tandon et al., 1982).

where

$$j_v{}^* = \frac{x\dot{m}''}{\sqrt{gD\rho_v(\rho_l - \rho_v)}} \tag{2.5}$$

Also according to Rohsenow et al. [33] for most of the tube, the flow regime is annular flow. At the higher end of the design flow range, there may be liquid droplets in the core -mist annular flow- and at the end of the tube when condensation is nearly complete there

may be stratified flow. Nevertheless, most of the practical range of operation can be well predicted by an annular flow model.

2.9.2 Single-Phase Flow

Once steam is fully condensed, fluid of a single phase (condensate) starts flowing inside the tubes. At the point of complete condensation, the liquid inside the tube will have slightly lower but similar temperature to that of saturated steam. Flow and heat transfer characteristics will also alter inside the tube, as a different kind of thermal boundary layer will be formed, which results in much lower heat transfer coefficients. Nevertheless, condensate's elevated temperature at that point witnesses that there is more energy which can be transferred to the cargo in the form of heat.

For the fully developed region, where the velocity profile is stabilised, the Reynolds number for flow in circular tube is defined as

$$Re_D = \frac{u_m D}{\nu} \tag{2.6}$$

where $u_m = \frac{\dot{m}}{\rho A_c}$ is the mean fluid velocity over the tube cross section and D is the tube internal diameter. In a fully developed flow, the critical Reynolds number corresponding to the onset of turbulence is

$$Re_{D,c} \approx 2300$$

although much larger Reynolds number are needed ($Re_D \approx 10^4$) to achieve fully turbulent conditions.

Under the assumptions that viscous dissipation is negligible and net heat transfer by conduction in the axial direction are neglected, we can apply an energy balance to a tube of finite length dx, where fluid moves at a constant flow rate $\dot{m}$, and convection heat transfer occurs at the inner surface. The energy balance equation, is expressed as:
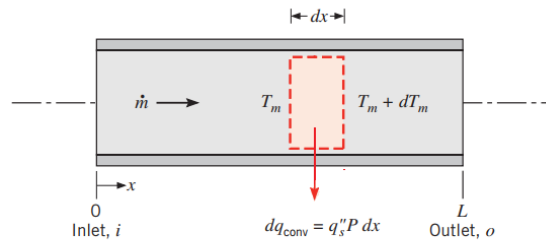
Figure 2.15: Control volume for internal flow in tube (Bergman et al., 2011).

$$dq_{conv} = \dot{m} c_p [(T_m + dT_m) - T_m] \tag{2.7}$$

Note that dT_m should be negative, as condensate reduces in temperature along the length of the heating coil. That amount of heat is transferred to the surrounding fluid through the circumference of the tube, thus :

$$dq_{conv} = \bar{h} \, dA_s \, (T_m - T_s) \tag{2.8}$$

where A_s is the tube surface area ($dA_s = P \cdot dx$), $\overline{h}$ is the average convective heat transfer coefficient for the length dx and T_m, T_s are the tubes core and inner surface temperatures. From equations Eq.2.7 and Eq.2.8 we can get that

$$dT_m = \frac{\overline{h}\,dA_s}{\dot{m}c_p}(T_m - T_s) \tag{2.9}$$

This expression is an extremely useful result, from which the axial variation of T_m may be determined. Both for single and two-phase flow, pressure drop occurs when frictional forces, caused by the resistance to flow, act on a fluid as it flows through the tube.

As fluid flows through the tubes, pressure drop occurs when frictional forces, caused by the resistance to flow, act on a fluid. The main determinants of resistance to fluid flow are fluid velocity through the pipe and fluid viscosity. Pressure drop increases proportional to the frictional shear forces within the piping network. High flow velocities and/or high fluid viscosities result in a larger pressure drop across a section of pipe or a valve or an elbow. Low velocity will result in lower or no pressure drop. We are concerned about pressure drop, as pressure is the predominant factor to determine steam's thermophysical properties. More on pressure drop for two-phase and single phase flows, can be found in pages 107 -110 of the Appendix.

Chapter 3

Calculation Process

3.1 Introduction

The model described in this thesis was developed in Matlab environment. In Matlab, programs are developed using some programming principles and rules in the so called m-files. Every sub-model described in chapter 2, was programmed in a separate m-file. As Matlab makes matrix manipulation easily accessible, the under investigation vessel's cargo tanks, were modelled as 2x7 matrix, where the first and second row of the matrix illustrate the port and starboard tanks respectively. The first column of the matrix refers to the slop tanks, while columns 2 to 7 refer to the cargo tanks.

Then we proceeded with heat transfer calculations from each seperate cargo tank towards it's environment. Thus, all results were obtained in a 2×7 matrix format. Our calculations were based on the existing analogy between heat transfer and electricity and under the assumption that heat transfer is one-dimensional, which means that it is significant only towards one dimension and negligible in the other two. Heat flow from each surface was modelled by the existing analogy to an electrical circuit, where heat flow is represented by current, temperatures are represented by voltages and thermal resistances are represented by resistors.

In this chapter, we will begin by introducing the needed input data required for the matlab program to run properly. Then, input data handling will be demonstrated, in order to acquire more informations based on simple assumption. Heat transfer calculation processes are performed, based on the order mentioned in chapter 2. Our aim is to calculate the equivalent thermal resistances for each mode of heat transfer occuring on the ship during cargo carriage and cargo heating processes at the best possible approximation, based on some fundamentals assumptions for heat flow.

3.2 Input Data Handling

Input Data are provided by the user by means of an Excel file. An xlsx file was chosen because it was considered the most user friendly way for data input, as most people are familiar with that computer application. The requested input data for heat losses calculations are illustrated in Table 3.1. Note that notations in the first column are exactly the same as those used in the code. This was done in order to assist the reader associate what is writen in this chapter, to the code attached to the Appendix.

Ambient Conditions	
$T_{ambient}$	Air temperature, $[°C]$
T_{sea}	Sea temperature, $[°C]$
Sailing Conditions	
V_{ship}	Ship's speed, $[kn]$
$V_{ship-dir}$	Ship's Direction, $[deg]$
V_{wind}	Wind's speed, $[kn]$
$V_{wind-dir}$	Wind's Direction, $[deg]$
$V_{current}$	Sea current speed, $[kn]$
$V_{current-dir}$	Sea current Direction, $[deg]$
T_{sail}	Draft, $[m]$
$COTK_{fillratio}$	Cargo tank filling ratio , $[\%]$
Loaded Cargo Properties	
d_{15}	Cargo density at $15°C$, $[kg/m^3]$
T_b	Boiling temperature, $[°C]$
T_{v1}	Kin. Viscosity Measurement temperature , $[°C]$
T_{visc1}	Cargo kinematic viscosity at T_{v1} , $[cSt]$
T_{v2}	Kin. Viscosity Measurement temperature , $[°C]$
T_{visc2}	Cargo kinematic viscosity at T_{v2} , $[cSt]$
$T_{c-loc1}, T_{c-loc2}, T_{c-loc3}$	Cargo temperatures at three different levels, $[°C]$

Table 3.1: Input Data for Heat Loss Calculations

Other data needed for our calculations, such as ship's dimensions, cargo tank capacities and other miscellenous geometry details were stored by default, as the code was developed for a specific ship. Finally, deck and bottom areas were measured by the ship's capacity plan for each cargo tank and were given at the form of a 2x7 matrix.

Based on the data compiled by the user, the program proceeds by calculating other problem parameters, such as :

- Wetted surface area for each tank (A_{sea}), where $A_{sea} = (T_{sail} - D_{db})L_{tank}$

- Freeboard surface area for each tank (A_{air}), where $A_{air} = (D_{ship} - T_{sail})L_{tank}$,

- Height of cargo inside the tank and ullage space above the free surface

  Assuming the cargo tank to be of a rectangular cross section, then cargo height inside the tank measured from the tank's bottom can be estimated by the equation

$$H_{cargo} = (D_{ship} - D_{db})\frac{COTK_{fillratio}}{100}$$

  The height of the cavity (H_{cav}) formed above the free surface and below the deck plating can then easily be determined.

- Cargo volume inside cargo tank,

- Area of cargo exposed to air flow,

- Average cargo temperature above and below sea level (Tc_{asl}, Tc_{bsl}).

  As mentioned in Chapter 2.2.2, temperature inside the cargo tank is considered to vary significantly only in the vertical direction, as temperature drop near tank walls

occurs in a very slim layer. A common practice in cargo monitoring is temperatures for each tank to be measured at three different levels. In the present work, we regarded this levels to be a)1m above tank top, b)at the middle of cargo height (H_{cargo}) and c) just below the oil's free surface. Considering that temperature varies inversely with H_{cargo}, as heat sources are placed at the bottom of the tank, temperature readings may vary even by $5°C$. Assuming cargo temperature distribution to be linear across the z-axis, it is possible to estimate the bulk cargo temperature at any height inside the tank by an equation of the form $T_{c,\infty} = (\alpha \times H) + \beta$, where α, β are constants.

Calculating the average cargo temperatures above and below sea level at that stage, will serve as well during heat transfer calculations from the ship's side.

- *Relative velocities between ship-seacurrent-wind*

  During data input, the user has submitted the velocities of ship, sea current and wind. However in heat transfer calculations, we are intrested on the relevant velocities between the seacurrent-ship system and wind-ship system, defined by an "inertial observer" located onboard the ship. In that aspect, lets assume that the ship sails with a velocity V_s at a random course (Φ degrees from North), and that wind originates from NE, as shown in Figure 3.1. This is a random example and in any case we could swap the wind vector with a sea current vector, as the procedure is the same for both.

  In order to calculate the relative velocities, we analyse the initial wind vector (W) into two components along axes xx' and yy' (Wxx' and Wyy' respectively), which describe the equivalent effect of the wind vector on the direction of each axis. Note that wind vector Wxx' will always by parallel to the ship's centerline and wind vector Wyy' will always be perpendicular.
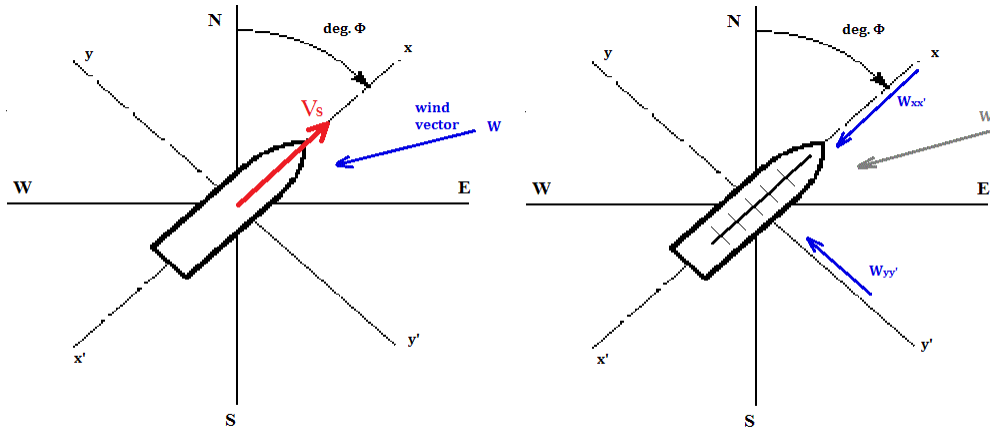
Figure 3.1: Analysis of wind vector to ship's axis

For vertical surfaces like the ship's side, the relative velocity above the flat surface is the conjugate effect of V_s and wind vector ($W_{xx'}$) which is parallel to xx' axis , while vector $W_{yy'}$ won't provoke any heat transfer. On the other hand, for horizontal surfaces (such as the ship's deck and bottom), vector $W_{yy'}$ will contribute to heat transfer, as it flows transversly to the ship's motion. The effects of that lateral flow will be discussed later on.

3.3   Heat Loss Calculations

3.3.1   Side Shell Plating

In order to calculate heat flow rate through the ship's side, we must first determine the respective heat transfer coefficients for each mode of heat transfer mentioned in Chapter 2.2. Our aim is to model heat exchange from the cargo space towards the environment, via an equivalent thermal circuit. While the ship's side is surrounded by two different fluids, each at a different temperature, it is not possible to conclude in a single thermal circuit. Hence, two different thermal circuits should be constructed; one for the heat transferred to air, and one for the heat transferred towards the sea.

Nonetheless, as heat transfer was deemed to be one dimensional, only the amount of cargo situated below sealevel will exchange heat with sea. The same will apply for the amount of cargo situated above sea level, which will exclusively exchange heat with ambient air. As we have regarded temperature distribution between the three levels of measured temperatures to be linear, we can easily estimate the average cargo tamperatures both above and below sea level, which will serve as the starting point of heat transfer in the constructed thermal circuits.

Summarizing the heat transfer modes analyzed in Chapter 2.2 for the amount of cargo situated below sea level, heat will be transferred from the bulk mass of the cargo to the inner side shell of the tank via natural convection. From there it will be conducted towards the double hull through the inner hull plating. Reaching the double hull space, heat will be simultaneously transferred through i)natural convection by the secluded fluid in the ballast tanks (air or seawater) and ii) through conduction from the web frames and stringers to the opposing side of the double hull. From there, heat will be conducted by the outer side shell plating to the outer surface of the ship, where it will be transferred under forced convection by the sea flowing around the hull. The same will apply for heat flow from the cargo situated above sea level, only this time the fluid flowing outside the ship's hull is air.

Furthermore we notice that initially the only known temperatures, are those of the cargo (above and below sea level), the temperature of sea and that of ambient air. All other intervening temperatures are unknown, and have to be determined in order to estimate the total heat flow rate from the ship's side. So we proceed by defining the following temperatures:

- $T_{inner.bsl}$: the average temperature of the inner hull plating, situated below sealevel,

- $T_{inner.asl}$: the average temperature of the inner hull plating, situated above sealevel,

- $T_{db1.bsl}$: the temperature of the wall inside the enclosure, adjacent to the cargo side and below sealevel,

- $T_{db1.asl}$: the temperature of the wall inside the enclosure, adjacent to the cargo side and above sealevel,

Figure 3.2: Heat transfer towards the ship's side shell. Intervening temperatures are annotated in the double hull area
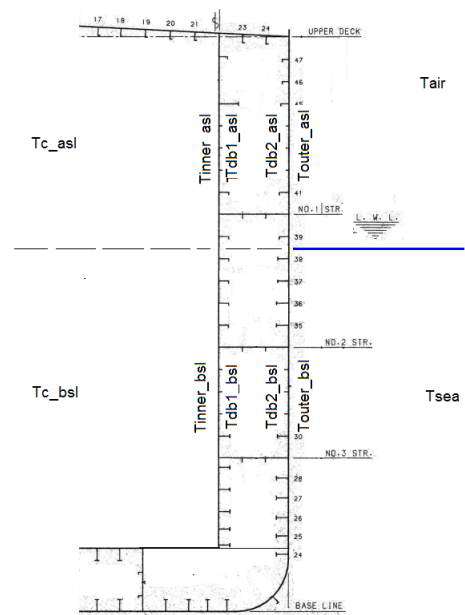
- $T_{db2.bsl}$: the temperature of the wall inside the enclosure, adjacent to the sea side,

- $T_{db2.asl}$: the temperature of the wall inside the enclosure, adjacent to the air side,

- $T_{outer.bsl}$: the temperature of the ship's external hull situated below sealevel,

- $T_{outer.asl}$: the temperature of the ship's external hull situated above sealevel,

The calculation process for the ship side is illustrated below :

1. **Calculate the properties of seawater**

   Seawater properties depend on three factors: i) temperature, ii) salinity and iii)pressure at the depth of reference. As a rule of thumb, fluid properties in heat transfer calculations are evaluated at the arithmetic mean of free stream and surface temperatures, the so called *film temperature*, $T_f = (T_s + T_\infty)/2$. Thus, properties of sea water surrounding the ship's hull should be calculated at the arithmetic mean temperature of sea and ship's outer plating.

   However, results of this work, as well as those of Mavrakos [6] showed that the temperature at the outside shell plating does not diverge significantly from that of sea. Specifically Mavrakos [6] calculated for a single hull tanker, carrying crude oil at 60 °C and a sea temperature of 10 °C, that the resulting outer side shell temperature would be around 10.05 °C. Thus, more correctly, the sea water properties should be estimated at 10.025 °C instead. However, that alteration would have a trivial impact on seawater properties. In addition, the effect's of cargo temperature on the outer plating temperature of a single hull ship, are much greater compared to that on modern double hull designs of crude oil carriers, where the double hull acts as an insulation to the cargo tanks. Thus in our case, we anticipate the outer side shell plating temperature to be even more similar to that of sea.

   Salinity has been taken to be constant, and equal to 35 g/kg(ppt), although it varies subject to the ship's location and along different seasons. Finally, pressure increases with the ship's draft. We decided that an appropriate depth to calculate the thermophysical properties of seawater is half of the ship's design draft. Calculations were based on correlation proposed by Nayar et al [43] and Sharqawy, Lienhard & Zubair [44] and are attached to the Appendix pg.82.

2. **Calculate the local Reynolds number for sea water flowing over the hull**

   Sea water flows over the sides of the ship, with a velocity equal to the relative velocity of the ship-sea current system. However, only the vector parallel to the ship's centerline should be considered. Characteristic length x, is measured from the ship's bulb. The crude oil tanker under investigation has 6 pairs of cargo tanks, each one of which has a total length of 29.6 meters and a set of slop tanks, extending 4.7 meters aft of Cargo tank No.6. The distance from the bulb to the foremost bulkhead of cargo tank No.1 is 16m. Increment was set equal to 0.1 m. Thus, for each cargo tank, the local Reynolds number is calculated from the beginning to the end of the tank, for every 0.1 meters of plate's length.

3. **Calculate local (h_x) and average (h_L) heat transfer coefficient for forced convection around ship hull**

   The local heat transfer coefficients (h_x) at the exterior of each cargo tank were also calculated for every 0.1 m, since each value of Re_x corresponds to a single value of h_x through Eq.A.2. Equation A.2 applies for the entire plate only when the flow is turbulent over the entire range of the plate, or when the laminar flow region is comparatively small. In our study, we considered the plate's length to coincide with the total range of the ship's cargo tanks. Also, laminar flow region extends approximately a couple of meters from the ship's bulb, so that region can be disregarded with certainty. The overall heat transfer coefficient over each cargo tank, can be determined by estimating the mean average value of the local values h_x over the respective tank.

4. **Assume a temperature $T_{outer.asl}$**

   That temperature should be somewhere between the ambient air tamperature and cargo temperature located at the upper portion of the tank. Considering that the cargo secluded in the tanks has an elevated temperature compared to ambient environment and that the double hull area serves as an insulation to the cargo tank we figure that Tout-asl should be closer to tha ambient temperature, rather than that of cargo. Initially, it is taken to be $8°C$ higher than T_{air}.

5. **Calculate film temperature for air flow outside the side shell**,

   Following the same rules as above, the properties of air flowing past the ship's hull should be calculated at the average temperature of air and the ship's outer plating, $T_{film} = \frac{(T_{outer.asl} + T_{air})}{2}$.

6. **Estimate the thermophysical properties of air flowing around the ship's hull at temperature T_{film},**

   For our calculations, we are going to need the following air properties : i)density ρ_{air}, ii)thermal conductivity k_{air}, iii)kinematic viscosity ν_{air} and iv) the Prandtl number Pr_{air}. The formulas used to calculate the thermophysical properties of air are included at the end of this paper (see Appendix for the code).

7. **Estimate local Reynolds number an determine the nature of flow**

   The boundary layer develops around the ship's freeboard, where air moves with the relative velocity of the ship-wind system. The kinematic viscosity of air was calculated at the previous step and the characteristic length is measured, in accordance with step 2, from the ship's stem. Similarly to the flow of sea around the hull, air flow in most of the cases will be turbulent.

8. **Calculate the heat transfer coefficient for forced convection over the shear strake plating**

   Again, we can use equation A.2 to calculate the local heat transfer coefficientc of air flowing over the ship's side plating. The average heat transfer coefficient h_m results from integrating the local values over the entire surface.

9. **Assume temperatures $T_{inner.bsl}$, $T_{inner.asl}$**

   Cargo properties are calculated again, at a film temperature, which strongly depends on the assumed surface condition at the tank's surface. Correlations used in the present thesis for the estimation of the heat transfer coefficient inside the cargo tank have been obtained by various investigators under the assumption that the plate is isothermal (constant T_s along the plate's height). Nonetheless, cargo temperature inside the tank is not uniform, but varies along the z-axis. Thus, the plate's temperature will also vary along the z-axis and cannot be considered isothermal.

   Assuming that the surface condition is instead, one of uniform heat flux (constant q_s''), both Churchill [9] and Sparrow [11] were led to the conclusion that temperature difference $(T_\infty - T_s)$ will vary with z, increasing from the leading edge. In our case, the temperature difference indeed varies along the z-axis, increasing while cargo moves downwards from the top of the tank, as core cargo temperature rises as we move towards the bottom of the tank. Hence we can accept the condition of uniform heat flux. Correlations obtained for the isothermal plate may still be used to an excellent approximation, if $\overline{Nu_L}$, Ra_L and Gr_L are defined in terms of the temperature difference at the midpoint of the plate $\Delta T_{L/2} = T_s(L/2) - T_\infty$.

   As the cargo tank's height is equal to 18.7 m and the scantling draft of the ship is 14.6 m, it is evident that even for partially or half filled tanks, the midpoint of the plate will always be below sea level. Thus, T_∞ will always coincide with the average bulk cargo temperature below sea level. Surface temperature T_s will also coincide with $T_{inner.bsl}$, the value of which is not known at the beginning of our calculation. Hence we proceed by assuming temperatures $T_{inner.bsl}$ and $T_{inner.asl}$. Based on the fact that $Tc_{bsl} > Tin_{bsl}$, since temperatures as we move towards the outer of the ship are reduced, we considered $T_{inner.bsl}$ to be 10°C lower than Tc_{bsl}. The same is also made for $T_{inner.asl}$, which is assumed initially to be 10°C lower than Tc_{asl}.

10. **Estimate film temperature and temperature difference at the midpoint of the plate**

    The temperature difference at the midpoint of the plate can now be determined by $\Delta T = Tc_{bsl} - Tin_{bsl}$. Furthermore, the film temperature at which the properties of crude oil are calculated is equal to $T_{film} = (T_\infty + T_s)/2 \Rightarrow \quad T_{film} = (T_{c\_bsl} + Tin_{bsl})/2$.

11. **Calculate the thermophysical properties of crude oil**

    The cargo properties we need for our calculations are the density of the cargo (ρ_c), thermal expansion coefficient (b_c), kinematic viscosity (ν_c), thermal conductivity (k_c), specific heat of cargo (Cp_c) and the Prandtl number (Pr_c). The calculation formulas for petroleum products are attached to the relevant chapter at Appendices(see ch. page.) .

12. **Estimate Grashof-Rayleigh numbers and determine nature of flow inside the cargo tank**

    Next we calculate the Grashof (eq.2.1) and Rayleigh numbers. An appropriate increment for our calculations was considered to be 0.1 m, thus from the bottom of the tank until the cargo's free surface, we estimated the local Grashof number for every 0.1 meters. In that manner, we can easily determine whether and where transition

to turbulence occurs. If Grashof number exceeds the critical value of 10^9, there is no need to continue our calculations, as correlations for turbulent natural convection include overall values for Grashof and Rayleigh numbers (Gr_L and Ra_L respectively.)

13. **Estimate the heat transfer coefficient for natural convection inside each tank**

    If the flow above the plate remains laminar, we use equation Eq.A.11 to find the local heat transfer coefficients for the entire plate. The average heat transfer coefficient over the entire plate can be decided by calculating the average of the local values h_x, as well as from equations A.9 and A.10. The average heat transfer coefficient over the cargo tank's side occurs by the arithmetic mean of the results of the aforementioned equations. If the flow over the plate becomes turbulent at some point, the average heat transfer coefficient over the entire surface is calculated exclusively by equation A.12.

14. **Asssume temperatures T_{db1} and T_{db2} above and below sea level**

    In order to investigate the heat transfer mode inside the double hull space, we must first be aware of the temperatures at the two vertical walls. However, these temperatures are initially unknown. Hence,an assumption has to be made for the temperature at the side of the ballast tanks located closer to the cargo tank (T_{db1}) and closer to the atmospheric air/sea T_{db2} respectively. These temperatures will be quite similar to the ones inside the cargo tank and outside of the ship's hull, as heat is conducted through thin metallic sheets forming the inner and outer hull, the thermal conductivity of which is considerably high, as they are made out of steel.

15. **Calculate fluid properties inside the ballast tank**

    For rectangular enclosures heated from one side and cooled from the other, film temperature is defined as the average temperature of the two vertical walls. In Fig.2.5, we observed that all ballast tanks are vertically segregated by three stringers, forming four different compartments. Also, 7 web frames seperate those four compartments in the longitudinal direction, thus raising the number of subcompartments to 32. Manholes formed in those structural frames allow the inspection of ballast area, as well as permit ballast to be uniformly distributed in the double hull space. As we assumed ballast tanks to be empty, air is free to flow inside each of the four spaces. Although manholes allow air flow inside these four spaces, we will assume that air inside each tank is secluded and cannot escape to any of its neighbouring spaces located above and/or below. For areas (1), (2) and (4), properties of air are calculated at the mean temperature $(T_{db1}+T_{db2})/2$ according to the corresponding correlations for air in page 89.

16. **Estimate Grashof and Rayleigh numbers**

    Grashof and Rayleigh numbers are calculated in respect to the enclosures width (Gr_L) and the enclosures height (Gr_H), as correlations are available for both dimensions (see pg.78-79).

$$Gr_H = \frac{g\beta(T_h - T_c)H^3}{\nu^2} \tag{3.1}$$

where T_h and T_c are the temperatures of the hotter and colder vertical wall respectively.

17. **Calculate the total heat transfer coefficient inside the ballast space**

For the purpose of this study, the horizontal surfaces of the deck and bottom platings forming the top of compartment number 4 and the bottom of compartment number 1 (as depicted in Fig.2.5) are considered to be adiabatic, as $L << H$ and heat dissipation is considered to be one-dimensional, thus heat transfer to other dimensions can be neglected. For space area (3), we acknowledge that during loaded voyages is seperated into to portions; the upper portion is located above sealevel while the other part will be below. In that case we decided to calculate the Nusselt numbers inside this enclosure, based on the percentage of area located below or above sea level. For example if sealevel reaches 80% of space (3) height, the total Nusselt number results from :

$$\overline{Nu} = 0.8 \times \overline{Nu}(Pr_{bsl}, Ra_{bsl}) + 0.2 \times \overline{Nu}(Pr_{asl}, Ra_{asl}) \tag{3.2}$$

From equations A.13-A.21 we can calculate the convective heat transfer coefficients using numbers Gr_L, Gr_H, Ra_L, Ra_H as needed.

18. **Compute the radiative heat transfer coefficient**

The net radiation exchange (q) and the radiative heat transfer coefficient in an enclosure can be calculated by the equation :

$$q = \frac{\sigma A(T_1{}^4 - T_2{}^4)}{\frac{1}{\epsilon_1} + \frac{1}{\epsilon_2} - 1} \quad \Rightarrow \quad h_{rad} = \frac{\sigma(T_1{}^4 - T_2{}^4)}{\frac{1}{\epsilon_1} + \frac{1}{\epsilon_2} - 1} \frac{1}{T_1 - T_2} \tag{3.3}$$

where T_1, T_2 and ϵ_1, ϵ_2 are the temperatures and the normal emissivities of the hotter and colder surface respectively, while σ is the Stefan-Boltzmann constant. It is important to mention that in equation 3.3, the units of T_1 and T_2 are in degrees Kelvin [^oK] and not Celsius [^oC].

Emissivities of different materials are illustrated in the adjacent figure, taken by Bergman (2011 p.796) [2]. We can see that for as received, unpolished metals, the surface emissivity varies from 0.1-0.4, while polishing is found to reduce the normal emissivity values to below 0.1. Emmissivities for steel platings is taken to be equal to $\epsilon1 = \epsilon_2 = 0.2$.

The total heat transfer coefficient inside each enclosure can be calculated by summing the relevant convective and radiative heat transfer coefficients.
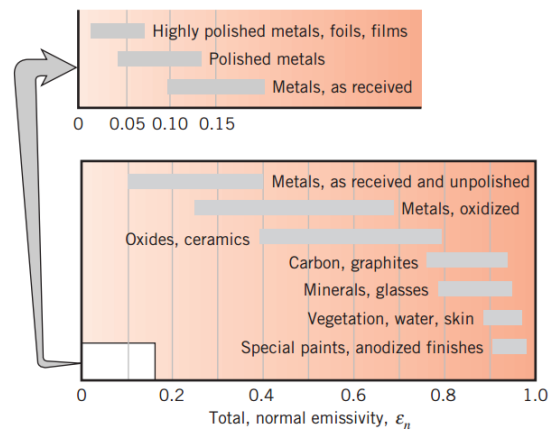
19. **Estimate the equivalent thermal resistances caused by the finned surfaces**

By following the calculation process mentioned in Bergman et al [2], we can infer an expression for the thermal resistance of a fin array, by amending the total htc found, due to the existence of extended surfaces. The methodology of this process is attached to the Appendix.

20. **Calculate the total thermal resistance of ballast tanks**

   The resistances of webs (R_{webs}), stringers ($R_{str.}$) and the amended resistances due to natural convection in the ballast tanks, are all connected in parallel, as they have the same origin and end temperature. We may figure the equivalent resistance of the double hull area by following the same principles as in an electric circuit. Then, all resistances are connected in series, so we can add them in order to export the total thermal resistances ($R_{tot.asl}$) and ($R_{tot.bsl}$).

21. **Calculate the equivalent total thermal resistances for heat flow towards the ship sides**

   The final thermal circuits are illustrated in page105, Fig.E.1 and Fig.E.2 respectively. As c we denoted the percentage of area (3) located below sealevel.
   Finally from equation C.9 we calculate the total amount of heat that is transferred towards the environment ($Q_{tot.side} = Q_{tot.asl} + Q_{tot.bsl}$). However, along the calculation process, we assumed temperatures for the inside of the cargo tank (T_{in}), for the two vertical walls of the ballast area (T_{db1} and T_{db2}), and for the surface of the side plating ($T_{out.asl}$). From equations C.5 and C.6 we get that each of the assumed temperatures must satisfy the equations :

$$Q_{tot.asl} = \frac{T_{c.asl} - T_{air}}{R_{tot.asl}} = \frac{T_{c.asl} - T_{in.asl}}{R_{cargo}} = \frac{T_{in.asl} - T_{db1.asl}}{R_{cond}} = \frac{T_{db2.asl} - T_{out.asl}}{R_{cond}} = \frac{T_{out.asl} - T_{air}}{R_{air}}$$

Hence :

$$T_{in.asl} = T_{c.asl} - Q_{tot.asl}\ R_{cargo} \tag{3.4a}$$

$$T_{db1.asl} = T_{in.asl} - Q_{tot.asl}\ R_{cond} \tag{3.4b}$$

$$T_{out.asl} = T_{air} + Q_{tot.asl}\ R_{air} \tag{3.4c}$$

$$T_{db2.asl} = T_{out.asl} + Q_{tot.asl}\ R_{cond} \tag{3.4d}$$

   If the outcome of the above equations is different than the initially assumed temperatures, the calculation process starts again, only this time the new assumed temperatures are the results of equations 3.4a - 3.4d. This is repeated numerous times, until convergence is succeeded at all temperatures. Furthermore the same is valid for the calculations below sealevel, where the intervening temperatures are given by equations:

$$T_{in.bsl} = T_{c.bsl} - Q_{tot.bsl}\ R_{cargo} \tag{3.5a}$$

$$T_{db1.bsl} = T_{in.bsl} - Q_{tot.bsl}\ R_{cond} \tag{3.5b}$$

$$T_{out.bsl} = T_{sea} + Q_{tot.bsl}\ R_{sea} \tag{3.5c}$$

$$T_{db2.bsl} = T_{out.bsl} + Q_{tot.bsl}\ R_{cond} \tag{3.5d}$$

Annotations

Ship's hull is constructed by steel, the thermal conductivity of which is equal to 52 W/mK. The thickness of plates forming inner and outer hulls were found in the ship's midship section drawing. Plate's thickness for both the inner and outer hull varies in the transverse direction, as metal sheet located closer to the ship's bottom have increased thicknesses in order to support the forces induced to the hull externally and internally by waves and cargo.

3.3.2   Deck

In order to depict this thermal circuit, first of all he have to clarify which temperatures are known and which are not. The overall temperature difference will be that between the cargo's free surface and atmospheric air ($T_{c.fs} - T_{air}$), where the subscript c.fs denotes "cargo at free surface". As mentioned above, the cargo temperature is monitored by the crew regularly and measurements are taken at three different levels, one of which was considered to be just below the free surface. Hence we have to determine two more temperatures; one at the inner surface of the deck plating ($T_{in.deck}$) and another one at the upper surface (T_{deck}) in order to find the total heat transferred through the tank's deck. The thermal circuit is illustrated in page106 Fig.E.3. The calculation process begins by:

1. Assume temperatures $T_{in.deck}$ and T_{deck}. These temperatures will be closer to the respective temperature of ambient air, rather than that of cargo's free surface.

2. Calculate the properties of fluid contained inside the tank's ullage space. This fluid is a mixture of air, inert gas and hydrocarbon vapours, the analogy of which constantly fluctuates as ingress of air can occur from the pressure/vacuum valve and purging operations can take place. As we cannot determine its exact composition, we are going to assume that the properties of this gas mixture do not differ significantly by those of ambient air. The source of inert gas can either be flue gases from the auxiliary boiler exhaust gas uptakes, either from an inert gas top-up generator, which aims to complement any leakages or air ingress inside the cargo tank.

   At the following table, typical compositions of ambient air and flue gases from the auxiliary boilers are illustrated. We can see that the prevailing constituent in both gases is nitrogen, the amount of which remains rather constant, while the concentrations of oxygen and carbon dioxide vary considerably.

   Table 3.2: Flue gases and ambient air compostition in % mol

	Flue Gases	Ambient Air
Nitrogen (N_2)	83%	78%
Carbon Dioxide (CO_2)	11-13%	0.04%
Oxygen (O_2)	2-4%	21%

   Based on atmospheric air formulas attached at the end of this paper, we calculate the thermal expansion coefficient b, thermal conductivity k, kinematic viscosity ν and Prandtl number Pr of the fluid at the mean temperature $T_m = (T_{c.fs} + T_{in.deck})/2$.

3. Calculate the Grashof and Rayleigh numbers, in order to determine the type of flow inside the cavity. As far as equations A.22 - A.25 are expressed based on different enclosure dimensions (the enclosure's height and width), we must calculate both numbers for each characteristic length separately.

4. Calculate the Nusselt number from equations A.22 - A.25 Equations A.24 and A.25 have to be amended, in order to express Nusselt number as a function of height (H_{cav}) instead of width (B_{cav}). For the conversion, we used an equation given in Rincon et al.([17],2016,p.13) where

$$\overline{Nu_B} = 2\frac{B}{H}\ \overline{Nu_H} \tag{3.6}$$

Furthermore, correlation A.22 applies for values of H/B sufficiently small to ensure a negligible effect of the sidewalls, where B and H are the cavity's width and height respectively.

5. Calculate the mean Nusselt number from the above methods and thus the convective heat transfer coefficient inside the cavity

6. Calculate the total htc inside the cavity by summing the radiative and convective heat transfer coefficients. Thermal radiation plays an important role in heat transfer during natural convection modes as both the free surface of the oil, as well as the deck plating emit heat via electromagnetic waves. In order to compute the radiative heat transfer coefficient through equation 3.3, we need the emissivities of each surface ϵ_1 and ϵ_2. According to Robinson and Davis [68], the emissivity of petroleum fractions is found to be slighly lower than that of water. For crude oil, experiments showed that the normal emissivity is equal to 0.95. The normal emissivity for high tensile steel at the lower side of the deck plating, is assumed equal to $\epsilon = 0.2$.

7. After the calculation of the total heat transfer coefficient, we consider the effects of extended surface (longitudinal stiffeners) to the total heat transfer rate. The equivalent thermal resistance for the space below the main deck and above the cargo free surface, $R_{tot.cav}$ is estimated following the methodology of finned surface areas as refered to the appendix.

8. Estimate thermophysical properties of air flowing above the deck plating

   Air properties are computed at the arithmetic mean of the environment (T_{air}) and upper surface of deck plating (T_{deck}) temperatures were the latter was assumed during step no.1.

9. Calculate the heat transfer coefficient above the deck plating deck. On deck, heat is transferred by means of forced convection. We treat the deck's plating as a flat horizontal plate. We note that wind can originate from various angles compared to the ship's velocity. Speed vectors are measured in degrees clockwise from due north both for ship and wind. Let's assume that the ship is heading north, and wind blows from south east. The speed's of ship and wind are V_{ship} and V_{wind}, while the direction of speed vectors are $V_{ship.dir} = 0°$ and $V_{wind.dir} = 270 + \phi°$ for ship and wind respectively, as illustrated in Fig.3.3.

   We decide to analyze the wind velocity vector into two components, one parallel to the ship's centerline (V_x) and one lateral (V_y). To do so, we calculate the relative angle between velocity vectors $\theta = V_{wind.dir} - V_{ship.dir}$. Then, for the wind's speed component vectors : $V_x = V_{wind} \cdot cos\theta$, $V_y = V_{wind} \cdot sin\theta$.

   Hence, two velocities contribute to heat transfer. One emerges from adding vectors V_{ship} and V_x and one because of wind vector V_y. As V_y is perpendicular to the ship's motion of movement, we can say that the deck plating is also exposed to a cross flow of air. Similarly, the resulting wind flow from the addition of vectors V_{ship} and V_x can
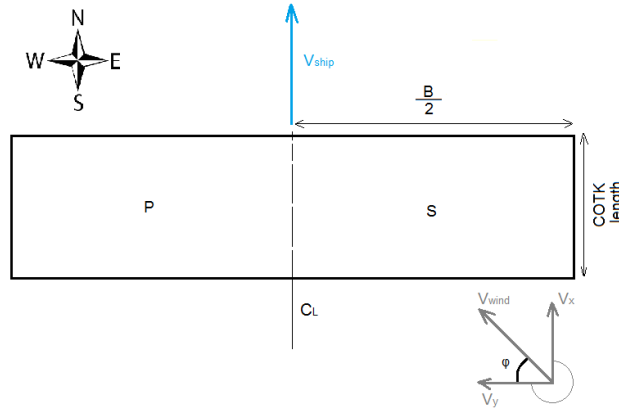
Figure 3.3: Forced convection on deck

be called axial flow. For the purpose of using equation A.1(p.76), we have to calculate the Reynolds number both for axial and cross flow. In the first occasion, Reynolds number uses as a characteristic length the cargo tank's length, albeit in cross flow the ship's half breadth. Then, the average heat transfer coefficients ($h_{ax.deck}$ and $h_{cr.deck}$) are calculated by integrating the local htc over the entire surface, for each respective characteristic length.

Although radiation can be neglected in forced convection modes, we computed the radiative htc based on equation 3.3(p.36), which however will be minor compared to that of forced convection. We assume that the emissivity for the upper side of the deck plating is $\epsilon = 0.1$, lower than that for inner surface of the deck plating, due to the effect of paints and coatings. The total average external heat transfer coefficient over the entire deck surface occurs from the summation of $h_{rad.deck}$, $h_{ax.deck}$ and $h_{cr.deck}$. Finally, we can calculate the thermal resistance of air flowing above the deck plating, R_{deck}.

10. Calculate the total thermal resistance $R_{tot.deck}$ as all component resistances are connected in series. The total loss of heat through the deck plating ($Q_{tot.deck}$) can be determined by dividing the overall temperature difference with the total thermal resistance results.

11. Temperatures assumed at the beginning of this process must satisfy the following equations :

$$T_{in.deck} = T_{c.fs} - Q_{tot.deck}\ R_{tot.cav} \tag{3.7a}$$
$$T_{deck} = T_{air} + Q_{tot.deck}\ R_{deck} \tag{3.7b}$$

If the outcome of the above equations is different than the initially assumed temperatures, the calculation process restarts from the beginning, only this time the new assumed temperatures are the results of equations 3.7a - 3.7b. This is reapeated numerous times, until convergence is succeeded for both temperatures.

Annotations

For considerably loaded cargo tanks, vertical walls were considered to be adiabatic, as $H_{cavity} \ll L_{tank}$ and $H_{cavity} \ll B_{tank}$. Nevertheless, for partially filled tanks, the cavity's

dimension alter and one might assume that heat will begin to transfer from the free surface of cargo towards the ship's side. In the present work, we considered that heat transfer through vertical walls should be neglected. First of all, for thermal circuit illustration, heat transfer was assumed to be one dimensional. Secondly, a study in the relevant literature and available exercises for natural convection inside rectangular enclosures, reveals that all researchers and authors make the adiabatic vertical wall assumption as well. Thus, correlations suggested by the bibliography would be rather useless, if not conditions and restriction are met.

Thirdly, heat losses towards the ship's deck are favoured in comparison to heat losses towards the ship's vertical walls. That is because forced convective heat transfer coefficient on deck is larger than the respctive for the sides, as air flow on deck is caused by the conjugate effect of the parallel and lateral velocity vector. Finally, for semi filled tanks, gas flow inside the ullage space obtains a similar behavior with that of oil inside the cargo tank; inert gas will commence to rise from the center of the tank and it will move downwards while cooling at the sides. Hence, hot gas will initially touch the inner deck plating and then move along its surface until it reaches the sides, thus intensifying heat losses towards the main deck.

3.3.3   Bottom

As mentioned in chapter 2.4, above the tank top plating and below the heating coils, a thick viscous layer of crude oil is formed during loading procedures. Using the publication [32] as a reference, we can safely assume that the sludge layer thickness would be approximately 9cm.

We decided to begin the calculation process from the temperature exactly above the viscous layer of cargo ($T_{ab.layer}$), as measured by thermometers at the bottom of the tank. Likewise with deck's calculation process, assumptions have to be made for all the intervening temperatures between $T_{ab.layer}$ and T_{sea}. The total thermal circuit is presented in page 106, Fig.E.4

where :

- $R_{v.oil}$ = thermal resistance of viscous oil layer,

- R_{cond} = thermal resistance of tank top / bottom plating,

- R_{db} = thermal resistance of double bottom area, due to radiation and conduction

$$R_{db} = \frac{1}{\left(\frac{1}{R_{rad.db}} + \frac{1}{R_{cond.air}} + \frac{1}{R_{web.db}} \right)} \tag{3.8}$$

- R_{bottom} = thermal resistance due to forced convection under the bottom plating

  and

- $T_{tk.top1}$ / $T_{tk.top2}$ = temperature above / below the tank top plating,

- T_{bp1} / T_{bp2} = temperature above / below the bottom plating,

1. Assume temperatures $T_{tk.top1}$, $T_{tk.top2}$, T_{bp1} and T_{bp2}. The latter two are closer to sea's temperature and the former two closer to that of the viscous oil layer.

2. Calculate the heat transfer coefficient and the thermal resistance of seawater flowing below the bottom plating. The procedure is similar with that described during calculations of the heat transfer coefficient of air flowing above the deck plating, page39, step no.8. This time, instead of wind, the medium causing forced convection is sea water, hence the relative velocity in respect to an inertial observer onboard the ship should be calculated accordingly.

3. Calculate the thermal conductivity of the viscous oil layer at a mean temperature of $T_f = (T_{ab.layer} + T_{tk.top1})/2$, where $T_{ab.layer}$ is given and $T_{tk.top1}$ is assumed in step 1.

4. Estimate the thermal resistance of viscous oil at the bottom of the tank, based on relevant assumption made for its thickness.

5. Calculate the thermal resistances of the tank top and bottom platings. For conduction, $R_{cond} = L/kA$. L is the thickness of the plate and k it's thermal conductivity, which is assumed equal to $52W/mK$,

6. Find the thermal conductivity of air trapped inside the double bottom area at the mean temperature of $T_{tk.top1}$ and T_{bp1}.

7. Compute the radiative htc for the double bottom area based on equation 3.3, where ϵ_1 and ϵ_2 are equal to 0.2

8. Calculate the the total thermal resistance of the web frames. As mentioned earlier, each cargo tank is supported by 7 web frames. The average thickness of the web frames was measured by the ship's miship section drawing and it was found to be equal to 16 mm.

9. Determine the equivalent thermal resistance inside the double bottom area, where for conduction, L=2.3m

10. Calculate the total thermal resistance of the bottom side by summing each individual resistance component,

11. Estimate the total amount of heat transferred towards the bottom of the ship $(Q_{tot.bot})$.

12. Calculate circuit's new intervening temperatures by equations:

$$
\begin{aligned}
T_{tk.top1} &= T_{ab.layer} - Q_{tot.bot}\ R_{v.oil} & \text{(3.9a)} \\
T_{tk.top2} &= T_{tk.top1} - Q_{tot.bot}\ R_{cond.} & \text{(3.9b)} \\
T_{bp.2} &= T_{sea} + Q_{tot.bot}\ R_{bottom} & \text{(3.9c)} \\
T_{bp.1} &= T_{bp.2} + Q_{tot.bot}\ R_{cond} & \text{(3.9d)}
\end{aligned}
$$

13. If the assumed temperatures of step 1, do not coincide with that of step 9, our calculations must be repeated, only this time, the new temperatures assumed during step 1 will be that calculated from equations 3.9a - 3.9d. This process is repeated until the assumed and calculated temperatures do not differ more than $0.1°C$.

Annotation

As approximately a third of the bottom surface area is covered by heating coils, we could possibly commence our calculations for the total heat transfer coefficient, from the heating coils surface temperature and proceed outwards towards the bottom. However that would mean that we will have to investigate the interaction between the two layers of heating coils. In addition to this, wall temperature of each heating coil varies along it's length as heat is transfered to the cargo; supposedly steam condensation has been completed and inside the exhaust tubes, condensate flows back to the engine room. Thus the overall temperature difference between the coil's external temperature and sea will continuously change, for every single part of the coil. Nevertheless, striving for that kind of precision would have an insignificant impact to the total heat loss, as there are two layers between the coils and sea that "resist" heat transfer; one is the viscous crude oil at the bottom of the tank, and the other is the double bottom area, where in both these spaces heat is transferred via conduction.

3.3.4 Adjacent Cargo Tanks

Looking at the arrangement of cargo tanks, we can understand that each cargo tank has at least one tank located forward or backwards, and surely one cargo tank located sideways. For cargo tanks located in the longitudinal direction of the ship, we assumed that the cargo height in all tanks is the same. Figure 3.4 illustrates two different loading conditions.
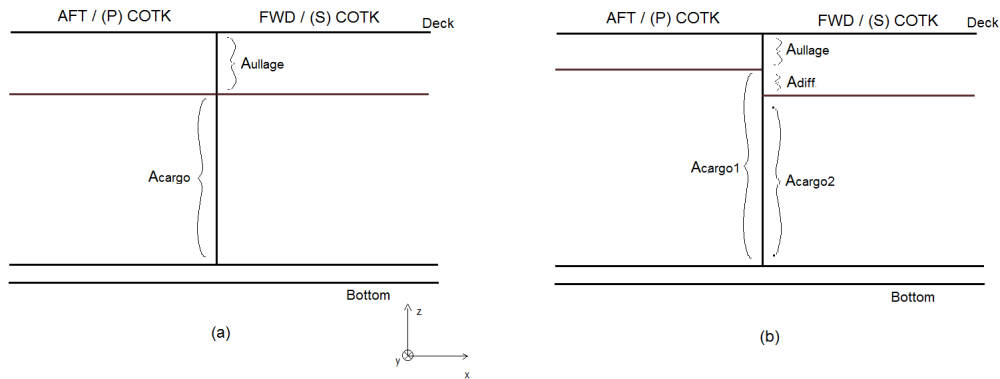
Figure 3.4: Loading conditions for adjacent cargo tanks

In Figure 3.4 (a), heat is transferred from the cargo of one tank to the other through area A_{cargo}. Someone might think that heat is also transferred, from cargo to the gas situates above it's free surface and from there towards the adjacent tanks. Heat transfer coefficients for laminar oil flow can fluctuate from 6-10 W/m^2K and extend to 25-30 W/m^2K for turbulent flows. However, for turbulent air flows in natural convection, the heat transfer coefficient rarely surpasses the value of 2-3 W/m^2K, mainly due to the large deficit in the air's Prandtl numbers compared with that of petroleum liquid products. A small heat transfer coefficient means that thermal resistance will have relatively large values, hence on both sides of the bulkhead, the resistances will be great enough to constrict heat transfer through the upper sections of the tanks surrounded by gas. Also heat, likewise electric current, chooses the path of lower resistance, consequently heat exchange through area A_{cargo} will be much greater than that of area A_{ullage}, which will be considered as insulated. This acceptance also enhances the foundations of our choice to neglect the effects of sidewalls during heat loss calculations through the ship's deck (see p.38). Similarly in

Fig.3.4 (b), heat transfer will be done primarily through area A_{cargo2} and again we assume that areas A_{ullage} and $A_{diff.}$ act as insulating layers. Nevertheless, the code was mainly developed to face situations like this of Figure3.4 (a) and provide a rough estimation for the interaction between tanks, as heat losses towards the environment are much greater compared to those among the cargo tanks.

In case (a) of Fig. 3.4, we have assumed that both tanks are equally filled. Heat is transferred from the hotter tank to the cooler via natural convection above a vertical plate of area $A_{cargo} = H_{cargo} \times B_{COTK}$. The breadth of the tank is taken to be equal to the half breadth of the ship, minus the width of the double hull area. The temperatures at either side of the bulkhead are initially unknown, however we know the bulk temperature of each tank, at the middle of the plate (in order to satisfy the requirement for uniform heat flux, see page 34). The equivalent thermal circuit is quite simple with three thermal resistances connected in series, as shown in page 106, Fig.E.5. $R_{conv.aft}$ and $R_{conv.fwd}$ are the thermal resistances due to natural convection in the aft and fore tanks respectively and R_{cond} is the conduction thermal resistance of the bulkhead wall between the tanks.

1. So let's consider two different temperatures on either side of the bulkhead, $T_{bhd.aft}$ and $T_{bhd.fwd}$. Obviously the temperature closer to the warmer tank will be elevated in comparison with the one towards the side of the cooler tank.

2. Calculate the properties of cargo at the film temperatures $Tfilm_{aft} = (T_{aft} + T_{bhd.aft})/2$ and $Tfilm_{fwd} = (T_{fwd} + T_{bhd.fwd})/2$

3. Calculate the Grashof and Rayleigh numbers to determine the type of flow in each side of the bulkhead.

4. Subject to the type of flow, calculate the relative heat transfer coefficient based on equations for natural convection over a vertical plate Eq. A.9-A.12, p.78.

5. Calculate equivalent thermal resistances adversarially of the bulkhead, as well as the thermal resistance of the bulkhead based on it's average thickness (measured from the Midhip Section) and a thermal conductivity equal to 52 W/mk. Finally the total thermal resistance is found by summing the component resistances

6. Find the total amount of heat exchanged between the tanks $Q_{tot.adj}$

7. Calculate temperatures $T_{bhd.aft}$ and $T_{bhd.fwd}$ by equations:

$$T_{bhd.aft} \quad = T_{aft} \pm Q_{tot.adj} \; R_{conv.aft} \tag{3.10a}$$
$$T_{bhd.fwd} \quad = T_{fwd} \mp Q_{tot.adj} \; R_{conv.fwd} \tag{3.10b}$$

As we study the amount of heat loss from a tank, possitive signs denote heat loss while negative signs for heat loss denote heat gains. For example, if an aft tank is cooler than a fwd tank, the temperature at the former's bulkhead ($T_{bhd.aft}$), will be higher than the bulk temperature of the cargo inside the same tank T_{aft}, hence plus sign should be used. Similarly, for the warmer tank, the bulkhead's temperature towards the colder tank will have a lower temperature than the bulk volume of the cargo, so minus sign is appropriate.

8. If temperatures of step 7 are different than those initially assumed in step 1, a new circle of calculations must commence, using as intervening temperatures those exported by equations 3.10a and 3.10b.

Clearly this process can be used for port and starboard tanks as well, by swaping T_{aft} and T_{fwd} with T_{port} and T_{stbd} respectively (see figure 3.4) and following the same procedure.

3.3.5 Overall Heat Losses

Finally we can calculate the total heat loss rate from each tank by the summation of all individual heat loss rates :

$$Q_{total} = Q_{tot.asl} + Q_{tot.bsl} + Q_{tot.deck} + Q_{tot.bot} + Q_{tot.adj}$$

where $Q_{tot.adj}$ stands for the total heat transfer rate from each tank to it's surrounding tanks, whether these are located aft, forward or at their sides.

Up until now we haven't addressed the effects of stochastic factors such as cargo sloshing due to the ship movements (mentioned in Ch.2.8 of the present thesis.), sea spraying etc. That wasn't done directly, but through four correction factors introduced to heat losses from the ship's deck, sides and bottom. For the topside and deck, that increase on heat losses was set to 15 %, while for the rate of heat transfer below sea level and towards the bottom, that correction factor was 20% and 30%. The final augmentation to total heat losses was estimated to be around 15 %.

3.4 Auxiliary Boiler Parameters

As mentioned earlier, the boiler's working pressure is 10 kg/cm^2 gauge. The formulas that we use to estimate the properties of steam are given as a function of absolute pressure in MPa. Conversion between the units is made based on the following equations:

$$
\begin{aligned}
P_{MPa} &= P_{kg/cm^2} \times 0.0980665 \\
P_{MPa.abs} &= P_{MPa.g} + 0.101325
\end{aligned}
$$

The fuel used in the marine boiler (MGO or HFO) and boiler's load are both variables given by the user during data input. Depending on this two parameters, we are able to calculate the amount of steam produced by the boiler and fuel consumption, based on performance curves provided by the boiler's maker [1]. However, these performance curves were given based on HFO. In order to determine fuel oil consumption when boilers are running on Marine Gas Oil (MGO), we made use of the boiler efficiency equation.

Boiler efficiency is considered as the ratio between the boiler's energy output to the boiler's energy input and can be expressed by the equation :

$$\eta_B = \frac{\dot{m}_s(h_s - h_f)}{\dot{m}_f H_u}$$

where :

- $\dot{m}_s$ = production of steam per hour [kg/h],

- $\dot{m}_f$ = fuel consumption per hour [kg/h],

- h_s = the specific enthalpy of steam, estimated at 16 kg/cm^2 which is the pressure at the boiler's outlet,

---

[1]See Appendix, pg.111

- h_f = the specific enthalpy of feedwater, estimated at 1 atm $\approx$ 1.03323 kg/cm^2 and $T = 60^oC$,

- H_u = the net calorific or lower heating value of fuel.

As boiler efficiency and steam production are only influenced by the boiler's working load and the specific enthalpies of steam and feedwater depend exclusively on pressure and pressure and temperature at the boiler's outlet and inlet respectively, we conclude on the following equation :

$$\dot{m}_{f_{MGO}} = \dot{m}_{f_{HFO}} \frac{H_{u_{HFO}}}{H_{u_{MGO}}}$$

For Heavy Fuel Oil (HFO), $H_{u_{(HFO)}}$ = 39550 kJ/kg, while for Marine Gas Oil (MGO), $H_{u_{(MGO)}}$ = 42700 kJ/kg.

3.5   Steam Pipeline on Weather Deck

In order to figure the amount of heat available for a tank's heating, we must first be aware of the steam condition at the entrance of each tank. Hence we must know the steam flow rate, steam quality and pressure at that point. It is evident that we must investigate the steam condensation along the ship's hull, as the only informations available initially are the steam properties at the engine room exit. There, dry saturated steam, that is, steam with a unity dryness fraction is provided on a pressure equal to 10 kg/cm^2g and a flow rate equal to that respective to the predetermined boiler load.

Our approach to this subject was to use a kind of finite element method, by dividing the total main steam pipeline length, into smaller elements having a finite length Δz. Commencing from the engine room's exit, main steam pipeline runs down along the ship's main deck, until the foremost cargo tanks. Steam distribution from the main pipeline to a pair of cargo tanks (out of the 6 total) is done by means of a flow-through branch, followed by a t-junction to divide the steam into the two tanks. All pipe lengths were measured based on the ship's general arrangement, while the pipeline's diameter, which gradually reduced, was taken based on the ship's hull piping arrangement drawing.

In order to assist the reader comprehend the calculation process more easily, as well as explain the issues that arise during such a calculation, let's try to estimate steam properties at the first flow-through branch, which feeds with cargo tanks no.6 and the slop tanks with steam .

For a predetermined boiler load, we can calculate steam output at the engine room exit, based on the boiler's performance curve. Steam pressure is considered to be 10 kg/cm^2g while steam's dryness fraction is equal to unity. As measured in the GA drawing, the first flow-through branch is located 6 meters ahead of the engine room exit. We divide the total length L=6m, into smaller finite lengths of pipe Δz. As $\Delta z \to 0$, the accuracy of our calculations is theoretically improved, at the expense of calculation time. We decided that a reasonable value for the increment's length on deck is 0.5 m, thus we have seperated the initial pipe length into 12 smaller pieces.

The pipeline's internal diameter D_{in}, external diameter D_{out} and entry quality $x_1 = 1$. The flow rate of steam is considered to be $\dot{m}_{steam}$ and the pressure at the pipe's entry is P_1. We look to determine the steam's quality x_2 and pressure P_2 at the pipe's exit. To do so, we first estimate the quality and pressure at the exit of the first pipe segment.
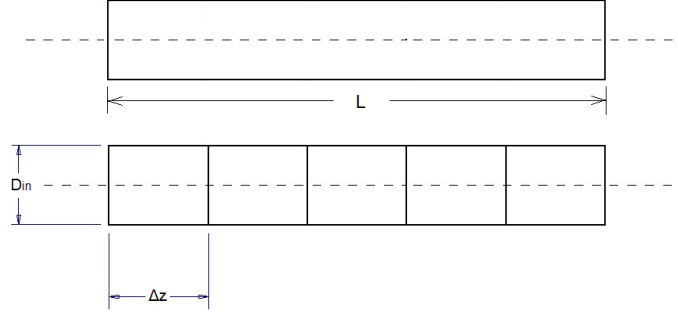
Figure 3.5: Pipeline Segmentation

Estimate steam quality x_2

1. Calculate the steam properties at the pipes entry for pressure P_1.

2. Assume a value for x2

3. Calculate the mid-quality magnitude x inside each pipe of length Δz, $x = \dfrac{x_1 + x_2}{2}$

4. Calculate the Reynolds number for condensate Re_l, the Martinelli parameter X_{tt} and function F_2 by equations of page 81

5. Calculate the heat transfer coefficient for steam (h_z) from equation A.32, p.81, assuming that it is uniform in the particular quality range $\Delta x = x_1 - x_2$.

6. Assume values for the internal and external temperature of the pipe ($T_{in.tube}$ and $T_{out.tube}$ respectively). Both of these temperatures should be comparable to that of saturation temperature calculated during step 1, as the pipeline is not insulated,

7. Determine the heat transfer coefficient over the pipeline h_{ext}

   From research to the available literature, no correlations were found for external forced convection over a circular cylinder while air flows from a random origin. However, external forced convection of a circular cylinder in cross flow (the axis of the cylinder is normal to the fluid motion) is largely investigated. More recently, Wiberg et al. [65] suggested correlation from experimental data acquired from the unexplored until then, phenomenon of heat transfer from a cylinder in axial flows. Thus, we concidered that the total heat transfer coefficient over the ship's pipeline will be the summation of the heat transfer coefficients in axial and in cross flow, plus the heat transfer coefficient due to radiation.

   Similarly to chapter page , we analyze the wind's speed into two component vectors, one parallel to the ship's main pipeline (V_x) and one perpendicular (V_y). Assuming θ to be the angle between velocity vectors $V_{ship.dir}$ and $V_{wind.dir}$, we get that:

$$\begin{aligned} \theta &= V_{wind.dir} - V_{ship.dir} \\ V_x &= V_{wind.dir}\ cos\theta \\ V_y &= V_{wind.dir}\ sin\theta \end{aligned}$$

   The ship's main pipeline, based on the inertial observer assumption, will face an axial and a cross flow of air equal to

$$\begin{aligned} V_{axial} &= |V_{ship} - V_x| \\ V_{cross} &= |V_y| \end{aligned}$$

while for the branches of the main pipeline, the flow regime would be the exact opposite. In order to find the heat transfer coefficient for the air flow above the pipe, we have to:

(a) Determine the orientation of the pipe, with respect to the ship's centerline. If the pipe is perpendicular to the centerline, then $V_{axial} = |V_y|$ and $V_{cross} = |V_{ship} - V_x|$, and vice versa if the pipe is parallel,

(b) Find the film temperature of the pipe, $T_{film} = (T_{out.tube} + T_{ambient})/2$,

(c) Calculate the air's thermal conductivity, kinematic viscosity and Prandtl number for the ambient and film temperature,

(d) Estimate the Reynolds number in respect to the axial and cross flow velocity,

(e) Determine the Nusselt number for axial and cross flow, based on the correlations proposed in pages 76 - 77, using each time the appropriate Reynolds number,

(f) Calculate the heat transfer coefficients for axial and cross flow respectively,

(g) Compute the radiative heat transfer coefficient based on equation 3.14. The emissivity ϵ of carbon steel is taken to be equal to 0.3. In order to calculate the radiative heat transfer coefficient we are going to transform equation **ref**, so as :

$$h_{rad} = \frac{\epsilon\sigma(T_{surface}{}^4 - T_\infty{}^4)}{(T_{surface} - T_\infty)} \tag{3.14}$$

(h) Find the total heat transfer coefficient above the pipe by equation 3.20

8. Calculate the thermal conductivity of carbon steel pipeline k_{pipe}

   The thermal conductivity of carbon steel equipped on deck is equal to 46 W/mK at 20 °C. However in reality the average temperature of the pipe is much higher, as steam flowing inside reaches 180 °C. The thermal conductivity of carbon steel pipes used in the above calculations was determined by a formula attached to the appendix, based on the arithmetic mean of the internal and external temperature of the pipe. This formula returns higher values for thermal conductivity k_{pipe} than the nominal value at 20 °C.

9. Calcuate the component resistances of the thermal circuit, as illustrated in page 106, Fig. E.6 .

   Note that for circular geometries :

$$R_{steam} = \frac{1}{h_z\pi\Delta z D_{in}} \tag{3.15a}$$

$$R_{cond} = \frac{log(D_{out}/D_{in})}{2\pi\Delta z k_{pipe}} \tag{3.15b}$$

$$R_{ext} = \frac{1}{h_{ext}\pi\Delta z D_{out}} \tag{3.15c}$$

10. Calculate the equivalent total thermal resistance $(R_{tot.})$ of pipe section Δz , the heat loss from the pipe (Q_{pipe}) and the amended external and internal temperatures of the pipe from equations:

$$Q_{pipe} = \frac{T_{sat} - T_{ambient}}{R_{tot.}}$$

$$T_{in.tube} = T_{sat} - Q_{pipe}R_{steam} \tag{3.16a}$$

$$T_{out.tube} = T_{in.tube} - Q_{pipe}R_{cond} \tag{3.16b}$$

11. From an energy balance at the length of the tube Δz, we can calculate the steam quality change Δx from equation

$$\Delta x = \frac{4 \ h_z \ \Delta T \ \Delta z}{D_{in}G \ h_{evap}} \tag{3.17}$$

where $\Delta T = T_{sat} - T_{in.tube}$.

12. From equation 3.17, we can calculate the steam quality at the pipe's exit x_2'. Obviously $x_2' \neq x_2$ assumed in step 2.

13. By replacing $x_2' \to x_2$, we repeat steps 2-12 until $x_2' \simeq x_2$ (precision was set to 10^{-8}, hence when $x_2' - x_2 < 0$ the program will exit the for loop)

Calculate pressure P_2

We calculate the pressure drop (ΔP) in length Δz by equation:

$$\Delta P = \frac{dP}{dz} \ \Delta z \Leftrightarrow P_2 = P_1 + \frac{dP}{dz} \ \Delta z \tag{3.18}$$

where $\frac{dP}{dz} < 0$ and is given by equations F.1-F.5. For horizontal tubes, Eq.F.4 is equal to zero , as it reflects pressure drop caused by gravitational field.

Then, we proceed to the next piece of equal increment Δz, where this time x_1 and P_1 which are the calculation outputs of the first segment are considered to be the entry for the second. The aforementioned calculation process is repeated numerous times and is the same for all intervening tube segments. Also, the external and internal temperatures of two consecutive increments should be comparable, thus during step 6 of the next piece, the assumed temperatures can be those calculated for the previous pipe segment and achieve convergence faster.

If at some point along the pipeline, a fitting, a valve or a bend is equipped, we use the equivalent length method in order to simulate the added pressure, as explained in page 107. If at the end of any investigated pipe length Δz a fitting is attached, Eq.3.18 is altered and the pressure at the exit of that fitting is given by

$$P_2 = P_1 + \frac{dP}{dz} \ (\Delta z + L_{equiv.}) \tag{3.19}$$

Another assumption that had to be made was that of steam quality at the exits of a tee branch. For example, let's assume that at the inlet of a tee junction, steam/condensate mixture flows with a flow rate of $\dot{m}_1$ and a dryness fraction x_1. As shown in Fig.3.6 , flow rates at the left and right branches will be $\dot{m}_2$ and $\dot{m}_3$ respectively.

From the law of mass conservation, $\dot{m}_1 = \dot{m}_2 + \dot{m}_3$, where we assume that the steam qualities remain constant, thus $x_1 = x_2 = x_3$. Practically that means that the amount of steam and condensate divide uniformly between the two branches.
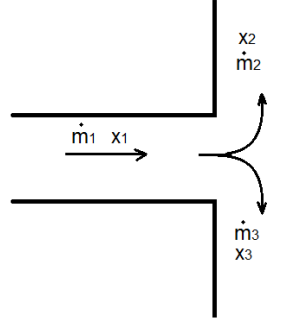
Figure 3.6: Flow inside a tee branch

3.5.1 Annotations

Steam Distribution to the Various Cargo Tanks

Another issue that we face with steam is that it's difficult to decide the amount of steam that will enter each tank, assuming that all valves are fully open. A network study similar to that done for incompressible fluids would be pointless, exactly because steam as a gas, is compressible. To solve this, we considered that the amount of steam flowing inside each tank is initially a function of a tank's volume, hence a larger tank loaded with more cargo would have larger heating demands and thus needs a higher steam flow rate. In that aspect, steam distribution to the various cargo tanks and along the deck's pipeline was determined a priori. After the completion of the program, if we deem that a tank is under excess or insufficient heating, we can reduce the steam flow rate by means of the globe valves equipped at the entrance of each tank.

Each tank has its own steam and exhaust valves, which enables steam flow rate to be shut off or reduced at will. Typically globe valves are used as the main steam feed valves and are placed at the entrance of each tank, followed by a number of angle valves, one for each heating coil. These angle valves allow the heating coil to shut down in case of damage, due to corrosion for example, in order avoid ingress of cargo in the condensate return line. Thus, simulation results for each tank, can also be carried out with less than four operating heating coils.

Effects of Neighbouring Tubes on Heat Transfer Coefficient Above Steam Pipeline

Finally we notice that in the literature, tubes were totally exposed to the flow and tests were carried out for a single isolated tube. Nonetheless the main steam supply pipe and its branches are located centrally on deck and are surrounded by other pipes, such as the inert gas pipe or the fuel oil pipe, the existence of which affects both the flow pattern around the tube and heat transfer characteristics. Generally, based on experiments carried out by Goel [59] on different amount of pipes and arrangements, for pipes of similar diameter, the turbulence generated by leading tube enhances heat transfer and this change is more significant at higher Reynolds number. Although tubes of similar diameter tend to enhance heat transfer, tubes of greater diameter tend to do the exact opposite, as the generated turbulent layer flows well above the boundaries of the under investigation tube.

Similarly, the axial flow above the pipeline is impeded by various objects and equipments on deck. Hence we understand that the true heat losses from the pipeline will be reduced, compared to those calculated based on correlations for isolated cylinders, because

of the presence of neighbouring tubes. Due to the lack of other data, we will assume that this reduction is equal to 20 percent, and thus the total heat transfer coefficient above the pipeline will be determined by equation :

$$h_{out.pipe} = \left[(h_{cross} + h_{axial}) \times 0.8\right] + h_{rad} \qquad (3.20)$$

3.6   Heating Coils

Before entering the tank, steam is distributed into four heating coils. The equipped heating coils are made out of an alloy of copper and aluminium. The reason for this is that the heating surfaces are subjected to excessive corrosion from the lighter fractions in the crude, and ordinary steel pipes would not stand up to the corrosive action. Before each heating coil, an angle valve is equipped so as to control the steam flow through the coil. Similarly to the assumption shown in 3.6, we consider the steam quality to be unchanged throughout the four heating coils entries. Steam mass flow is equally distributed between the active heating coils.

Heating coils run down the aft bulkhead and are initially surrounded by the gas mixture of inert gas, hydrocarbon and air mentioned in Ch.3.3.2. Energy dissipation from the heating coils towards the gas at the ullage space is not considered as cargo heating at that stage, although gas temperature might eventually increase. Cargo heating calculations begin when the coils submerge below the free surface of liquid cargo and stop immediately after coils re emerge above the surface.

Identically to steam deck pipeline, we divide each heating coil in increments of finite length, only this time, as we aim for a higher accuracy to our calculations, the increment is set to 0.1 m. Heating coil lengths were manually measured in all 14 tanks by the heating coil arrangement inside cargo and slop tanks drawing provided by Thenamaris Inc. The cargo's temperature varies linearly between measurement points, hence at any tank height, we can calculate the bulk temperature of cargo surrounding the heating coils ($T_{c,\infty}$). There are two occasions we have to investigate seperately; one is that of two-phase flow inside the coils and single phase flow. The calculation course is quite similar although some differences do exist

Two-phase flow

For a finite pipe length of 0.1 meters, we begin by calculating the bulk temperature of cargo at the height of reference. The under investigation pipe might be at some height on the aft bulkhead or it might be at the bottom of the tank. Nevertheless, at any height H measured from tank bottom, the temperature is given by the equation defined in Ch.3.2. Then:

1. Determine whether the heating coil is submerged in cargo or it is exposed to ullage space gas,

2. Determine the orientation of under investigation heating coil. This can be vertical to the ship's bottom plane or horizontal,

3. For steam-condensate mixture flowing inside the tube, calculate the following thermophysical properties based on entry pressure, P_1:

    (a) saturation temperature (T_{sat}),

    (b) density of steam and condensate,

    (c) condensate's specific heat,

    (d) condensate's thermal conductivity,

    (e) dynamic viscosity of steam and condensate,

    (f) enthalpy of evaporation,

4. Assume a temperature for the external surface of the coil, $T_{out.coil}$. That temperature should be closely related with that of saturation, found in step 3(a),

5. Calculate oil's thermophysical properties such as thermal conductivity, kinematic viscosity, thermal expansion coefficient and the Prandtl number, all accounted at the film temperature, $T_{film} = (T_{out.coil} + T_{c,\infty})/2$

6. Calculate the Grashof and Rayleigh numbers and determine the type of flow around the tube,

7. For vertically oriented tubes, check which condition between 2.3 and 2.4 is fulfilled.

8. Calculate the mean Nusselt number and heat transfer coefficient above the heating coil, $h_{c.ext}$.

   If the coil has a vertical orientation, equations A.12 of page 78 and A.26, A.27 of page 80 are to be used. The former is subject to whether conditions for the thermal boundary layers thickness, in the previous step are met.

9. Assume a value for x2

10. Calculate the mid-quality magnitude $x = \frac{x_1 + x_2}{2}$,

11. Calculate the Reynolds number for condensate Re_l, the Martinelli parameter X_{tt} and function F_2 by equations of page 81

12. Calculate the mean heat transfer coefficient (h_z)

   For steam flow inside vertical cylinders, this is done throug equations A.33 - A.34, p.81, while for steam flow inside horizontal tubes from equation A.32, p.81. It is noted that h_z is assumed to be uniform in each particular quality range Δx.

   Concerning the latter, the method discribed to the appendix agrees well with data, and according to [33], [64], we will assume that annular flow extends to the whole length of the pipeline, even for very low steam qualities, until the whole mass of steam is condensed. In reality that is not the case, as for low steam qualities, flow is not characterised by shear forces acting on the condensate layer but from gravitational forces and flow pattern is similar to that of slug or bubble flow.

13. Calculate the component resistances of the thermal circuit shown in figure E.6, only this time $h_{ext} \equiv h_{c.ext}$.

For the thermal conductivity of aluminum brass, we assumed that under temperature variations, it behaves similarly with regular brass. Table on the right illustrates the thermal conductivity curve of brass and other metals in respect to their temperature. We can see that the thermal conductivity of brass slightly increases with temperature. We conclude that it is safe to consider an approximate value of $k_{pipe} = 120W/mK$ for every temperature range.
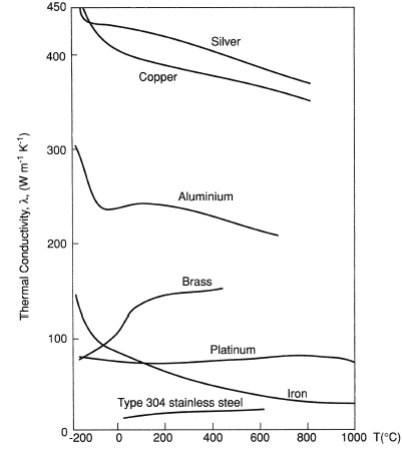
14. Calculate the equivalent total thermal resistance of this coil section ($R_{tot.coil}$), the heat loss from the pipe (Q_{coil}) and the external and internal temperatures from equations:

$$Q_{coil} = \frac{T_{sat} - T_{c,\infty}}{R_{tot.coil}}$$

$$T_{in.coil} = T_{sat} - Q_{coil} \cdot R_{steam} \tag{3.21a}$$
$$T_{out.coil} = T_{in.coil} - Q_{coil} \cdot R_{cond} \tag{3.21b}$$

15. From an energy balance, we can calculate the steam quality change Δx from equation

$$\Delta x = \frac{4 \ h_z \ \Delta T \ \Delta z}{D_{in} G \ h_{evap}} \tag{3.22}$$

where $\Delta T = T_{sat} - T_{in.coil}$.

16. From equation 3.22, we can find the steam quality at the coil's exit x_2'. Obviously x_2' will be different than the steam quality assumed during step 9,

17. For the new steam quality x_2' and the external wall temperature $T_{out.coil}$ calculated in step 14, repeat steps 4-16 until $x_2' \simeq x_2$.

Q_{pipe} is the amount of heat rate transfered to the cargo, due to steam condensation inside the finite dimension's coil. If coil is not surrounded by oil, this amount of heat transfers to the gas mixture occupying ullage space.

Pressure drop (ΔP) in a finite length $\Delta z = 0.1$ can be calculated by equations F.2 - F.5, so

$$\Delta P = \frac{dP}{dz} \ \Delta z \Leftrightarrow P_2 = P_1 + \frac{dP}{dz} \ \Delta z$$

where

$$\frac{dP}{dz} = \left(\frac{dP}{dz}\right)_f + \left(\frac{dP}{dz}\right)_m + \left(\frac{dP}{dz}\right)_g < 0$$

By the heating coils arrangement inside the cargo tanks, we figure that steam supply line equips 40 DN tubes, which means that $D_{out} = 44.5mm$ and $D_{in} = 39.5mm$. Also, various heating coil bends have the same radius, which is equal to 145 mm. In order to determine the equivalent length of each bend, we advised the tables attached to the appendix. In page 121, for smooth bend elbows and a nominal pipe diameter of 40 DN, equivalent lengths are given to be 1.2 and 0.8 meters for standard 90° and for 90° long radius bends. That is for a radius to pipe diameter ratio (r/d) equal to 1 and 1.5 respectively.

In our case, $r/d = 145/40 = 3.671$, which is way above the available data. By examining data available on that table, and by the way equivalent length varies with r/d, we concluded that the equivalent length would be somewhere in the region of 0.4-0.6 meters. By Crane and Co. 118 we get that for a ratio equal to 3, resistance coefficient K is $12f_T$, while for a ratio of 4, $K = 14f_T$. By linear interpolation, we derive that K=13.342 f_T, where f_T is given in page 115 for a 40 mm inside pipe diameter to be 0.021. Then, based on equation F.12, p.109 we have

$$\frac{L}{D} = K \Rightarrow L_{eq} = 13.342 \times 0.04 = 0.534m$$

Correspondingly to the previous chapter, the pressure after a bend would be given by equation 3.19. Consider the arrangement of Fig. 3.7 and assume that we investigate heat transfer from tube element (1)-(1'). Then, P_1 is the pressure at the inlet of the tube and dP/dz the pressure drop calculated at the increment (1)-(1').
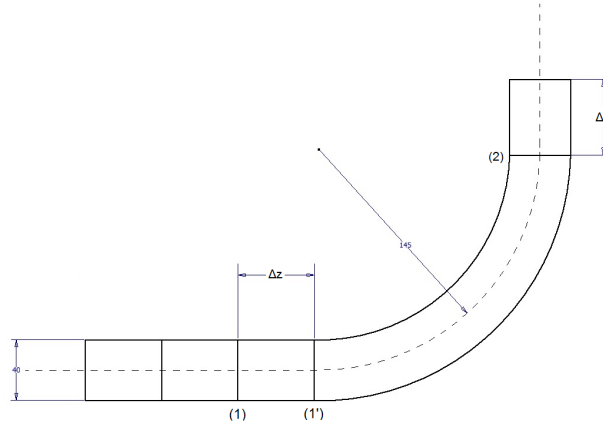
Figure 3.7: Pressure drop in a bend fitting

Single-phase flow

At some point, steam will fully condense and will be replaced by superheated water. The temperature at this point is equal to that of saturation, so heat is still stored in that amount of water. As it flows inside the coils, temperature will drop and heat will be transfered to cargo. To investigate this occasion we follow the following procedure for each increment of length $\Delta z = 0.1m$:

1. Determine whether the heating coil is submerged in cargo or it is exposed to ullage space gas,

2. Determine the orientation of under investigation heating coil. This can be vertical to the ship's bottom plane or horizontal,

3. Calculate condensate's thermophysical properties based on temperature T_1 and pressure P_1 at the coil's entry

4. From the principle of mass conservation, mass flow rate inside the coil will be the same with that of steam at the top of the tank, since no steam/condensate leakage occurs. Hence, we are able to estimate the velocity of condensate at point (1) by equation:

$$v_{cond.1} = \frac{\dot{m}_{coil}}{A\rho_1}$$

   where A is the cross section area of the coil and ρ_1 the density at position 1,

5. Determine whether the flow is laminar or turbulent by calculating the Reynolds number by Eq.2.6, pg.26.

6. Estimate the Darcy friction factor f for the corresponding flow from equations F.8-F.10,

7. Calculate the Nusselt number by equations A.35-A.37

8. Compute the heat transfer coefficient for the internal flow h_{in},

9. Find the oil thermophysical properties at the film temperature $T_{film} = (T_{out.coil} + T_{c,\infty})/2$, where $T_{out.coil}$ the external temperature of the coil at point (1)

10. Compute the Grashof and Rayleigh numbers, in order to determine the nature of flow around the heating coil,

11. For vertically oriented tubes, check which condition between 2.3 and 2.4 is fulfilled.

12. Calculate the mean Nusselt number around the tube, from equations A.35-A.37 pg.82 and then the mean heat transfer coefficient h_{ext}.

    If the coil has a vertical orientation, equations A.12 of page 78 and A.26, A.27 of page 80 are to be used. The former is subject to whether conditions for the thermal boundary layers thickness, as described in the previous steps are met.

13. Calculate all relevant thermal resistances from equations 3.15a-3.15c, only this time h_z is subtituted with h_{in} of step 8,

14. Find the total thermal resistance for the condensate flow, $R_{tot.cond}$

15. Estimate the amount of heat transferred to cargo from equation

$$Q_{cond} = \frac{T_1 - T_{c,\infty}}{R_{tot.cond}}$$

16. From the conservation of energy equation 2.9, $Q_{cond} = mc_v\Delta T$. Thus we can estimate the condensate's temperature at position (2), T_2.

    In order to determine the fluids properties at position (2), we also have to know the pressure P_2 at that location. However, a direct application of Bernoulli's equation wouldn't be convenient, as heat transfer takes place. In addition to this, condensate's density increases as temperature drops, thus $\rho_2 \neq \rho_1$. From mass conservation law, between two consecutive cross sections of the tube :

$$\dot{m}_1 = \dot{m}_2 \iff v_1\rho_1 A = v_2\rho_2 A \iff v_1\rho_1 = v_2\rho_2$$

    Hence, it is evident that while $\rho_2 > \rho_1$ then $v_2 < v_1$.

17. Assume magnitudes for density and velocity at the coil's exit $v_{cond.2}$, ρ_2

18. Estimate the average density of condensate flowing through the finite element, $\rho = (\rho_1 + \rho_2)/2$,

19. Use the extended Bernoulli equation Eq.F.6 for the mean value ρ calculated above,

$$\frac{u^2_{cond.1}}{2g} + \frac{P_1}{\rho g} + z_1 = \frac{u^2_{cond.2}}{2g} + \frac{P_2}{\rho g} + z_2 + H_{tot} \Leftrightarrow$$

$$P_2 = P_1 + \frac{\rho}{2}(u^2_{cond.1} - u^2_{cond.2}) + \rho g(z_1 - z_2) - \rho g H_{tot}$$

where

$$H_{tot} = h_L + h_B = f\frac{L}{D}\frac{u^2}{2g} + K_b\frac{u^2}{2g}$$

For horizontal tubes, $z_1 - z_2 = 0$, while for vertical tubes, $z_1 - z_2 > 0$ for downflow and $z_1 - z_2 < 0$ for upflow. Friction factor f was calculated during step 6 and $h_B = 0$ if we refer to a straight pipe. Nevertheless, if a bend follows position (2), $h_B \neq 0$ and K_b is given by equation F.15, pg.110 where:

- n is the number of 90 degree bends, i.e. a 180 degrees return bends consists of two 90 degree bends, thus $n = 2$

- $f_T = 0.021$, is the turbulent friction factor as given at table in pg. 115 for a nominal pipe diameter of 40mm.

- K_1 is the resistance for a single bend. Values for K_1 are given in pg. 118 for various ratio of bend radious (r) to pipe internal diameter(d). By linear interpolation for $r/d = 3.671$, $K_1 = 13.342 \times f_T = 0.2802$

20. Using P_2, T_2, calculate the condensate's density at position (2), ρ'_2

21. For the flow inside the coil of finite length Δz, we know from the conservation of mass that:

$$u'_{cond.2} \times \rho'_2 = u_{cond.1} \times \rho_1 \Leftrightarrow u'_{cond.2} = \frac{u_{cond.1} \times \rho_1}{\rho'_2}$$

22. If $u'_{cond.2} \neq u_{cond.2}$ and $\rho'_2 \neq \rho_2$ inferred during step 17, we repeat steps 17-21 until convergence for velocity and density is achieved.

It is important to highlight that in the aforementioned process, properties of condensate used in heat transfer calculations where based on the thermophysical properties of condensate at position (1) and not on the average properties over the entire pipe length Δz. However, we assumed Δz to be small enough, so as condensate properties between points (1) and (2) can be considered relatively constant. Summing the values of Q_{coil} and Q_{cond} estimated from each finite element of heating coil, we calculate the total rate of heat transferred towards the cargo Q_{in}.

Furthermore, the use of Bernoulli equation is *prohibited* in cases where the under investigation flow is compressible and heat transfer takes place. However, calculations of condensate temperature at the cargo tanks exit, showed good agreement with data provided by the ship's constructor. As stated at the hull and piping diagram of the

ship, condensate's temperature at the cargo tanks exit is approximately $100°C$, while our estimations returned values of $85-90°C$. This pressure drop study for the single phase flow was carried out for completeness purposes. An alternative method, would be to estimate the amount of heat transferred by the condensate by equation $Q = mc_v(T_{cond.} - T_{exit})$, where $T_{cond.}$ is the saturation temperature at the point where the dryness fraction becomes zero, and T_{exit} is the condensate's temperature at the tank's exit, as given by the ship's constructor.

3.7   Cargo Temperature Estimation

The net rate of heat flow from or to the cargo tank system can be determined by equation:

$$\dot{Q}_{net} = \dot{Q}_{in} - \dot{Q}_{tot.loss}$$

where $\dot{Q}_{in}$ represents the rate of heat flow from the ship's heating coils towards the transported cargo and $\dot{Q}_{tot.loss}$ is the rate of heat flow from the cargo to it's surroundings. If auxiliary boilers are not operating, then obviously $\dot{Q}_{in} = 0$ and there is no heat provision to the transported cargo.

As heat rate is measured in Watts, the question arises on how we will be able to estimate cargo temperature on a daily basis. If we simply multiply $\dot{Q}_{net}$ with the desired time interval (i.e. for a daily prediction, $24h \times 3600\frac{sec}{h} = 86400sec.$), we will be led to a faulty prediction for cargo temperature. That is because, as cargo temperature is reduced (or increased), the rate of heat transfer provided to the system is increased (or reduced) respectively, as the temperature difference between the main heat source, which is the steam flowing inside the heating coils, and cargo is increased (reduced). Similarly for heat losses, while cargo temperature decreases, rates of heat transfer will also begin to drop, as cargo temperature tends to achieve equilibrium with its surroundings, and vice versa if cargo temperature increases.

To compensate for that dynamic instability into our steady-state system, we decided to estimate the amount of energy offered and subtracted from the cargo tanks on an hourly basis, thus getting an hourly prediction. Then average temperature variation in each tank, can be determined through equation :

$$Q_{net} = mc_p\Delta T \Leftrightarrow \Delta T = \frac{Q_{net}}{mc_p} = \frac{\dot{Q}_{net}}{mc_p} \times 3600 \tag{3.23}$$

Daily temperature predictions are achieved through continuous repetitions. That means that for a daily temperature estimation, the code should run 24 consecutive times. That was achieved through a for loop statement. Apparently, the smaller the time interval of our calculations, the better the aqcuired results accuracy will be. However, that superior precision would be achieved through sacrificing calculation time.

Furthermore, heat losses are strongly connected to weather conditions, so in order to obtain an accurate prediction for the cargo's temperature, we also need a trustworthy weather forecast. As a rough approximation, we could pressume stable weather conditions throughout the whole day. However, better results will be acquired if during data input, we insert the average temperature of the under investigation date and the next, provided by the weather forecast.

Chapter 4

Results Presentation

4.1 Introduction

Previous chapters discussed the theoretical background behind the generated matlab code and presented a brief overview on it's development by demonstrating reasoning of the calculation process. This chapter aims to validate the constructed model, by comparing it with two different case studies of two sister vessels. Data source for these two case studies were the ship's noon reports and heating logs, provided by the ship's operator, maritime company Thenamaris Inc. The results are presented in form of comparative diagrams between the program's predictions and available data. Accuracy at which the developed Matlab code can predict given data, under the same conditions and restrictions, is expressed in the form of an average percentage error. Finally, for the first case study, where cargo is heated up to a specific temperature, an attempt is made to suggest an optimum heating procedure and assess any potential financial benefits.

4.2 Model Validation

4.2.1 Applicable Data

Data Handling

In order to validate the constructed model, we made use of heating logs and noon reports provided by the company for two different voyages. Heat logs include informations such as date, sea and ambient temperature, fuel oil consumption, type of fuel oil used and the average temperature of the cargo oil tanks both including and excluding the Slop tanks. Noon reports include all other information like ship's draft, vessel status, vessel's speed (recorded by GPS and speedlog), hull course, seacurrent speed and absolute direction, wind relevant speed and relevant directions and finally running hours and daily fuel oil consumptions by the auxiliary boilers. In order for Matlab to be able to read all the aforementioned informations during data input, a single excel file had to be constructed.

With some data manipulation, we managed to correlate data between heating logs and noon reports, in order for each reported value in the heating logs to correspond to those mentioned in the noon reports.

Data Filtering and Selection

At this point, it should be noted that available data are a product of measurements taken by the ship's crew, in not so favorable conditions. The human factor greatly influences data at hand. As we will see later on, some measurements can be trusted more than

others. In order to determine which sets of data are untrustworthy, we used the following procedure to estimate steam demands to compensate for heat losses from the cargo tanks during the ship's voyage.
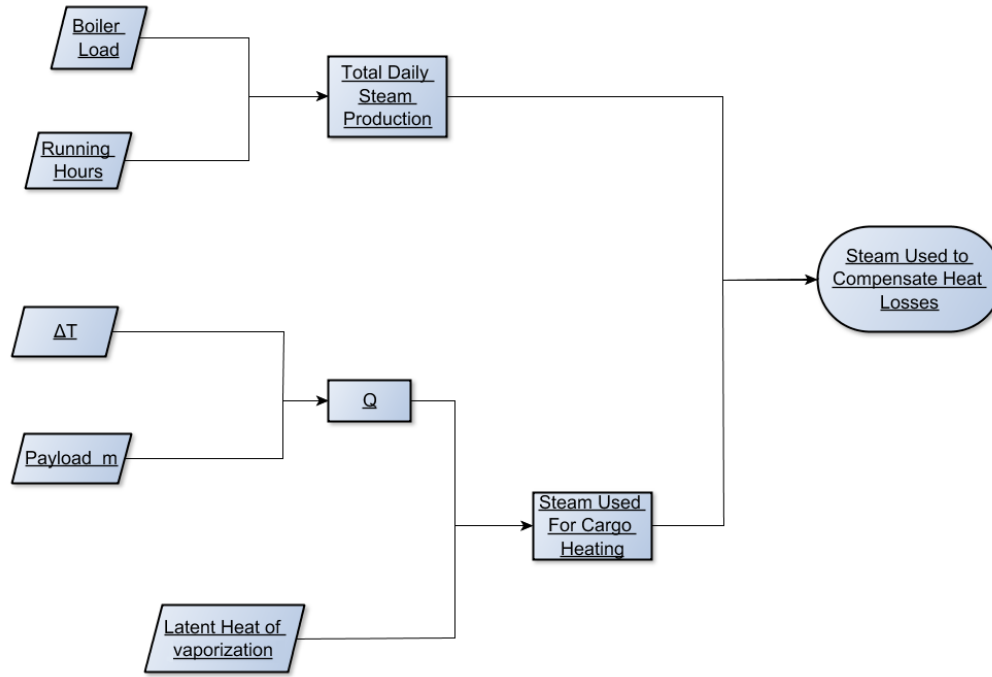
Figure 4.1: Data Filtering Flow Chart

From the applicable data, we are aware of the daily cargo temperature variation (ΔT), as well as the total amount of transferred cargo (Payload m). The amount of energy which caused that alteration in temperature, can be estimated through equation Eq.3.23, pg.57. That energy is provided predominantly by steam condensation inside the heating coils, during which the latent heat of vaporization is emitted. Hence if we divide the requested amount of energy to cause an alteration ΔT in cargo temperature, to steam's latent heat of vaporization, we will conclude to the total mass of condensed steam. Furthermore, as we are aware of the boiler's daily fuel oil consumption and operating hours, we can determine the boiler's load (assumed to be constant throughout the day) and thus the total daily steam production by the boiler. By subtracting from the total steam production, the amount of steam needed to cause temperature change of ΔT, we are left with the total amount of steam condensed to compensate heat losses towards the environment.

The first case study investigates the occasion of initial heating and then maintaining cargo temperature. The second case study solely investigates the occasion of maintaining cargo temperature. Thus, in the first case, steam consumption to compensate for heat losses is anticipated to increase periodically, as cargo temperature rises and so does the overall temperature difference between cargo and ambient temperatures. Furthermore, in the second case, as cargo temperature is maintained constant, steam consumption is expected to be rather stable and only vary due to the effects of stochastic factors that we haven't include in our calculations, such as solar radiation, cargo sloshing, sea spraying etc.

4.2.2   Case Study No 1

Parameters for the first case study are illustrated in Table 4.1. First of all, we must determine an acceptable value for the kinematic viscosity of the transferred cargo. To achieve that, we rely predominantly on it's density, as liquids with higher density tend to be more viscous.

Duration	16	Days
Loaded Cargo	Diluted Crude Oil	
Cargo Density	960	kg/m^3
Cargo Kin. Viscosity	Not Given	
COTK Fill Ratio	61.8	%
Ship's Draft (T)	11.2	m
Loaded Cargo Temperature	48.5	^oC
Requested Discharge Temperature	60	^oC
Charterer's Requirement	Heat Up & Maintain	

Table 4.1: Case Study No.1 Parameters

Then, we have to change the format of the data provided by the company[1]. Cargo temperature, which is reported in the heating logs, was measured daily at 16:00 pm. On the other hand, noon reports are reported at more frequent intervals (i.e. when the vessel departs port, berths, commences purging procedures, switches fuel etc.). Hence, noon reports should be adjusted in respect of time, to reflect the correct consumption on regular intervals. This amended excel table, will pose the basic data input source for the simulation code and can be found in page 93. In this case study, agreement between the data reported in the noon reports and those reported in the heating logs were satisfactory.

Loaded Cargo

Diluted Crude Oils are crude oil blends primarily consisted of heavy crude oil mixed with other lighter distillate fractions, the so called diluents. Crude oils are classified as light, heavy or extra heavy based on different physical properties, the most common of which is API gravity. According to worldwide definition, an API gravity ranging from 10° to 20° marks a crude oil as heavy. In addition, heavy crude oil reach values of kinematic viscosity which can even raise to 10000 cSt at 20^oC. Without reducing the viscosity, the transportation of heavy crude oil can be quite costly, which is due to the high energy demands required to handle the high pressure drop in pipelines.

In order to assure the transportation of crude oils is possible, we mix the initial heavy crude oil with diluents, in order to reduce their viscosity. The most commonly used diluents are natural gas condensates, naptha, kerosene, n-heptane and toluene. Specifically toluene and n-heptane are light hydrocarbons with extremely low viscosities, hence only a small amount is needed (in %wt) in order to reduce the blends viscosity drastically. Dehaghani and Badizad (2016) [60] tested two different diluted crude oils and calculated their viscosity with different solvents at various temperatures ranging from $20 - 40^oC$. They concluded that the final diluted crude oil viscosity is strongly depended upon the used solvent and it's concentration inside the blend.

As we are unaware of the cargo's solvent and concentration, we understand that we are unable to determine the exact loaded cargo viscosity. To tackle this problem, we decided to use three different types of diluted crude oils, with similar API gravities of 16°. The tested cargoes are illustrated below :

---

[1] Heating Logs and Noon Reports for case study No.1 can be found in pages 91-92.

1. Diluted Crude Oil (DCO) with Toluene Solvent of 4%wt.

   Toluene achieves to effectively reduce oil viscosity in a similar trend to n-heptane, in spite of being of slightly higher viscosity. With 4% wt content, at 20°C the DCO viscosity is 1490 cp $\approx$ 1555 cSt, while at 40°C that figure drops to 407 cp $\approx$ 390 cSt $(v_{50°C} = 220cSt)$[1].

2. Diluted Crude Oil (DCO) with n-Heptane Solvent of 4%wt.

   This is a blend of a heavy oil and n-Heptane, a light solvent with quite low kinematic viscosity which manages to reduce viscosity mixture asymptotically towards n-heptane viscosity (0.397 cp at 25°C). With 4% wt content, at 20°C the DCO viscosity is 1843 cSt, while at 40°C that figure drops to 550 cSt $(v_{50°C} = 378cSt)$. The purpose of using that oil was to cover the spectrum of heavy crude oil blends, with similar viscosities to HFO 380 .

3. Diluted Crude Oil (DCO) with Naptha Solvent of 4%wt.

   Naptha is not as effective as toluene or n-heptane in reducing viscosity because it is a petroleum fraction of fairly high API gravity composed mainly of paraffinic components. At 20°C the dco viscosity is equal to 6200cSt, while at 40°C that figure drops to 1230 cSt. $(v_{50°C} = 507cSt)$.

Temperature Data Verification

Average cargo temperatures were taken by the ship's heating logs. Daily fuel oil consumption were acquired by the ship's time adjusted noon reports. Both are presented below in the form of a graph :
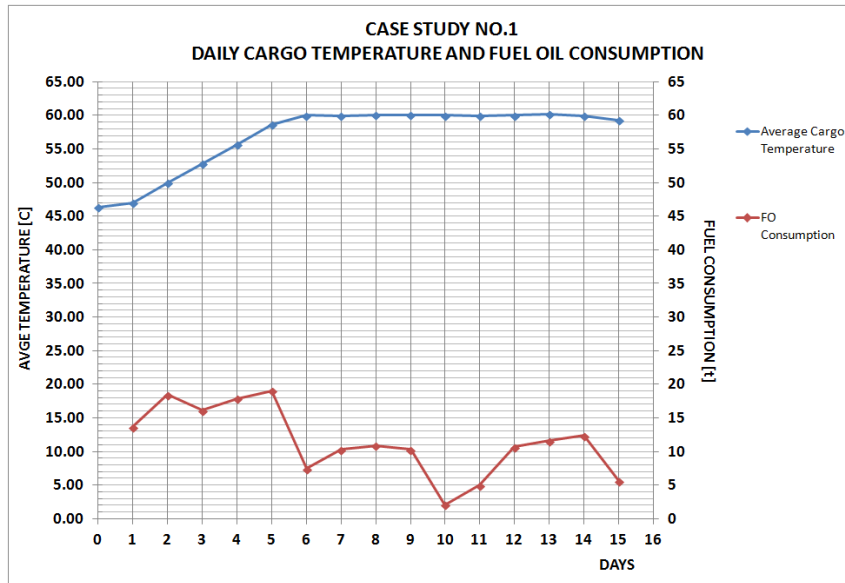
Figure 4.2: Case No.1 - Daily Average Temperatures and Fuel Consumptions

By investigating the available data for cargo temperature and fuel consumption shown in Fig.4.2, we can perceive that data points for days number 6, 10, 11 can be considered dubious. That is because, although fuel oil consumption is reduced significantly, the expected temperature drop does not occur. For example, fuel consumption during day number 5 is around 19 MT, while at day 6, that figure drops to approximately 7.5 MT

---

[1]Calculated according to Walther's Law, $loglog(\nu + 0.7) = A + BlogT$

of fuel (60 % reduction). However, average cargo temperature for day number 6 is elevated compared to that of day number 5, which is not consistent to the aforementioned statement.

To verify our claims, we used the method described in the flow chart of Fig. 4.1, aiming to acquire an approximate estimation of the total amount of steam used to compensate for heat losses. We anticipate steam consumption to remain rather constant or increase slightly until day 5 of the voyage, as up until then, the vessel remains docked in the harbor and cargo is heated. From days 6 to 12, heat losses and thus steam demands for cargo keeping should rise as the ship sails towards its final destination. Finally, for days 12 to 15, estimated data should show some consistency and steam demands should be higher than those at the earlier stages of the voyage. That is due to the fact that cargo inside the tanks is at a comparatively elevated temperature, besides ambient temperatures which are also lower.

Figure Fig.4.3 illustrates our estimations for the daily steam consumption to compensate for heat losses. For our calculations we used:

a) crude oil specific heat capacity $c_p = 1.8$ kJ/kgK,

b) total cargo mass $m = 68746.8$ t, which corresponds to the given cargo tank fill ratio of 61.8%,

c) steam latent heat of vaporization $\Delta h = 2000$ kJ/kg, estimated at a mean absolute pressure of 0.9 MPa.
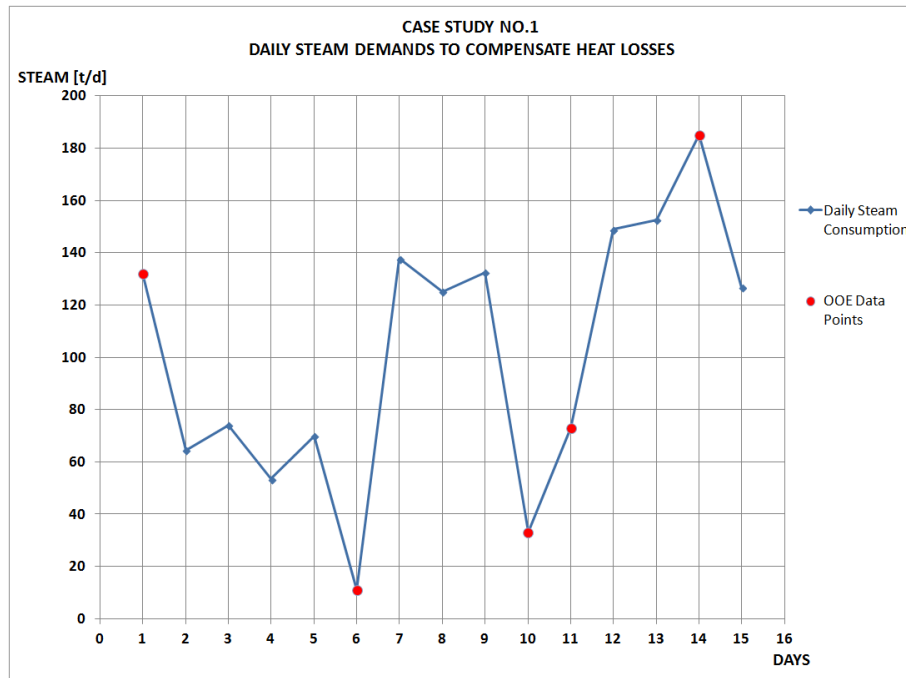
Figure 4.3: Case No.1 - Estimation for daily steam consumption used to compensate heat losses

Indeed, data points for days 6, 10 and 11 are not consistent with steam consumption trend of the previous days, and along with data points of days 1 and 14 can be characterized as outliers. For the given boiler operation parameters, steam consumption to compensate heat losses should be higher for days 6,10 and 11, which means that the amount of steam available for cargo heating should be reduced respectively. Flowing in the

opposite direction of the flow diagram in Fig.4.1, it is easy to understand that ΔT should be lower than that reported, and thus at each of the aforementioned dates, a temperature drop should occur.

Using the same reasoning, we can assess that cargo temperature for days number 1 and 15 should be higher than that reported in the heating logs, as the respective total steam production is considerably increased. Steam demands for cargo temperature keeping are correctly elevated during the second time the vessel enters port (days 13-15) compared to days 1-5, as ambient temperature dropped around 9 °C, as well as cargo temperature has increased by approximately 12 °C.

Simulation Results

Simulation results for the three different diluted crude oils mentioned in section 4.2.2 are presented below. Percentage error lines are fitted to the heating log data points, spanning to ±2%. Data points which are out of expectation (OOE data points), according to Fig.4.3 are marked in yellow. In general, the results of the present thesis model were satisfying. As we can observe, there is a pattern match in the various figures. The assumption that data points for days 6, 10 and 11 should indicate a lower temperature, is confirmed by the simulation results.
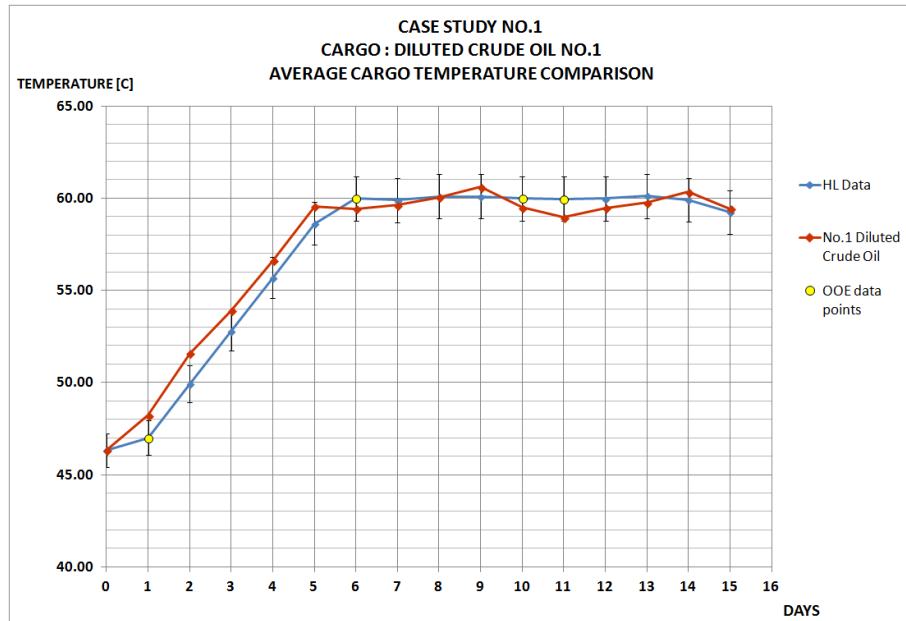
Figure 4.4: Case No.1 - DCO No.1 - Average Cargo Temperature Estimation

Diluted Crude Oil with Toluene Solvent of 4 % wt, appears to best fit the reported data. In addition, final temperature during day 15 appears to be almost identical. Average percentage errors throughout the voyage for all three simulations are given in the following table:

Finally, the fact that we used cargoes of different viscosities, gave us the opportunity to compare their behavior under the same heating input. We can observe that, as cargo viscosity rises, slightly higher average temperatures are achieved. This happens predominantly because more viscous cargoes tend to have lower heat transfer coefficients, since transition to turbulence is impeded by viscous forces developed within the transfered cargo and agitation occurs in a slower manner, thus heat transfer rates to the outer side shell
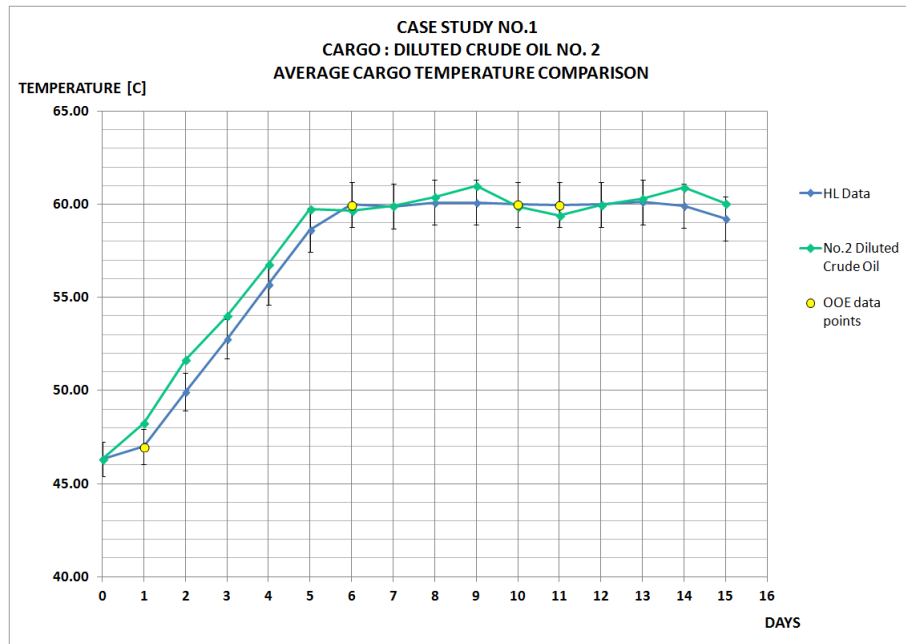
Figure 4.5: Case No.1 - DCO No.2 - Average Cargo Temperature Estimation
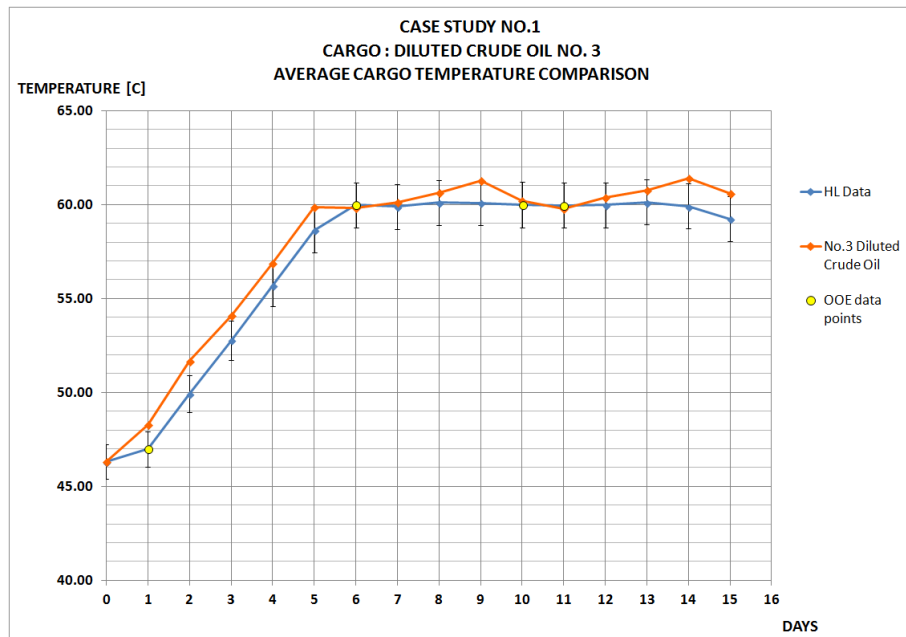
Figure 4.6: Case No.1 - DCO No.3 - Average Cargo Temperature Estimation

are reduced. As shown in the simulation results table included in the appendix[2], fuel oil consumption is almost equivalent between data and simulation.

Furthermore, it's plausible that during day number 1, a portion of the total amount of steam produced by the auxiliary boilers, is consumed in bringing the pipework up to operating temperature, something that we didn't include in our calculations. If we had, the estimated average cargo temperature emerging from the simulation results would be lower, thus being closer to the curve of the reported average cargo temperature. Furthermore, this would also affect the rest data points, resulting in an overall decrease to the divergence

[2]see page94

Crude Oil	Average Percentage Error
DCO No.1	1.17 %
DCO No.2	1.21 %
DCO No.3	1.48 %

Table 4.2: Case Study No.1 - Average Percentage Error

between the two curves.

4.2.3   Case Study No 2

Parameters for the second case study are illustrated below :

Duration	23	Days
Loaded Cargo	Fuel Oil	
Cargo Density	990	kg/m^3
Cargo Kin. Viscosity	Not Given	
COTK Fill Ratio	54.6	%
Draft (T)	14.65	m
Loaded Cargo Temperature	54.7	^oC
Requested Discharge Temperature	54.7	^oC
Charterer's Requirement	Maintain Loading Temperature	

Table 4.3: Case Study No.2 Parameters

Again, the kinematic viscosity of the loaded cargo is not given. Based on its relatively high density and elevated transportation temperature, we can assume that we refer to a quite viscous fuel oil. For this case study, we are going to assume that the loaded cargo is heavy marine fuel oil HFO 380, as it is the most widely used marine fuel at the present time.

Data Handling

Comparing provided data of case study No.2, a large discrepancy was observed between the fuel oil consumptions reported in the heating logs, and of those stated in the noon reports. For large periods of time, noon reports express null values for fuel consumption and auxiliary boilers were not operating. On the contrary, for the same time interval, heating logs state that fuel oil consumption is non - zero and that, for the biggest part of the voyage, consumption remains rather constant. The results of that fuel consumption is the average cargo temperature to remain fairly stable as well. The later would be impossible if auxiliary boilers weren't operating, as heat losses towards the environment will emanate reduced cargo temperatures.

Conclusively, we understand that we cannot rely solely on the noon reports for our estimations. The instruction we got from the company was to assume that boilers operate at the optimum boiler load (50 %) for days where fuel consumption is reported to be zero in the noon reports. Hence, we can estimate the daily boiler running hours by dividing the respective daily fuel consumption stated in the heating logs by the hourly fuel oil consumption given by the boiler's performance curve. For the remaining data points, we used the consumption values stated in the noon reports.

Temperature Data Verification

Daily fuel oil consumption were compared between the ship's heating logs and noon reports[3]. Fuel oil consumption from the noon reports have been altered slightly, as measurements between the two were not held at the same time or at the same intervals. Thus, noon reports consumptions were modified to illustrate fuel oil consumption per day, by means of an average hourly consumption. That is if we assume that the boiler's operate under constant load, steady state conditions and that the pipework is already brought up to operating temperature, so warm up load can be neglected.

Fig.4.7 shows how large discrepancy between fuel consumption reported in the noon reports (represented by the green line) and fuel consumption reported in the heating logs is (represented by the red line). As the chart demonstrates, heating log data are by far more fitting if we aim to maintain cargo temperature constant. Noon reports consumption present profound inconsistencies, which will result in intense fluctuations to the average cargo temperature. Nonetheless, summation of fuel oil consumptions throughout the voyage, results in approximately the same figures, both for noon reports and heating logs. So we can understand that noon reports were reported over longer intervals, but included the aggregate amount of burned fuel, which was correctly reported in the heating logs.
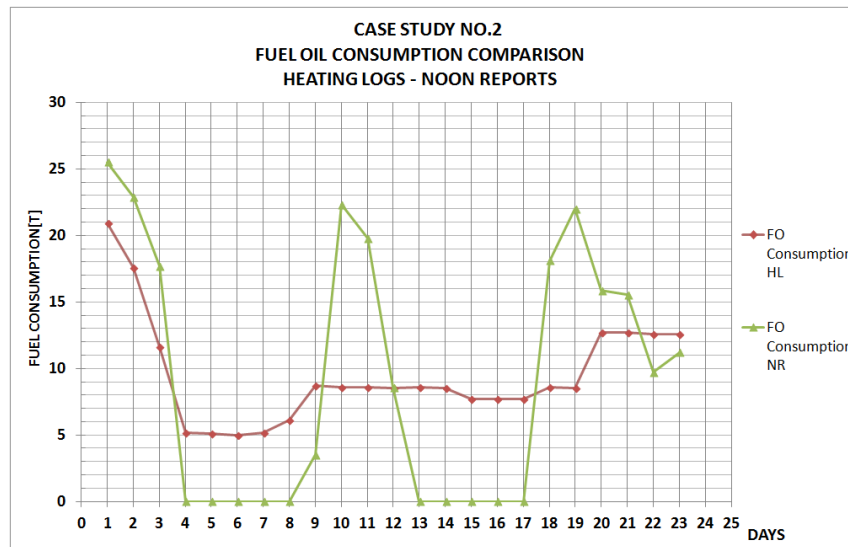
Figure 4.7: Case No.2 - Reported Consumptions Comparison

Average cargo temperatures as well as weather information were also drained by the ship's heating logs. Similarly to the previous case study, a graph was constructed displaying the average cargo temperature in correlation to the fuel oil consumption (Fig.4.8a). Finally, it was deemed necessary to include a graph which will demonstrate ambient temperature variation as a function of time (Fig.4.8b), since it varies considerably along the duration of the voyage, unlike case study no.1 were ambient temperature showed little fluctuations.

In figure Fig.4.8a, we observe that fuel consumption decreases from 21 t in day 1 to 5.2 t in day 4. From there up until day 8, fuel consumption remains around the same levels, rising slightly between days 8 and 9 of the journey. Furthermore, for the same interval, cargo temperature drops at almost steady rate, thus we conclude that the generated steam does not suffice to satisfy cargo heating demands. In contrast to the time interval between days 4 to 9, fuel consumption appears multiple times larger during the earlier stages of

---

[3]see appendix, pg.95-96

(a)   (b)
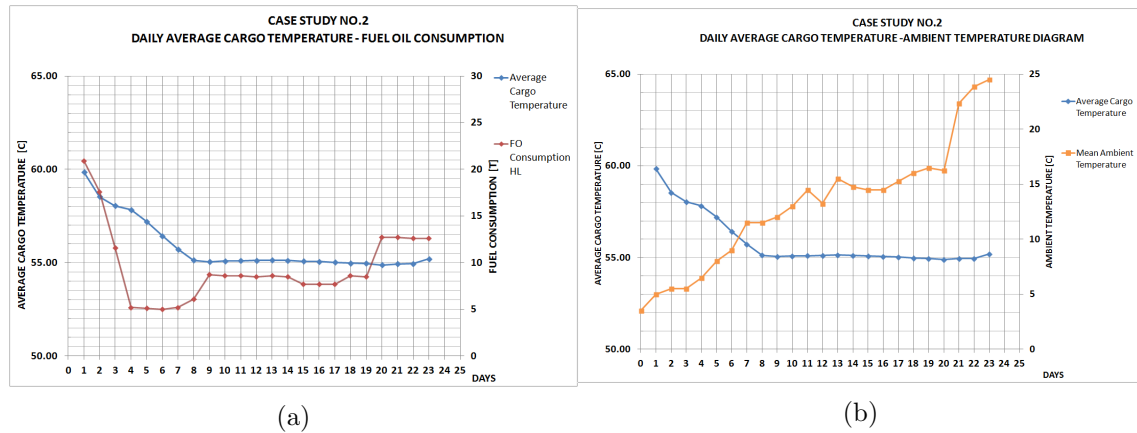
Figure 4.8: FO Consumption, Average Cargo Temperature and Mean Ambient
Temperature fluctuation throughout the journey

the voyage. In case all burned fuel was used solely to produce steam for cargo heating, we would foresee cargo temperature to rise. Hence, data of days 1-3 can be considered controversial, since they disagree with our expectations.

Likewise, for the final four days of the voyage, fuel consumption increases from 9 MT to 13 MT, without the expected cargo temperature rise. Simultaneously, ambient temperature rises substantially, and thus the overall temperature difference between the secluded cargo and surrounding temperature is reduced. Obviously the validity of data points 20 - 23 is also in dispute. For the majority of the journey however, fuel consumption appears to be rather constant, which coincided well with our efforts to maintain cargo at a standard temperature.
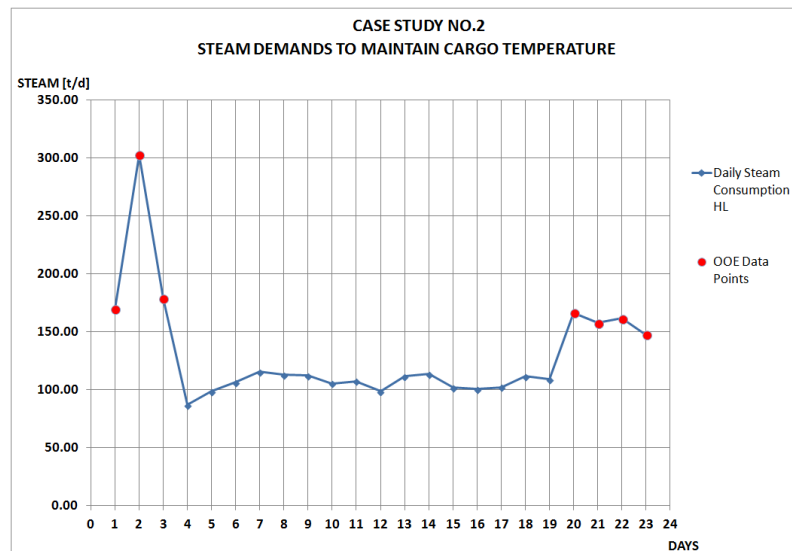
Figure 4.9: Case No.2 - Estimation for daily steam consumption used to compensate
heat losses

Simulation Results

Simulation results while transferring heavy fuel oil are demonstrated in Fig.4.10 . Percentage error lines are fitted to the heating log data points, spanning to ±2%.
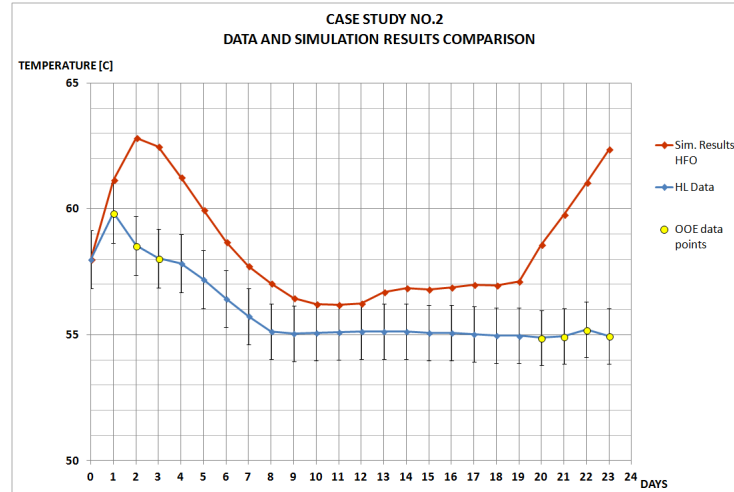
Figure 4.10: Case No.2 - Average Cargo Temperature Estimation

Again, data points which were out of expectation (OOE data points), according to Fig.4.9 are marked with yellow. Simulation results for the second case study were acceptable. As we can observe in Fig.4.10, the developed temperature patterns match satisfactorily as long as days 4 to 19 are concerned. The assumption that data points from days 1-3 and 20-23 should indicate higher temperatures, is also confirmed by the developed model.

An alleged rise in cargo temperature of the data set, for days 2 and 3, would also provoke deviations between the two curves to shrink, as it would eventually evoke higher temperatures for the remaining days of the voyage. Thus, divergence between data set and simulation results would fall below the established error margin of 2%. In addition, low ambient temperatures during the early stages of the voyage can also pose a substantial source of error, as they are usually linked with unfavorable weather conditions, rain, intense wind gust etc. factors which are totally stochastic and we cannot take under consideration.

As we noticed in both study cases, deviations always occur during the first day of the voyage, approximately during or slightly after cargo loading has completed. As mentioned above, this can be caused if the reported consumption in the data set does not solely refer to cargo heating, and a part of it refers to other ship operations that took place onboard. Since boiler load is determined through the boiler's performance curve, we understand that a decrease in the reported fuel oil consumption will result in lower boiler load and thus less production of steam. Conclusively, the initially calculated cargo temperatures would be an overestimation, as in reality less steam is provided to the cargo tanks.

By excluding the first day of the voyage from the data set, another simulation was carried out, commencing from the point at which the ship departs port (see relevant noon reports, pg. 96, 29/12/2017 at 16:00). Cargo temperature is given by the heating logs, where for the 29/12/2017 09:00 (day 1) temperature was measured to be 59.84 $°C$, while for the 30/12/2017 09:00, cargo temperature was 58.54 $°C$. Assuming that the temperature varies linearly between the two days, we determined the average cargo temperature at the time when the ship leaves port, which was taken equal to 59.5 $°C$. As shown in Fig.4.11, much greater convergence between simulation results and available data was achieved. Finally, after day 19 of the voyage, we notice that temperature curve tends to rise , and will most likely follow a similar pattern with that of Fig.4.10, further increasing the deviation between the two curves. Average percentage errors for both simulation runs of case study No.2 are demonstrated in Table 4.4. It is evident that excluding OOE data points led us to much more accurate results in terms of the average cargo temperature.
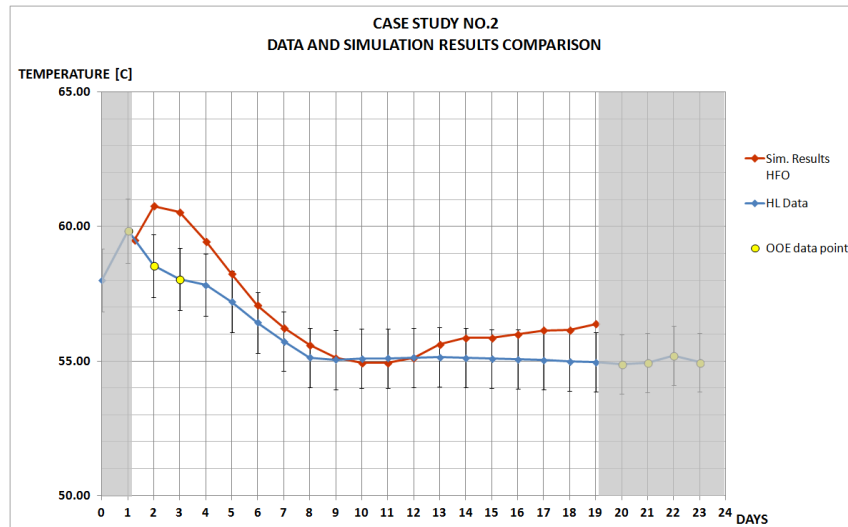
Figure 4.11: Case No.2 - Average Cargo Temperature Estimation (excluding days in port)

	Simulation Run No.1 (Complete Voyage)	Simulation Run No.2 (Excluding 1st and last OOE data points)
Overall	4.79 %	1.59%
OOE data points excepted	3.33%	1.29%

Table 4.4: Case Study No.2 - Simulation Results Percentage Errors

Aggregate tables including simulation results in respect of the average cargo temperature and fuel oil consumption are attached to the appendix, page98.

4.3   Heating Processes Optimization

In case study No.1, cargo was loaded at an approximate temperature of 46.3 °C and discharge temperature was set by the charterers to be equal to 60 °C. The most reliable heating plan, is to begin heating the cargo while the vessels stays at port and benefit from the prevailing lower heat transfer rates. Then, heating is continued until cargo temperature reaches the desired levels, where temperature maintenance begins. In that manner, one will always be on the safe side when it comes to being on time with the correct cargo temperature for discharge.

On the other hand, this method is the less fuel efficient, as throughout the voyage energy is consumed in order to maintain cargo temperature high, which in turn increases heat losses towards the environment. Maintaining cargo temperature constant or to the minimum possible value is the best way to minimize heat losses, and thus being energy efficient. Then cargo heat up must be carried out as quickly as possible and at the correct time, in order to diminish additional heat losses caused be the temperature rise. However, the question arises, when is the correct time to start heating in order to achieve the required discharge temperature and expend as little energy as possible.

The developed model achieves exactly that, as it provides an overall perspective of cargo temperature on board on different time intervals and operating parameters, with a considerable small margin of error. Since only case study no.1 includes cargo heating, we will attempt to suggest a fuelwise improved heating plan. Cargo temperature must be at

the required levels (60°C) before the ship arrives at its destination and enters anchorage status, awaiting to berth and commence discharge. That is because it is possible, although unlikely, for a ship to enter port right away, hence cargo temperature should be at the desired levels. Boiler efficiency is another factor which can vary according to the boiler load and can be very poor at partial loads below a certain level. In order to take this factor into account, we considered boilers to operate at the optimum load of 50%. Furthermore, since DCO No.1 returned the best results during model verification, we are going to assume that this is the loaded cargo for our optimization example.

Cargo heat up should under no circumstances be conducted under 24 hours. That is because extreme and abrupt heating may cause local overheating of crude oil, formation of flammable vapors above the cargo free surface and/or even cause thermal stresses and final deformation of the ship's integral structure. For that reason, heating is usually held for 2-3 days or more, but should never be inferior to 24 hours. In this test run, cargo heating expanded for three days, where boilers were under constant operation.

(a)   (b)
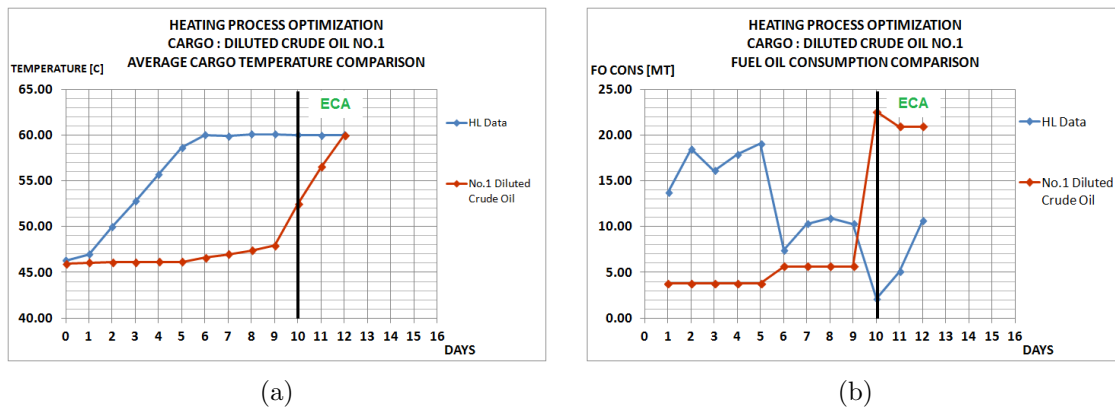
Figure 4.12: 1st Proposal - Minimize duration of cargo heat up

As demonstrated in Fig.4.12, for the first five days of the voyage, cargo temperature remains constant by burning almost 4 MT of fuel per day. Favorable weather conditions encourage low fuel consumptions, since they greatly influence the rate of heat losses. After the ship departs loading port (days 5 to 6), a higher amount of fuel is required to neutralize heat losses. Finally, during the tenth day of the voyage and three days prior reaching its destination, cargo heating load is at its maximum as boiler has to operate all day at the optimum load. The result is a steep increase to the average cargo temperature, measured to around 4°C per day.

In both figures, the bold vertical line denotes fuel switchover from HFO to MGO. Day number 10 is the last day where HFO is used. After that, the ship enters an emission control area (ECA). That also explains the ever so slightly drop in fuel consumption, for days 11 and 12, caused by the difference in the lower heating value of the two fuels. A fuel consumption and cost comparison is presented at table 4.5. Heavy fuel oil (HFO) was considered to cost US$ 600/ton and marine gas oil (MGO) is US$ 1000/ton.

	HFO		MGO		TOTAL	
	MT	$	MT	$	MT	$
Initial Method	126.3	75780	15.8	15800	142.1	91580
Suggested Method	63.9	38340	41.9	41900	105.8	80240
Comparison	**62.4**	**37440**	**-26.1**	**-26100**	**36.3**	**11340**

Table 4.5: Estimation of the financial benefits from the first suggestion

We notice that our suggestion managed to save around 36 MT of fuel in total, which corresponds to savings of up to US$ 11340. From this table however, we can deduce the importance of used fuel in our effort to optimize the heating process; although we achieved to almost halve the consumption of HFO, the inevitable use of MGO in ECA areas combined with the eminent demand for heat supply almost tripled MGO consumption.

2nd Proposal - Minimize MGO consumption in ECA areas

The increased cost of MGO leads us to believe that an even better heating scenario would be to minimize the MGO consumption as much as possible. That can be achieved by heating the cargo prior entering the ECA, and then only consume MGO in order to maintain cargo temperature constant at $60°C$. The simulation results are illustrated below :

(a)

(b)
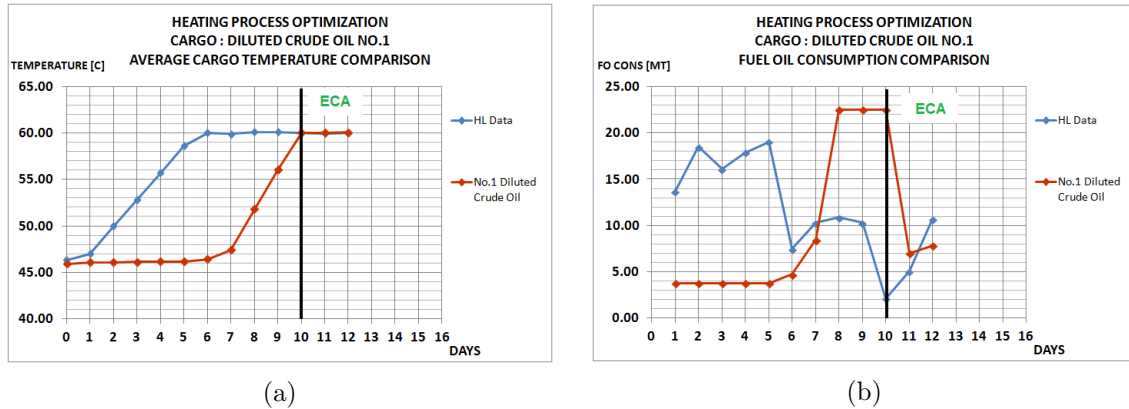
Figure 4.13: 2nd Proposal - Cargo temperature reaches desired levels before entering ECA

We observe that cargo temperature has reached the required levels on day 10, exactly before entering the ECA. The steep increase in fuel oil consumption prior day 10 was mainly because one boiler was operating for 3 days on 24 hour basis on 50% load. Fuel economy has improved, but not on a great extend. In Table 4.6, the financial benefits of our suggestion are illustrated.

	HFO		MGO		TOTAL	
	MT	$	MT	$	MT	$
Initial Method	126.3	75780	15.8	15800	142.1	91580
Suggested Method	99.6	59784	14.8	14830	114.5	74614
Comparison	**26.7**	**15996**	**1**	**1000**	**27.6**	**16996**

Table 4.6: Estimation of the financial benefits from the second suggestion

Compared to Table4.5, we note that HFO consumption has increased, by almost 36 MT. On the other hand, we achieved to decrease consumption of MGO proposed in the 1st suggestion from 42 MT to 14, which has the utmost impact on finances, since we managed to recover around USD$ 17000 compared to the practice applied in reality. That is also USD$ 5500 more than the savings from our first proposal, which proposed minimizing the duration of time cargo remains at elevated temperatures.

Taking everything into account, we can conclude that determining the optimum heating scenario cannot be considered univocal, as there are various parameters influencing cargo temperature and fuel consumption. However, the developed code can surely be considered

as an initial fundamental stepping stone towards developing such a software, which will assist ship operators in decision making on cargo heating procedures.

Annotation

The analysis run for each one of the study cases, as well as those done aiming to cargo heating optimization, took nearly 4-5 hours each, on a four-core, 3.6 GHz i7 processor equipped with a 8 GB memory. The reason why these simulations took so long is mainly due to the fact that the model is based on a trial and error basis, both for heat loss calculations, as well as for steam condensation inside the pipeline. However the biggest amount of time is obviously expended in steam pipeline and heating coils modeling, since we have decided to divide the total length of coils and pipeline into finite elements, the length of which varies from 0.1m to 0.5 m respectively. The total length of heating coils inside the tanks raises to 6719m; thus when steam is provided in all tanks, that means that at least 67190 repetitive calculations should be carried out, to determine the steam properties. In addition, steam pipeline on weather deck also increases the total calculation time.

In order to calculate the net heat transfer rate from or to the cargo tanks, Matlab needs to run for approximately 60-70 seconds, in case all tanks are heated, alike in our study cases. As heating intervals was set equal to one hour, that sums to approximately 1560 seconds or 26 minutes, to estimate cargo temperature after one day. On a 12 day voyage, with 24 hour heating, that will take almost 5 hours of simulation runs in real time, just to acquire a single set of results. In that aspect, we can increase the finite element length on board the ship and or increase the time interval, although that would eventually result in decreased accuracy. The optimum scenario would be to minimize both the finite elements length and the time interval, as feasibly possible and through that, achieve maximum precision in our calculations.

Chapter 5

Conclusions/Future Work

Conclusions

The present thesis focused on modelling the cargo heating practices on a crude oil carrier, by examining heat losses mechanisms towards the environment, as well as heat gain processes through steam distribution inside the tanks. In this context, a model capable of predicting cargo temperature inside each one of the ship's cargo tanks was generated by the author. For the implementation of this model, Matlab programming environment was used.

After extensive search in existing bibliographic sources, correlations for heat transfer phenomena taking place on ship were selected in order to be as accurate and up to date as possible. Two case studies were examined, to assess the developed model precision. Under the same operating parameters and weather conditions, the model showed to function properly and produce reasonable results. In the majority of occasions, simulation result trajectory agreed with that of available data. Average deviation was found to be less than $\pm 1°$C.

However, simulation results were not so favorable in cold weather conditions, where sea and ambient temperature were considerably low; that can be addressed by the stochastic factors prevailing during unfavorable weather conditions. Also, the developed model did not address the amount of heat required, in order to bring the ship's pipework up to operating temperature. Thus, a slight divergence was noted, during the first days of each simulated case study.

For the first case study, proposals for optimizing the cargo heating processes were also made. As the developed model showed satisfactory agreement during the validation phase, we deem that optimization results can be considered reliable. Simulation results showed that considerable profits can be made, when cargo temperature is brought up to the desired levels, prior entering an emission control area. However, the developed code was unable to define the optimum cargo heating plan. That was predominantly due to fact that drawing results out of the program was a severly slow procedure.

Future Work

According to the author's opinion, future research should focus predominantly on improving the accuracy of the suggested methodology in the present work. This can be achieved through realistic spatial design of the ship's steam piping system, which would also address the different forms of steam condensation taking place on board. Also, an in depth study of the steam distribution system seems necessary, so as steam flow inside the main steam pipeline and heating coils can be predicted precisely.

More case studies should be examined for further verification of the developed model.

Different case studies should also assist in establishing more precise correction coefficients for heat transfer augmentation due to stochastic events mentioned in this thesis. Furthermore, a means to accelerate result generation and improve simulation run duration should be investigated, without having to sacrifice precision.

It is worth noting that the present model accounts for a specific tanker, however vessel's particulars can be parameterized, in order for the model to be applicable to any tanker vessel. Another possible extension is the incorporation of the code in a block diagram environment, such as Simulink. In addition, the insertion of Graphical User Interface (GUI) would give the user a much friendlier interface, through which he/she would be able to provide and receive data. Finally, the present model can be evolved as a decision support tool for the optimization of cargo heating operation and the corresponding boiler fuel consumption.

Appendices

Appendix A

Correlations

A.1   Heat Transfer Correlations

A.1.1   Forced Convection Over a Flat Plate

In Chapter 2.2.1 we concluded that sea flow around the ship's hull will definetely be turbulent. However, for turbulent boundary layers, it is not possible to obtain exact analytical solutions as they are inherently unsteady. From experimental data, a correlation has been recommended for the local Nusselt number by Eckert and Drake [4], of the form :

$$\frac{Nu_x}{Re_x Pr} = \frac{0.0296 Re_x{}^{-0.2}}{1 + 0.87\, A Re_x{}^{-0.1}\,(Pr - 1)} \tag{A.1}$$

where A is a coefficient given from :

$$A = 1.5 Pr^{(-1/6)}$$

Replacing A into Eq.A.1 and transforming as needed, we get that the local heat transfer coefficient h_x is given by the equation :

$$\frac{h_x}{l_x k} = \frac{0.0296 Re_x{}^{0.8} Pr}{1 + 1.305\, Pr^{-1/6}\, Re_x{}^{-0.1}(Pr - 1)} \tag{A.2}$$

A.1.2   Forced Convection Above Cylinder

Cylinder in cross flow

According to Hilpert [45], the average Nusselt number over the external cylinder diameter is given by:

$$\overline{Nu_D} = \frac{\overline{h}D}{k} = C Re_D{}^m Pr^{1/3} \tag{A.3}$$

Equation A.3 is modified to account for various Prandtl numbers, while C, m are constants which depend on (Re_D), values for which can be found in the following table :

Re_D	C	m
4-40	0.911	0.385
40-4000	0.683	0.466
4000-40000	0.193	0.618
40000-400000	0.027	0.805

Also according to Churchil and Bernstein [42]

$$
\overline{Nu_D} = \begin{cases}
0.3 + \dfrac{0.62 Re_D{}^{0.5} Pr^{1/3}}{\left[1+(0.4/Pr)^{2/3}\right]^{0.25}} & \text{if } Re_D < 4000 \\[2em]
0.3 + \dfrac{0.62 Re_D{}^{0.5} Pr^{1/3}}{\left[1+(0.4/Pr)^{2/3}\right]^{0.25}} \left[1 + (\dfrac{Re_D}{282000})^{0.5}\right] & \text{if } 20000 < Re_D < 400000 \\[2em]
0.3 + \dfrac{0.62 Re_D{}^{0.5} Pr^{1/3}}{\left[1+(0.4/Pr)^{2/3}\right]^{0.25}} \left[1 + (\dfrac{Re_D}{282000})^{(5/8)}\right]^{0.8} & \text{if } Re_D = other
\end{cases}
\tag{A.4}
$$

Another correlation was proposed by Zukauskas [46] and is of the form

$$
\overline{Nu_D} = C Re_D{}^m Pr^{0.37} (\frac{Pr}{Pr_s})^{1/4}
\tag{A.5}
$$

which is valid for $Re_D \leq 10^6$. For the above equation, all properties are evaluated at T_∞, except Pr_s, which is evaluated at T_s. Values for C, m are listed in the table below.

Re_D	C	m
1-40	0.75	0.4
40-1000	0.51	0.5
1000 - 2×10^5	0.26	0.6
2×10^5 - 10^6	0.076	0.7

Cylinder in axial flow

For parallel flow above a cylinder, Sparrow & Geiger [63] suggested the following correlation for forced convection axial flow above a cylinder

$$
\overline{Nu_D} = 1.05 Pr^{0.36} Re_{axial}{}^{0.5}
\tag{A.6}
$$

Furthermore, another equation proposed from Wiberg et al. [65]

$$
\overline{Nu_D} = 0.096 Re_{axial}{}^{0.656}
\tag{A.7}
$$

A.1.3   Natural Convection Over Flat Plate

Although we understand the mechanism of natural convection well, the complexities of fluid motion make it very difficult to obtain simple analytical relations for heat transfer by solving the governing equations of motion and energy. Simple empirical correlations for the average Nusselt number $\overline{Nu}$ in natural convection are of the form :

$$
\overline{Nu} = \frac{\overline{h} L_c}{k} = C(Gr_L Pr)^n = C Ra_L{}^n
\tag{A.8}
$$

where all properties of the fluid are calculated at the *film temperature $T_f = (T_\infty + T_s)/2$.*

Laminar Flow

While the flow over a vertical plate remains laminar for the entire range of the plate, Ostrach [8] proposed that the mean Nussel number can be obtained by the equation :

$$
\overline{Nu_L} = \frac{4}{3} (\frac{Gr_L}{4})^{0.25} \frac{0.75 Pr^{0.5}}{(0.609 + 1.221 Pr^{0.5} + 1.238 Pr)^{0.25}}
\tag{A.9}
$$

Furthermore Churchill and Chu [9] proposed another correlation that may be applied over the entire range of a plate in laminar flow

$$\overline{Nu_L} = 0.68 + \frac{0.67 Ra_L{}^{0.25}}{[1 + (0.492/Pr)^{9/16}]^{4/9}} \tag{A.10}$$

Finally, a correlation for the local heat transfer coefficent was proposed by Eckert [5]

$$Nu_x = \frac{h_x x}{k} = \frac{0.508 Pr^{0.5}}{(0.952 + Pr)^{0.25}} Gr_x{}^{0.25} \tag{A.11}$$

Turbulent Flow

In case flow over a vertical flat plate becomes turbulent, there are various correlations that have been developed and are often of the form of equation A.8. However, results coming from equations of this form tend to have large margins of error. The most accredited correlation has been recommended by Churchill and Chu [9] and may be applied over the entire range of Ra_L :

$$\overline{Nu_L} = \{0.825 + \frac{0.387 Ra_L{}^{1/6}}{[1 + (0.492/Pr)^{9/16}]^{8/27}}\}^2 \tag{A.12}$$

A.1.4 Natural Convection in Vertical Enclosures (Double Hull)

For aspect ratios in the range of $1 \leq (H/L) \leq 10$, the following correlations have been suggested by Catton [25] :

$$\overline{Nu_L} = 0.22(\frac{Pr}{0.2 + Pr} Ra_L)^{0.28} (H/L)^{-0.25} \quad \begin{bmatrix} 1 \leq (H/L) \leq 10 \\ Pr \leq 10^5 \\ 10^3 \leq Ra_L \leq 10^{10} \end{bmatrix} \tag{A.13}$$

$$\overline{Nu_L} = 0.18(\frac{Pr}{0.2 + Pr} Ra_L)^{0.29} \quad \begin{bmatrix} 1 \leq (H/L) \leq 2 \\ 10^{-3} \leq Pr \leq 10^5 \\ 10^3 \leq \frac{Ra_L Pr}{0.2 + Pr} \end{bmatrix} \tag{A.14}$$

$$\overline{Nu_L} = 0.046 Ra_L{}^{1/3} \quad \begin{bmatrix} 1 \leq (H/L) \leq 40 \\ 1 \leq Pr \leq 20 \\ 10^6 \leq Ra_L \leq 10^9 \end{bmatrix} \tag{A.15}$$

Further research by ElSherbiny, Raithby & Hollands [27] suggested the following correlations

$$Nu_1 = 0.0605 Ra_L{}^{(1/3)}$$

$$Nu_2 = \left[1 + [0.104 Ra_L{}^{0.293}/(1 + (6310/Ra_L)^{1.36})]^3\right]^{(1/3)}$$

$$Nu_3 = 0.242(Ra_L/AR)^{0.272}$$

where the average Nusselt number is equal to the maximum value of Nu_1, Nu_2, Nu_3,

$$\overline{Nu_L} = \begin{bmatrix} Nu_1 & Nu_2 & Nu_3 \end{bmatrix}_{max} \tag{A.16}$$

and proposed various correlations, such as those of Bejan [20] (see eq.A.17) and Berkovsky and Polevikov [21] (see eq.A.18 and A.19).

$$\overline{Nu_H} = 0.364 \frac{L}{H} Ra_H^{1/4} \quad \begin{bmatrix} (H/L) > 1 \\ \frac{L}{H} Ra_H^{1/4} > 5 \end{bmatrix} \tag{A.17}$$

$$\overline{Nu_H} = 0.22 (\frac{Pr}{0.2 + Pr} Ra_H)^{0.28} (L/H)^{0.09} \quad \begin{bmatrix} 2 \leq (H/L) \leq 10 \\ Pr \leq 10^5 \\ Ra_H \leq 10^{13} \end{bmatrix} \tag{A.18}$$

$$\overline{Nu_H} = 0.18 (\frac{Pr}{0.2 + Pr} Ra_H)^{0.29} (L/H)^{-0.13} \quad \begin{bmatrix} 1 \leq (H/L) \leq 2 \\ 10^{-3} \leq Pr \leq 10^{13} \\ 10^3 \leq \frac{Ra_H Pr}{0.2 + Pr} (\frac{L}{H})^3 \end{bmatrix} \tag{A.19}$$

Finally, Rincon et al [17] recently proposed correlations from experimental data that show good agreement with the results of Bejan, Berkovsky and Polevikov. For an enclosure with vertical walls in the turbulent regime ($10^7 < Ra_H < 10^{11}$) and aspect ratios $0.5 < H/L < 2$, Rincon et al. suggested

$$\overline{Nu_H} = (0.433 Ra_H^{0.276})/2 \tag{A.20}$$

and Trias et al. [18] suggested

$$\overline{Nu_H} = c_1 (1 - exp(aRa_H^b)) Ra_H^{1/3} + c_2 exp(aRa_H^b) Ra_H^{1/4} \tag{A.21}$$

where $c_1 = 4.6847 \times 10^{-2}$, $c_2 = 3.2101 \times 10^{-1}$, $a = -1.5104 \times 10^{-4}$ and $b = 3.1874 \times 10^{-1}$.

A.1.5   Natural Convection in Horizontal Enclosures (Ullage Space)

As a first approximation, convection coefficients for the horizontal cavity heated from below may be obtained from the following correlation, proposed by Globe and Dropkin [31]

$$\overline{Nu_L} = \frac{\overline{h}L}{k} = 0.069 Ra_L^{1/3} Pr^{0.074} \quad 3 \times 10^5 \lesssim Ra_L \lesssim 7 \times 10^9 \tag{A.22}$$

where all properties are evaluated at the average temperature of the top and bottom wall.

Based on experiments with air, Hollands et al [26] recommended another correlation for horizontal enclosures,

$$\overline{Nu_L} = 1 + 1.44 \left[1 - \frac{1708}{Ra_L} \right] + \left[\frac{Ra_L^{1/3}}{18} - 1 \right] \quad Ra_L < 10^8 \tag{A.23}$$

The notation [ ], implies that, if the quantity in brackets is negative, it must be set equal to zero. More recent experiments produced correlations that are in good agreement with Eq.A.22 and Eq.A.23, such as those proposed by Rincon-Casado et al. [17] and Sharma et al [55]. However these equations were developed based on the cavity's width instead of height :

$$\overline{Nu_B} = 0.083 \ (\frac{H}{B})^{-0.095} Ra_B^{0.339} \tag{A.24}$$

$$\overline{Nu_B} = 0.152 \ (\frac{H}{B})^{0.267} Ra_B^{0.34} \tag{A.25}$$

A.1.6 Natural Convection from Vertical Cylinders

For natural convection above vertical cylinders in the turbulent region (i.e. for $Gr_H \geq 4 \times 10^9$) [51], a very approximate equation was recommended by McAdams [53] for practical applications, where

$$Nu_H = 0.13 Ra_H{}^{1/3} \tag{A.26}$$

An empirical equation was also suggested by Eigenson [56]

$$Nu_H = 0.148 Ra_H{}^{1/3} \tag{A.27}$$

An empirical equation was also suggested by Le Fevre and Ede [57]

$$\overline{Nu_H} = \frac{4}{3}\left[\frac{7 Ra_H Pr}{5(20 + 21Pr)}\right]^{(1/4)} + \frac{4(272 + 315Pr)H}{35(64 + 63Pr)D} \tag{A.28}$$

A.1.7 Natural Convection from Horizontal Cylinders

For horizontal orientations, Nusselt number is determined by Eq.A.29 and A.30. Churchill and Chu [10] have recommended a single correlation for a wide Rayleigh number range:

$$\overline{Nu_D} = \left\{0.6 + \frac{0.387 Ra_D{}^{1/6}}{\left[1 + (0.559/Pr)^{9/16}\right]^{8/27}}\right\}^2 \qquad Ra_D \lesssim 10^{12} \tag{A.29}$$

The foregoing correlation provide the average Nusselt Number over the entire circumference of an isothermal cylinder. Moreover Morgan [24] suggested an expression of the form

$$\overline{Nu_D} = \frac{\overline{h}D}{k} = C Ra_D{}^n \tag{A.30}$$

where C and n are given in the table below

Re_D	C	n
$10^{-2} - 10^2$	1.02	0.148
$10^2 - 10^4$	0.85	0.188
$10^4 - 10^7$	0.48	0.25
$10^7 - 10^{12}$	0.125	0.333

A.1.8 Steam Condensation Inside Tubes

Horizontal Tubes

Heat transfer correlations have been developed for the individual regimes, and recommendations for their use are included in Dobson and Chato [34]. Studies by Altman, Staub and Norris [35] for predicting the condensing heat transfer coefficient in the higher velocity range, verify experimental data to within +20% and −10%. In addition to this, studies by Akers [36] correlated the data to around ±50%. Attempts have been made to correlate average heat transfer coefficients for condensing inside tubes without much success. Data and prediction can disagree by over 100 percent(p.11-20) [33]. Dobson and Chato suggested an empirical correlation for a local heat transfer coefficient h_z of the form

$$\frac{h_z D}{k_l} = 0.023 Re_l{}^{0.8} Pr_l{}^{0.4}\left[1 + \frac{2.22}{X_{tt}{}^{0.89}}\right] \tag{A.31}$$

where :

- X_{tt} is the Martinelli parameter corresponding to the existence of turbulent flow in both the liquid and vapor phases.

- Re_l is the superficial Reynolds number of the liquid, or the Reynolds number based on the superficial velocity of liquid phase

- Pr_l is the Prandtl number for the liquid phase.

According to Rohsenow [33], the following procedure calculates local heat transfer coefficients along the tube and it had been found to agree with data within ±10 percent. Bae et al. [37] integrated momentum equations for the annular liquid layer and the vapor, employing the Martinelli two-phase-flow pressure drop relations, the analog between heat transfer and momentum transfer, and the universal velocity distribution in the liquid. Traviss et al. [38] simplified these prediction relations with the following result for the local coefficient:

$$\frac{h_z D}{k_l} = \frac{Pr_l Re_l^{0.9}}{F_2}\left[\frac{1}{X_{tt}} + \frac{2.85}{X_{tt}^{0.476}}\right] \tag{A.32}$$

where

$$Re_l = \frac{G(1-x)D}{\mu_l}$$

$$X_{tt} = \left(\frac{\mu_l}{\mu_g}\right)^{0.1}\left(\frac{1-x}{x}\right)^{0.9}\left(\frac{\rho_g}{\rho_l}\right)^{0.5}$$

$$F_2 = \begin{cases} Pr_l + 5ln(1 + 5\ Pr_l) + 2.5ln(0.0031\ Re_l^{0.812}) & \text{if } Re_l > 1125 \\ 5\ Pr_l + 5\ ln\big[1 + Pr_l\ (0.0964\ Re_l^{0.585} - 1)\big] & \text{if } 60 < Re_l < 1125 \\ 0.707\ Pr_l\ Re_l^{0.5} & \text{if } Re_l < 50 \end{cases}$$

Vertical Tubes

For steam condensation inside vertical tubes, Hebbard et al [47] used initially the mathematical relationship derived by Nusselt [49] for the case of vapor condensing on a smooth vertical surface, which is valid when the diameter of the pipe is larger in comparison to the film thickness.

$$h_{vert,sat} = 0.943\frac{\Delta h_{evap}\rho_l(\rho_l - \rho_v)gk_l^3}{(4\mu_l(T_{sat} - T_s)L)^{0.25}} \tag{A.33}$$

Moreover, Shah [48] proposed a correlation compared with a large amount of varied data from many sources with satisfactory agreement for practical designs. Defining as reduced pressure p_r, the ratio between the actual pressure p and the critical pressure p_c, Shah suggested an alteration of the Dittus-Boelter equation

$$h_{vert,sat} = h_{Dit-Boe}\left[(1-x)^{0.8} + \frac{3.8x^{0.76}(1-x)^{0.04}}{p_r^{0.38}}\right] \tag{A.34}$$

where $h_{Dit-Boe}$ the heat transfer coefficient calculated by the Dittus- Boelter equation assuming all the mass flowing as a liquid:

$$h_{Dit-Boe} = 0.023Re_L^{0.8}Pr_l^{0.4}\frac{k_l}{D}$$

A.1.9   Single Phase Flow in Horizontal Tubes

For fully developed laminar flow and uniform wall temperature in a circular tube, Nusselt number was proven to be constant and independent of Re_D, Pr or axial location

$$Nu_D = \frac{hD}{k} = 3.66 \tag{A.35}$$

For turbulent flows in a smooth circular tube, Gnielinski [50] provided a correlation valid over a large Reynolds number range, including the transition region, where :

$$Nu_D = \frac{(f/8)(Re_D - 1000)Pr}{1 + 12.7(f/8)^{1/2}(Pr^{2/3} - 1)} \tag{A.36}$$

which is valid for $0.5 \leq Pr \leq 2000$ and $3000 \leq Re_D \leq 5 \times 10^6$.

More recently, Faghri et. al (2010) [67] also suggested a correlation for fully turbulent $(Re_D > 10000)$ single phase flow inside horizontal tubes

$$\overline{Nu_D} = 0.027 Re_D{}^{0.8} Pr^{0.33} (\frac{\mu}{\mu_w})^{0.14} \tag{A.37}$$

where μ_w is the dynamic viscosity of the condensate evaluated at the wall temperature.

A.2   Thermophysical Properties Correlations

A.2.1   Seawater

t= Seawater temperature $[°C]$,
D = Depth [m]
P_0 = atmospheric pressure = 0.101325 [MPa],
$P = P_0 + (D \cdot 0.0101325)$ [MPa] S = Salinity [ppm]

Density

$$\rho_{sw}(t, S, P) = \rho_{sw}(t, S, P_0) \times F_P$$

where

$$\rho_{sw}(t, S, P_0) = \left(\alpha_1 + \alpha_2 t + \alpha_3 t^2 + \alpha_4 t^3 + \alpha_5 t^4\right) + \left(b_1 S + b_2 St + b_3 St^2 + b_4 St^3 + b_5 S^2 t^2\right)$$

$\alpha_1 = 9.9992293295 \times 10^2, \alpha_2 = 2.0341179217 \times 10^{-2}, \alpha_3 = -6.1624591598 \times 10^{-3},$
$\alpha_4 = 2.2614664708 \times 10^{-5}, \alpha_5 = -4.6570659168 \times 10^{-8},$
$b_1 = 8.0200240891 \times 10^2, b_2 = -2.0005183488, b_3 = 1.6771024982 \times 10^{-2},$
$b_4 = -3.0600536746 \times 10^{-5}, b_5 = -1.6132224742 \times 10^{-5}$

$$F_P = exp\left[(P - P_0) \times (c_1 + c_2 t + c_3 t^2 + c_4 t^3 + c_5 t^4 + c_6 t^5 + S \times (d_1 + d_2 t + d_3 t^2)) + \right.$$

$$\left. \frac{(P^2 - P_0{}^2)}{2} \times (c_7 + c_8 t + c_9 t^3 + d_4 S)\right]$$

$c_1 = 5.0792 \times 10^{-4}, c_2 = -3.4168 \times 10^{-6}, c_3 = -5.6931 \times 10^{-8},$
$c_4 = -3.7263 \times 10^{-10}, c_5 = 1.4465 \times 10^{-12}, c_6 = -1.7058 \times 10^{-15},$
$c_7 = -1.3389 \times 10^{-6}, c_8 = 4.8603 \times 10^{-9}, c_9 = -6.8039 \times 10^{-13},$
$d_1 = -1.1077 \times 10^{-6}, d_2 = 5.5584 \times 10^{-9}, d_3 = 4.2539 \times 10^{-11}, d_4 = 8.3702 \times 10^{-9}$

Validity : ρ_{sw} in (kg/m^3); $0 < t < 180\ °C$; $0 < S < 0.16$ kg/kg, $P = 0 - 12$ MPa
Accuracy: $\pm 0.1\%$

Dynamic Viscosity

$\mu_{sw} = \mu_w \left(1 + AS + BS^2\right)$

$A = 1.5409136040 + 1.9981117208 \times 10^{-2}\ t - 9.5203865864 \times 10^{-5}\ t^2$

$B = 7.9739318223 - 7.5614568881 \times 10^{-2}\ t + 4.7237011074 \times 10^{-4}\ t^2$

μ_w is based on the IAPWS 2008 data and given by:
$\mu_w = 4.2844324477 \times 10^{-5} + \left(0.15700386464(t + 64.9926201)^2 - 91.296496657\right)^{-1}$

Validity : μ_{sw} and μ_w in $(kg/m.s)$; $0 < t < 180\ °C$; $0 < S < 0.15$ kg/kg,
Accuracy: $\pm 1.5\%$

Thermal Conductivity

$k_{sw}(t, S, P) = \frac{k_w(t,P)}{1+0.00022 \times S}$

$k_w(t, P) = k_w(t, P_0) \times \left[1 + P^* \times (f_1 + f_2 T^* + f_3 T^{*2} + f_4 T^{*3} + f_5 T^{*4})\right]$

where

$k_w(t, P_0) = g_1 T^{*-0.193823894} + g_2 T^{*-4.7166384} + g_3 T^{*-6.38463554} + g_4 T^{*-2.13362102}$

$T^* = \dfrac{t + 273.15}{300}$; $P^* = \dfrac{P - 0.1}{139.9}$

$f_1 = 21.942, f_2 = -77.387, f_3 = 102.81, f_4 = -60.727, f_5 = 13.464$
$g_1 = 0.797015135, g_2 = -0.251242021, g_3 = 0.0964365893, g_4 = -0.0326956491$

Validity : k_{sw} and k_w in $(W/m.K)$; $0 < t < 90\ °C$; $0 < S < 120$ g/kg,
Accuracy: $\pm 2.57\%$

Specific Heat at Constant Pressure

$C_{p_{sw}} = c_{sw} + c_{sw_p}$

$c_{sw} = A + BT + CT^2 + DT^3$

$c_{sw_p} = (P - P_0) \times \left(c_1 + c_2 T + c_3 T^2 + c_4 T^3 + S(c_5 + c_6 T + c_7 T^2) + c_8 T^3\right)$

where

$A = 5.328 - 9.76 \times 10^{-2}\ S + 4.04 \times 10^{-4}\ S^2$

$B = -6.913 \times 10^{-3} + 7.351 \times 10^{-4} \; S - 3.15 \times 10^{-6} \; S^2$
$C = 9.6 \times 10^{-6} - 1.927 \times 10^{-6} \; S + 8.23 \times 10^{-9} \; S^2$
$D = 2.5 \times 10^{-9} + 1.666 \times 10^{-9} \; S - 7.125 \times 10^{-12} \; S^2$

$c_1 = -3.1118$, $c_2 = 0.0157$, $c_3 = 5.1014 \times 10^{-5}$, $c_4 = -1.0302 \times 10^{-6}$, $c_5 = 0.0107$,
$c_6 = -3.9716 \times 10^{-5}$, $c_7 = 3.2088 \times 10^{-8}$, $c_8 = 1.0119 \times 10^{-9}$

Validity : $C_{p_{sw}}$, c_{sw} and c_{sw_p} in (kJ/kg K); $273.15 < T < 453.15$ K ; $0 < S < 180$ g/kg
Accuracy: $\pm 0.28\%$

The aforemetnioned correlations can all be found in the works of Nayar et al. [43] and Sharqawy et al. [44].

A.2.2 Steam and Condensate

Due to the increased complexity of said correlations, the reader is referred to publications of the International Association for the Properties of Water and Steam. Specifically, the present work used the updated version released in 2007, which is called "IAPWS Industrial Formulation 1997 for the Thermodynamic Properties of Water and Steam" [79].

A.2.3 Crude Oil Fractions

API Gravity

$$API^\circ = \frac{141.5}{SG_{60^\circ F}} - 131.5$$

where

$SG_{60^\circ F}$ is the crude oil specific gravity at 60° F or 15.6° C.

Watson Characterization Factor, K_W

$$K_W = \frac{T_b^{1/3}}{SG_{60^\circ F}}$$

where

T_b is the normal boiling point or 50% boiling point in degrees Rankine.

Thermal Expansion Coefficient

Thermal expansion coefficient for crude oils depends more on density rather than temperature. For crude oils, values for the thermal expansion coefficient are given in the following table as a function of the liquid's density at 15°C [80]

Table A.1: My caption

Density $[t/m^3]$	Thermal Expansion Coefficient $[K^{-1})]$
$0.9246 <\rho_{15^\circ C} <1.0243$	0.00063
$0.8595 <\rho_{15^\circ C} <0.9245$	0.00065
$0.8280 <\rho_{15^\circ C} <0.8594$	0.00067
$0.8021 <\rho_{15^\circ C} <0.8279$	0.00068

Specific Heat

$$C_{p_1} = \alpha \ (b + c \ T) \ [77] \ \text{where}$$

$\alpha = 1.4651 + 0.2302 \ K_W$
$b = 0.306469 - 0.16734 \ SG_{60^\circ F}$
$c = 0.001467 - 0.000551 \ SG_{60^\circ F}$

Validity : C_{p_1} in (kJ/kg K); $T > 273.15$ K ; K_W is the Watson characterization factor as described above
Accuracy: $\pm 5\%$

$C_{p2} = A_1 + A_2 T + A_3 T^2$ [78]

where

$A_1 = -4.90383 + (0.099319 + 0.104281 SG)K_W + \dfrac{4.81407 - 0.194833K_W}{SG_{60°F}}$

$A_2 = (7.53624 + 6.21461K_W) \times (1.12172 - \dfrac{0.27634}{SG_{60°F}}) \times 10^{-4}$

$A_3 = -(1.35652 + 1.11863K_W) \times (2.9027 - \dfrac{0.70958}{SG_{60°F}}) \times 10^{-7}$
Validity : C_{p2} in (kJ/kg K); $T > 273.15$ K ; Accuracy: $\pm 5\%$

$Cp_3 = 4.185 \ (0.35 + 0.055K_w)((0.3065 - 0.16734 \ SG_{60°F}) + T_K(1.467 \cdot 10^{-3} - 5.508 \cdot 10^{-4} \ SG_{60°F}))$

Correction for $K_W \neq 11.8$

$c_p = Cp_3(0.35 + 0.055K_w)$

Finally, in the work of Mavrakos, another figure is given, expressing the specific heat capacity as a function of temperature (see Fig.A.2, p.88). The proposed correlation is:

$C_{p4} = ((0.6811 - 0.308SG_{60°F}) + (T_F(0.000815 - 0.000306 * SG_{60°F}))4.1855$

Thermal Conductivity

In [75], equation for k_1 is given as applying to any petroleum derived liquid:

$k_1 = \left(339 - 0.19 \ T\right) \times 418.4 \times 10^{-6}$

Furthermore, Mavrakos [6] achieved to deduce a linear expression for the correlation between thermal conductivity and temperature, as proposed by Cragoe [81] in the form of Fig.A.1 .

$k_2 = ((-2.424242424 \times 10^{-5}T_F) + 0.0816969697) \times 1.731$

where the multiplication to 1.731 intends to convert units from $BTU/hr.ft.°F$ to $W/m.K$.

$k_3 = \frac{0.137}{\rho_{15°C}}\left[1 - 0.00054(T_K - 273)\right] \times 10^3$ [76]

Kinematic Viscosity

The effect of temperature on the kinematic viscosity has been described by an empirical equation proposed by Walther. The Walther formula is as follows:

$$log_{10}log_{10}(\nu + 0.7) = A + B \ log_{10}T$$

where A,B are empirical parameters, ν in cSt and T in K. Parameters A and B are calculated if kinematic viscosity is known at two different temperatures.

THERMAL CONDUCTIVITY CONVERSION FACTORS

$\dfrac{BTU}{hr \cdot ft^2 \cdot °F/ft}$	$\dfrac{g\text{-}cal}{sec \cdot cm^2 \cdot °C/cm}$	$\dfrac{watts}{cm^2 \cdot °C/cm}$	$\dfrac{kg\text{-}cal}{hr \cdot m^2 \cdot °C/m}$	$\dfrac{BTU}{hr \cdot ft^2 \cdot °F/in}$
1	.004134	.01731	1.488	12
241.8	1	4.183	360	2901
57.8	.239	1	86.1	694
.672	.002778	.01162	1	8.06
.0833	.0003447	.001441	.1241	1
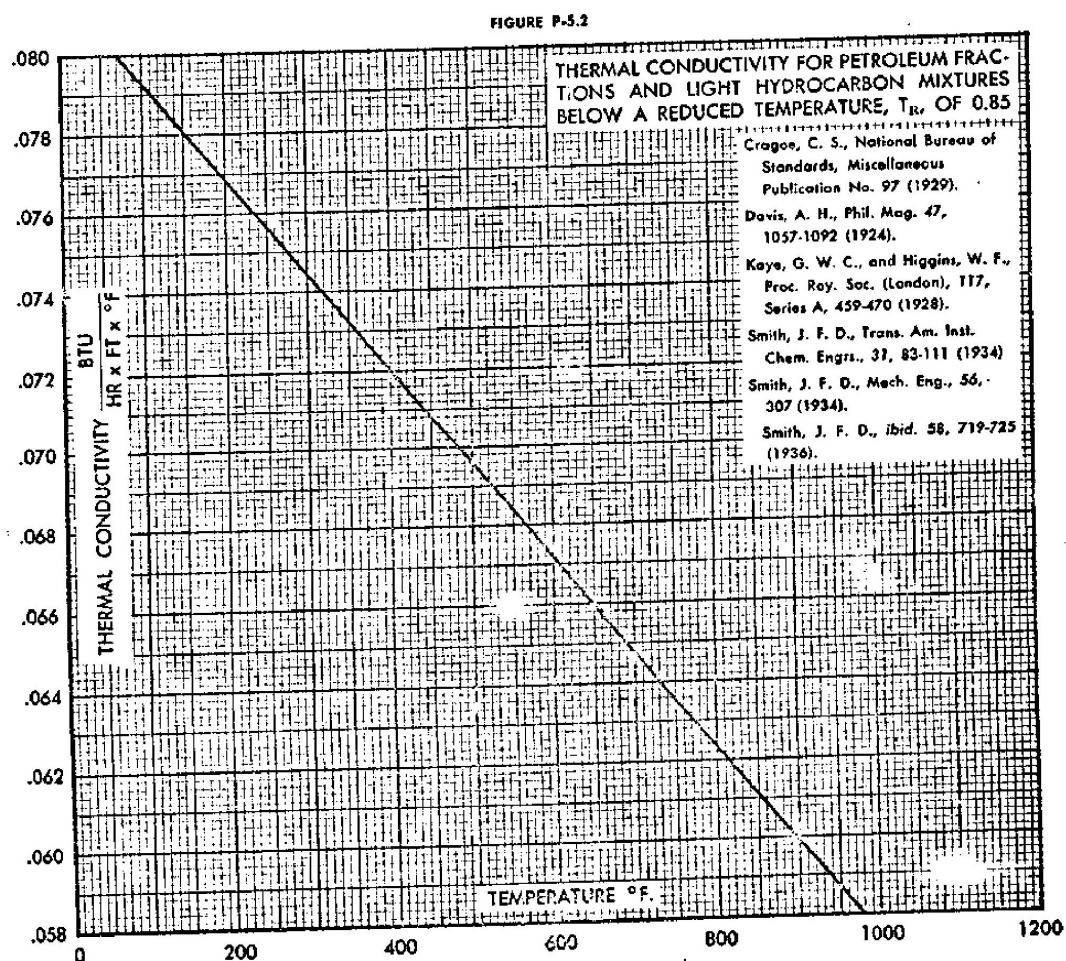
FIGURE P-5.2

Figure A.1: Thermal conductivity for petroleum fractions
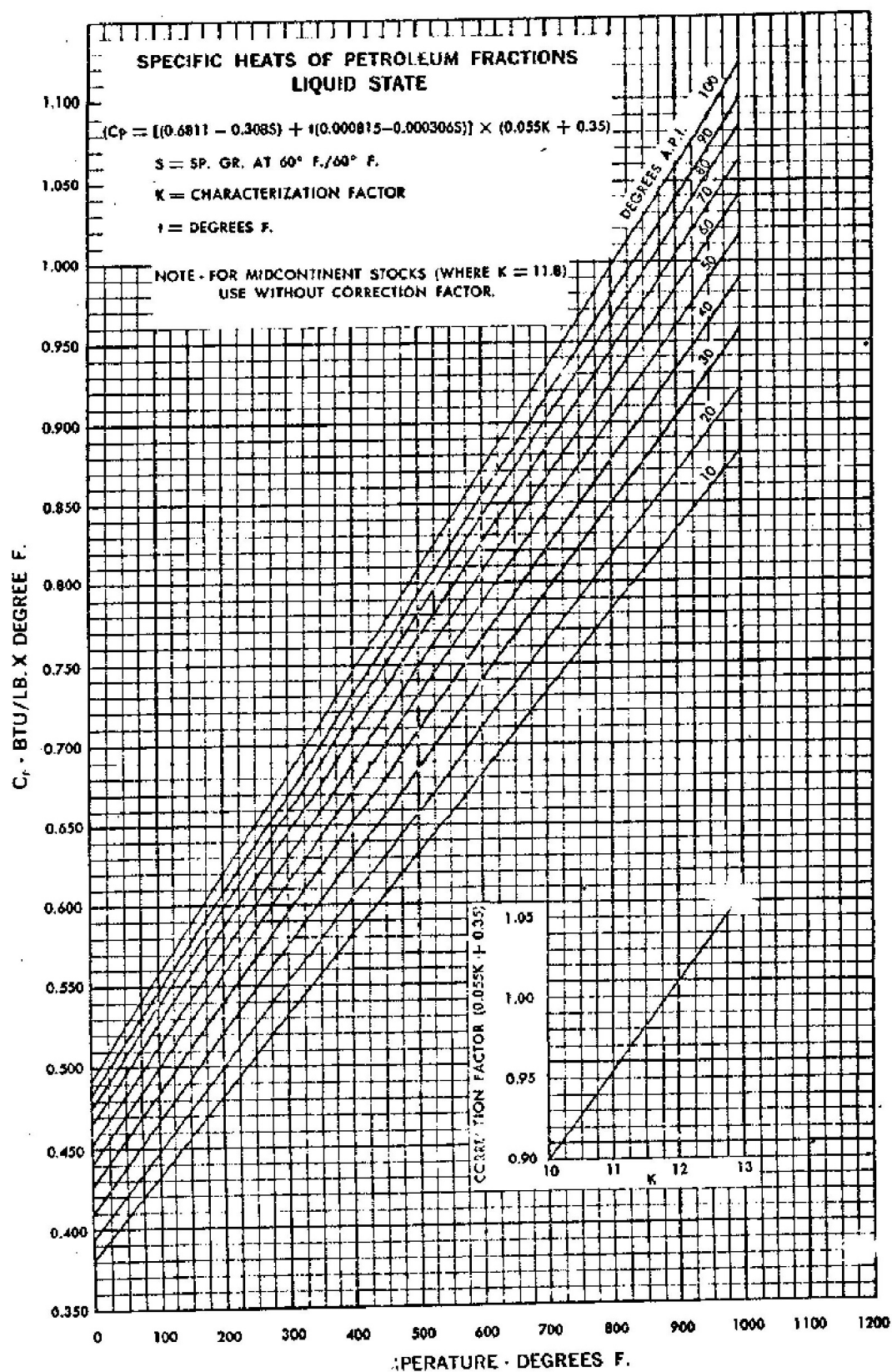
Figure A.2: Specific heats of petroleum fractions liquid state

A.2.4 Air

Dry air Pressure : 1 atm
T_{cr}=132.52 [K], ρ_{cr}=313 [kg/m^3]

Density

$$\rho_{air} = \frac{\rho_{air1} + \rho_{air2} + \rho_{air3}}{3}$$

ρ_{air1} is given by a 6th grade polynominal developed by Mavrakos while trying to interpolate tables illustrating dry air density as a function of temperature. Standard error of estimate for said polynomial rises to $4.80668072 \times 10^{-3}$

$$\rho_{air1} = a_0 + a_1 T + a_2 T^2 + a_3 T^3 + a_4 T^4 + a_5 T^5 + a_6 T^6$$

ρ_{air2} and ρ_{air3} are given under the ideal gas assumption, as air can be treated as such for most purposes. According to [71] and [72], good engineering accuracy can be achieved by the following equations.

$$\rho_{air2} = \frac{351.99}{T_K} + \frac{344.84}{T_K{}^2}$$
$$\rho_{air3} = \frac{P}{R_A T_K}$$

where

$a_0 = 1.249722929718$, $a_1 = -5.12211442 \times 10^{-3}$, $a_2 = 3.96395279 \times 10^{-5}$,
$a_3 = -8.88759333 \times 10^{-8}$, $a_4 = -1.84150422 \times 10^{-8}$, $a_5 = 2.65962325 \times 10^{-10}$,
$a_6 = -1.162129 \times 10^{-12}$
$R_A = 287.05 J/kg.K$

Validity : ρ_{air}, ρ_{air1} and ρ_{air2} in (kg/m^3); $200 < T_K < 400$ K ; P : absolute pressure in Pa
Accuracy: $< 0.15\%$

Thermal Expansion Coefficient

Again, under the ideal gas assumption, the volumetric thermal expansion coefficient at constant pressure can be approximated by the following equation:

$$b_{air} = T_K{}^{-1}$$

Dynamic Viscosity

Sutherland's equation was used by Reid [73], in order to correlate dynamic viscosity with temperature:
$$\mu = \frac{1.4592 T_K{}^{3/2}}{109.1 + T_K}$$
This expression is used for the production of reference tables so, presumably, is more than sufficiently accurate for enginnering purposes.

Validity : μ in (Ns/m^2); $100 < T_K < 800$ K ;

Thermal Conductivity

According to the work of Stephan and Laesecke [74], thermal conductivity of dilute air at atmospheric pressure can be determined by the equation :

$$k_{air1} = 4.358 \times 10^{-3} \Big(m_1 T_r^{-1} + m_2 T_r^{-2/3} + m_3 T_r^{-1/3} + m_4 + m_5 T_r^{1/3} + m_6 T_r^{2/3}$$
$$+ m_7 T_r + m_8 T_r^{4/3} + m_9 T_r^{5/3} \Big)$$

where

$T_r = T_K/T_{cr}$: reduced temperature, $T_{cr} = 132.52K$
$\rho_r = \rho_{air}/\rho_{cr}$: reduced pressure, $\rho_{cr} = 313kg/m^3$

$m_1 = 33.9729025, m_2 = -164.702679, m_3 = 262.108546, m_4 = -21.5346955,$
$m_5 = -443.455815, m_6 = 607.339582, m_7 = -368.790121, m_8 = 111.296674,$
$m_9 = -13.4122465$

In [71], another correlation can be found expressed based on the Sutherland equation form,

$$k_{air2} = \frac{2.334 \times 10^{-3} T_K^{3/2}}{164.54 + T_K}$$

Finally, in [72] and [73], the following equations are suggested for the thermal conductivity of air

$$k_{air3} = 1.5207 \times 10^{-11} T_K^3 - 4.8574 \times 10^{-8} T_K^2 + 1.0184 \times 10^{-4} T_K - 0.00039333$$

$$k_{air4} = 0.02624 \frac{T_K}{300}^{0.8646}$$

Validity : k_{air1} in (W/m.K); $70 < T_K < 1400$ K ;
$\qquad\quad k_{air2}$ in (W/m.K); $200 < T_K < 400$ K ;
$\qquad\quad k_{air4}$ in (W/m.K); $240 < T_K < 500$ K ;

Accuracy: $k_{air1} \pm 1.1\%$, $k_{air2} \pm 0.15\%$, $k_{air4} \pm 1\%$.

Specific Heat Capacity

According to [71], specific heat follows a quadratic relationship:

$$C_{p_1} = 1030.5 - 0.19975 T_K + 3.9734 \times 10^{-4} T_K^2$$

Finally, [72] suggested another correlation

$$C_{p_2} = 1002.5 + \left(275 \times 10^{-6} \left(T_K - 200 \right)^2 \right)$$

Validity : C_{p_1} and C_{p_2} in (J/kg K); $200 < T_K < 400K$;

Accuracy: $C_{p_1} \pm 0.15\%$, $C_{p_2} \pm 0.1\%$

Appendix B

Data Set and Simulation Results

B.1   Case Study No.1

General Info	
Cargo Type	DILUTED CRUDE OIL
Loaded Cargo Temperature [°C]	48.5
Heating Requirement	Heat Up & Maintain
Requirement Cargo Temperature [°C]	60
Total Heatup HSFO Consumption [MT]	66.2
Total Heatup LSFO Consumption [MT]	0
Total Heatup MGO Consumption [MT]	0
Total Maintain HSFO Consumption [MT]	36.8
Total Maintain LSFO Consumption [MT]	0
Total Maintain MGO Consumption [MT]	46.2
Total HSFO Consumption [MT]	103
Total LSFO Consumption [MT]	0
TotaL MGO Consumption [MT]	46.2
Heating Duration [hours]	143
Maintenance Duration [hours]	281
Total Duration [hours]	424
COTK fill ratio	61.8%
Cargo density at $15°C$ $[kg/m^3]$	960
Cargo viscosity	-

Table B.1: Case Study No.1 Data and Parameters

Heating Details										
UTCDT	Interval	Title	Temperature [C]		Total Boiler Consumption		Fuel Type	Average Cargo Temperature [C]	
			Sea	Air	for Heat Up[MT]	for Maintain [MT]		with Slop TK	without Slop TK
14/11/2017 3:00		Commenced Heatup	26	30	0	0		45.21	45.67
14/11/2017 16:00	13	In progress Heatup	27	29	2.5	0	HSFO	45.92	46.32
15/11/2017 16:00	24	In progress Heatup	25	30	9.5	0	HSFO	47.19	46.99
16/11/2017 16:00	24	In progress Heatup	25	30	13.5	0	HSFO	50.29	49.93
17/11/2017 16:00	24	In progress Heatup	25	29	11.1	0	HSFO	53.26	52.78
18/11/2017 16:00	24	In progress Heatup	25	29	12.7	0	HSFO	56.22	55.69
19/11/2017 16:00	24	In progress Heatup	26	28	13.7	0	HSFO	58.85	58.63
20/11/2017 2:00	10	Completed Heatup	27	28	3.2	0	HSFO	60.06	60.02
20/11/2017 2:00		Commenced Maintenance	27	28	0	0	HSFO	60.06	60.02
20/11/2017 16:00	14	In progress Maintenance	27	28	0	3.2	HSFO	60.03	59.98
21/11/2017 16:00	24	In progress Maintenance	29	29	0	10.3	HSFO	59.97	59.89
22/11/2017 16:00	24	In progress Maintenance	29	32	0	10.9	HSFO	60.12	60.10
23/11/2017 16:00	24	In progress Maintenance	29	31	0	10.3	HSFO	60.09	60.09
24/11/2017 16:00	24	In progress Maintenance	29	27	0	2.1	HSFO	59.95	59.99
25/11/2017 16:00	24	In progress Maintenance	24	27	0	5.5	MGO	59.95	59.97
26/11/2017 16:00	24	In progress Maintenance	18	17	0	10.5	MGO	59.99	59.98
27/11/2017 16:00	24	In progress Maintenance	18	14	0	10.7	MGO	60.10	60.13
28/11/2017 16:00	24	In progress Maintenance	18	18	0	11	MGO	59.89	59.91
29/11/2017 16:00	24	In progress Maintenance	17	20	0	3	MGO	59.23	59.24
30/11/2017 16:00	24	In progress Maintenance	18	21	0	3.1	MGO	59.66	59.62
1/12/2017 16:00	24	In progress Maintenance	17	20	0	2.1	MGO	59.75	59.75
1/12/2017 19:00	3	Completed Maintenance	0	0	0	0.3	MGO	59.85	0.00

Table B.2: Heating Logs for Case Study No.1

Noon Report Data

UTC From	UTC To	Time Interval	Draft AFT	Draft FWD	Draft Average	Vessel Status	Speed GPS [kn]	Speed LOG [kn]	Hull Course [deg]	Current Speed [kn] (Based On Maps)	Current Abs Direction	Wind Relative Speed [kn]	Wind Relative Direction [deg]	Composite Boiler Rhrs	Composite Boiler FOC	No1 Boiler Rhrs	No1 Boiler FOC	No1 Boiler FOC/Hour	No2 Boiler Rhrs	No2 Boiler FOC	No2 Boiler FOC/Hour	Total Boiler FOC
14/11/2017 16:00	15/11/2017 16:00	24	11.2	11.2	11.2	ANCHOR	0	0	0	0.5	N	5	80			24	13.7	0.571				13.7
15/11/2017 16:00	16/11/2017 16:00	24	11.2	11.2	11.2	ANCHOR	0	0	0	0.5	N	7	320			24	18.5	0.771				18.5
16/11/2017 16:00	17/11/2017 16:00	24	11.2	11.2	11.2	ANCHOR	0	0	0	0.5	N	7	330			24	16.1	0.671				16.1
17/11/2017 16:00	18/11/2017 16:00	24	11.2	11.2	11.2	ANCHOR	0	0	0	0.5	N	7	30			24	17.9	0.746				17.9
18/11/2017 16:00	19/11/2017 22:00	30	11.2	11.2	11.2	ANCHOR	0	0	0	0.5	N	7	75			29	23.1	0.797				23.1
19/11/2017 22:00	20/11/2017 00:00	2	11.2	11.2	11.2	MANOEUVER			0							0.4	0.2	0.5				0.2
20/11/2017 00:00	20/11/2017 16:00	16	11.2	11.2	11.2	SEAGOING	10.6	10.1	299	0.5	N	5	124									0
20/11/2017 16:00	21/11/2017 16:00	24	11.2	11.2	11.2	SEAGOING	13.3	12.4	299	0.5	W	4	100			22.5	10.3	0.458				10.3
21/11/2017 16:00	22/11/2017 16:00	24	11.2	11.2	11.2	SEAGOING	12	11.9	299	0.5	NW	2	120			24	10.9	0.454				10.9
22/11/2017 16:00	23/11/2017 16:00	24	11.2	11.2	11.2	SEAGOING	11	12.2	304	0.5	N	1	350			24	10.3	0.429				10.3
23/11/2017 16:00	24/11/2017 17:00	25	11.2	11.2	11.2	SEAGOING	11.9	11.5	343	1	N	0	20			3.2	2.1	0.656				2.1
24/11/2017 17:00	25/11/2017 17:00	24	11.2	11.2	11.2	SEAGOING	11.3	11.9	348	1	NE	25	355						12.5	5.5	0.44	5.5
25/11/2017 18:00	26/11/2017 15:30	21.5	11.2	11.2	11.2	SEAGOING	8.7	8	317	0.5	NE	7	100						21.5	9.8	0.456	9.8
26/11/2017 15:30	26/11/2017 17:00	1.5	11.2	11.2	11.2	MANOEUVER			0										1.5	0.7	0.467	0.7
26/11/2017 17:00	27/11/2017 18:00	25	11.2	11.2	11.2	ANCHOR	0	0	0	0.5	NE	12	350						25	12.2	0.488	12.2
27/11/2017 18:00	28/11/2017 18:00	24	11.2	11.2	11.2	ANCHOR	0	0	0	0.5	NE	10	355			21.5	11.3	0.526	2.5	1.3	0.52	12.6
28/11/2017 18:00	29/11/2017 12:00	18	11.2	11.2	11.2	ANCHOR	0	0	0	0.5	NE	10	355			6.8	3.7	0.544				3.7
29/11/2017 12:00	29/11/2017 17:00	5	11.2	11.2	11.2	MANOEUVER			0							0.9	0.5	0.556	0.3	0.2	0.667	0.7
29/11/2017 17:00	30/11/2017 18:00	25	8.85	3.95	6.4	BERTH	0	0	0							18.2	22	1.209	8	6.9	0.863	28.9
30/11/2017 18:00	1/12/2017 18:00	24	9.5	4.3	6.9	BERTH	0	0	0							12.6	11.1	0.881				11.1

Table B.3: Noon Reports for Case Study No.1

| UTC Date Time | | Time Interval | Temperatures | | Speed GPS [kn] | Speed LOG [kn] | Hull Course [deg] | Current | | Wind | | No1 Boiler | | | | No2 Boiler | | | | FO USED | OP MODE |
From	To		Sea	Air				Speed [kn] Based On Maps	Abs Direction	Relative Speed [kn]	Relative Direction [deg]	Running Hours	FOC	foc/hr	Load	Running Hours	FOC	foc/hr	Load		
14/11/2017 16:00	15/11/2017 16:00	24	26	29.5	0	0	0	0.5	0	5	80	24	13.7	0.570833333	29	0			0	HFO	2
15/11/2017 16:00	16/11/2017 16:00	24	25	30	0	0	0	0.5	0	7	320	24	18.5	0.770833333	41	0			0	HFO	2
16/11/2017 16:00	17/11/2017 16:00	24	25	29.5	0	0	0	0.5	0	7	330	24	16.1	0.670833333	34	0			0	HFO	2
17/11/2017 16:00	18/11/2017 16:00	24	25	29	0	0	0	0.5	0	7	30	24	17.9	0.745833333	39	0			0	HFO	2
18/11/2017 16:00	19/11/2017 16:00	24	25.5	28.5	0	0	0	0.5	0	7	75	24	19.05	0.79375	42	0			0	HFO	2
19/11/2017 16:00	20/11/2017 0:00	8	26.5	28	0	0	0	0.5	0	7	75	5	4.25	0.85	42	0			0	HFO	2
20/11/2017 0:00	20/11/2017 16:00	16	27	28	10.6	10.1	299	0.5	0	5	124	4	3.2	0.8	42	0			0	HFO	2
20/11/2017 16:00	21/11/2017 16:00	24	27	28	13.3	12.4	299	0.5	270	4	100	23	10.3	0.447826087	23	0			0	HFO	2
21/11/2017 16:00	22/11/2017 16:00	24	28	28.5	12	11.9	299	0.5	315	2	120	24	10.9	0.454166667	23	0			0	HFO	2
22/11/2017 16:00	23/11/2017 16:00	24	29	30.5	11	12.2	304	0.5	0	1	350	24	10.3	0.429166667	22	0			0	HFO	2
23/11/2017 16:00	24/11/2017 16:00	24	29	31.5	11.9	11.5	343	1	0	0	20	3	2.1	0.7	36	0			0	HFO	2
24/11/2017 16:00	25/11/2017 16:00	24	29	29	11.3	11.9	348	1	45	25	355	0			0	11	5.06	0.46	26	MGO	2
25/11/2017 16:00	26/11/2017 16:00	24	26.5	27	8.7	8	317	0.5	45	7	100	0			0	24	10.69	0.445416667	25	MGO	2
26/11/2017 16:00	26/11/2017 7:00	1	21	22	0	0	0	0.5	45	7	100	0			0	1	0.466	0.466	26	MGO	2
26/11/2017 7:00	27/11/2017 16:00	23	18	15.5	0	0	0	0.5	45	12	350	0			0	23	11.2	0.486956522	27	MGO	2
27/11/2017 16:00	28/11/2017 16:00	24	18	16	0	0	0	0.5	45	10	355	19	10	0.526315789	29	5	2.4	0.48	27	MGO	2
28/11/2017 16:00	29/11/2017 12:00	20	17.5	19	0	0	0	0.5	45	10	355	9	4.8	0.533333333	29	0			0	MGO	2
29/11/2017 12:00	29/11/2017 16:00	4	17.5	20.5	0	0	0	0.5	45	7	355	1	0.5	0.5	28	1	0.4	0.4	20	MGO	1

Table B.4: Amended Excel Table Used as Data Input for Simulation Purposes of Case Study No.1

a/a	Date	Data	DCO No.1	Error	DCO No.2	Error	DCO No.3	Error	FO Cons	
									Data	Simulation
0	14/11/2017 16:00	46.32	46.32	0.00%	46.32	0.00%	46.32	0.00%		
1	15/11/2017 16:00	46.99	48.23	2.64%	48.26	2.70%	48.28	2.74%	13.7	13.91
2	16/11/2017 16:00	49.93	51.59	3.34%	51.66	3.48%	51.68	3.52%	18	18.61
3	17/11/2017 16:00	52.78	53.91	2.15%	54.03	2.38%	54.08	2.47%	16.1	16.28
4	18/11/2017 16:00	55.69	56.63	1.68%	56.79	1.97%	56.86	2.10%	17.9	17.85
5	19/11/2017 16:00	58.63	59.56	1.58%	59.76	1.92%	59.85	2.08%	19.05	19.05
6	20/11/2017 16:00	59.98	59.43	0.92%	59.67	0.52%	59.81	0.29%	7.45	7.14
7	21/11/2017 16:00	59.89	59.62	0.45%	59.91	0.03%	60.11	0.36%	10.3	10.41
8	22/11/2017 16:00	60.10	60.05	0.08%	60.38	0.47%	60.64	0.90%	10.9	10.86
9	23/11/2017 16:00	60.09	60.6	0.85%	60.97	1.46%	61.27	1.96%	10.3	10.48
10	24/11/2017 16:00	59.99	59.5	0.82%	59.88	0.19%	60.22	0.38%	2.1	2.11
11	25/11/2017 16:00	59.97	58.95	1.70%	59.4	0.94%	59.77	0.33%	5.06	5.1
12	26/11/2017 16:00	59.98	59.47	0.86%	59.96	0.04%	60.37	0.64%	10.69	10.78
13	27/11/2017 16:00	60.13	59.76	0.61%	60.29	0.27%	60.75	1.04%	11.67	11.57
14	28/11/2017 16:00	59.91	60.34	0.72%	60.92	1.69%	61.41	2.51%	12.4	12.63
15	29/11/2017 16:00	59.24	59.43	0.32%	60.05	1.36%	60.6	2.29%	5.7	5.73
				1.17%		1.21%		1.48%	170.72	172.51

Table B.5: Case Study No.1 - Model Verification Simulation Results

B.2   Case Study No.2

Table B.6: Voyage Basic Parameters

General Info	
Cargo Type	FUEL OIL
Load Cargo Temperature [C]	54.7
Heating Requirement	Maintain at Load Temperature
Requirement Cargo Tempearature [C]	54.7
Total Consumption HSFO [MT]	138.8
Total Consumption ULSFO [MT]	116.7
Total Consumption MGO [MT]	26.8
Total Duration [hours]	637
COTK fill ratio or Ullage	54.6%
Cargo density @15C [kg/ m^3]	990
Cargo viscosity	-

Heating Details							
UTCDT	**Interval**	**Temperature**		**Total Boiler Consumption [MT]**	**Fuel Type Used**	**Average Cargo Temperature [C]**	
		Sea	**Air**			**with Slop TK**	**without Slop TK**
26/12/2017 12:00		4	3	0		54.36	54.38
27/12/2017 9:00	21	4	3	23.1	MGO	56.09	56.20
28/12/2017 9:00	24	4	3	3.7	MGO	57.79	58.00
				18.8	ULSFO		
29/12/2017 9:00	24	7	3	20.9	ULSFO	59.50	59.84
30/12/2017 9:00	24	7	4	17.6	ULSFO	58.48	58.54
31/12/2017 9:00	24	7	4	11.6	ULSFO	57.91	58.04
1/1/2018 9:00	24	8	5	5.2	ULSFO	57.74	57.83
2/1/2018 9:00	24	9	7	5.1	ULSFO	57.20	57.20
3/1/2018 9:00	24	11	7	5	ULSFO	56.45	56.43
4/1/2018 9:00	24	12	11	5.2	ULSFO	55.70	55.73
5/1/2018 9:00	24	12	11	4.2	ULSFO	55.10	55.13
				1.9	HSFO		
6/1/2018 9:00	24	14	10	8.7	HSFO	55.07	55.05
7/1/2018 9:00	24	15	11	8.6	HSFO	55.10	55.09
8/1/2018 9:00	24	15	14	8.6	HSFO	55.09	55.10
9/1/2018 9:00	24	14.5	12	8.5	HSFO	55.12	55.13
10/1/2018 9:00	24	16	15	8.6	HSFO	55.14	55.14
11/1/2018 9:00	24	15.5	14	8.5	HSFO	55.11	55.12
12/1/2018 9:00	24	16	13	7.7	ULSFO	55.09	55.08
13/1/2018 9:00	24	16	13	7.7	ULSFO	55.06	55.07
14/1/2018 9:00	24	16.5	14	7.7	ULSFO	55.02	55.03
15/1/2018 9:00	24	17	15	8.6	HSFO	54.99	54.98
16/1/2018 9:00	24	17	16	8.5	HSFO	54.99	54.96
17/1/2018 9:00	24	17.5	15	12.7	HSFO	54.90	54.88
18/1/2018 9:00	24	23.7	21	12.7	HSFO	54.95	54.94
19/1/2018 9:00	24	25.7	22	12.6	HSFO	54.96	54.95
20/1/2018 9:00	24	26	23	12.6	HSFO	55.17	55.20
21/1/2018 9:00	24	26	23	12.7	HSFO	55.15	55.18
22/1/2018 1:00	15	0	0	5	HSFO		

Table B.7: Case Study No.2 - Heating Logs

UTC Date Time From	To	Time Interval	Draft Aft	Draft Fwd	Draft Average	Vessel Status	Speed GPS [kn]	Speed LOG [kn]	Hull Course [deg]	Current Speed [kn] (Based On Maps)	Current Abs Dir.	Wind Rel. Speed [kn]	Wind Rel. Dir [deg]	Composite Boiler Rhrs	Composite Boiler FOC	No1 Boiler Rhrs	No1 Boiler FOC	No1 Boiler FOC/Hour	No2 Boiler Rhrs	No2 Boiler FOC	No2 Boiler FOC/Hour	Total Boiler FOC
26/12/2017 9:00	27/12/2017 8:00	23	11	11	11	BERTH	0	0	0					18	1.9	23	20.5	0.891				20.5
28/12/2017 10:00	29/12/2017 10:00	24	14.85	14.85	14.85	BERTH	0	0	0										24	26.6	1.108	26.6
29/12/2017 10:00	29/12/2017 14:20	4:20	14.85	14.85	14.85	BERTH	0	0	0										4.3	5	1.163	5
29/12/2017 14:20	29/12/2017 16:00	1:40	14.85	14.85	14.85	MANOEUVER													1.6	1.2	0.75	1.2
29/12/2017 16:00	30/12/2017 10:00	18	14.85	14.85	14.85	SEAGOING	12.4	12.3	213	0.1	SW	25	10						18	16.4	0.911	16.4
30/12/2017 10:00	31/12/2017 11:00	25	14.85	14.85	14.85	SEAGOING	11.9	11.9	255	0.1	SW	30	15						23	16.8	0.73	16.8
31/12/2017 11:00	1/1/2018 11:00	24	14.7	14.7	14.7	SEAGOING	12	12	30	0.1	SW	30	10									
1/1/2018 11:00	2/1/2018 11:00	24	14.7	14.7	14.7	SEAGOING	11.4	11.6	207	0.2	NW	30	10									
2/1/2018 11:00	3/1/2018 11:00	24	14.6	14.6	14.6	SEAGOING	11.5	11.6	205	0.2	W	45	5									
3/1/2018 11:00	4/1/2018 11:00	24	14.6	14.6	14.6	SEAGOING	10.1	10.4	258	0.3	SW	50	5									
4/1/2018 11:00	5/1/2018 11:00	24	14.6	14.6	14.6	SEAGOING	7.9	7.9	209	0.2	SW	45	10			3.5	3.5	1				3.5
5/1/2018 11:00	6/1/2018 11:00	24	14.6	14.6	14.6	SEAGOING	9.6	9.4	209	0.2	N	15	90			24	22.3	0.929				22.3
6/1/2018 11:00	7/1/2018 11:00	24	14.6	14.6	14.6	SEAGOING	11.1	10.7	180	0.4	N	15	180			24	19.8	0.825				19.8
7/1/2018 11:00	8/1/2018 11:00	24	14.6	14.6	14.6	SEAGOING	11.1	10.8	167	0.3	N	10	160			22.5	8.6	0.382				8.6
8/1/2018 11:00	9/1/2018 6:00	19	14.6	14.6	14.6	SEAGOING	12.1	12.1	71	0.1	NW	20	5									
9/1/2018 9:30	9/1/2018 19:00	9:30	14.6	14.6	14.6	ANCHOR	0	0	0	0.1	NW	10	10	9.5	0.9							
9/1/2018 19:00	9/1/2018 21:00	2	14.6	14.6	14.6	MANOEUVER			0					2	0.2							
9/1/2018 19:00	9/1/2018 21:00	2	14.6	14.6	14.6	MANOEUVER			0					2	0.3							
9/1/2018 21:00	10/1/2018 11:00	14	14.6	14.6	14.6	SEAGOING	12.9	12.6	73	0.2	W	5	90									
10/1/2018 11:00	11/1/2018 11:00	24	14.6	14.6	14.6	SEAGOING	12.6	12.3	85	0.3	N	15	150									
11/1/2018 11:00	12/1/2018 11:00	24	14.6	14.6	14.6	SEAGOING	12	11.7	104	0.3	W	15	160									
12/1/2018 11:00	13/1/2018 10:00	23	14.6	14.6	14.6	SEAGOING	12.6	12.3	107	0.3	SW	5	100									
13/1/2018 10:00	14/1/2018 10:00	24	14.6	14.6	14.6	SEAGOING	11.9	12.1	107	0.2	NW	10	60									
14/1/2018 10:00	15/1/2018 10:00	24	14.6	14.6	14.6	SEAGOING	11.6	11.8	107	0.2	NW	10	60			24	18.1	0.754				18.1
15/1/2018 10:00	16/1/2018 10:00	24	14.6	14.6	14.6	SEAGOING	12.1	12.1	123	0	SE	5	30			23	22	0.957				22
16/1/2018 10:00	16/1/2018 11:30	1:30	14.65	14.65	14.65	MANOEUVER			0							1.5	1.2	0.8				1.2
16/1/2018 11:30	17/1/2018 1:30	14	14.65	14.65	14.65	ANCHOR	0	0	0	0.1	NW	10	90			14	8.9	0.636				8.9
17/1/2018 1:30	17/1/2018 16:00	14:30	14.65	14.65	14.65	MANOEUVER	0	0	0							14.5	9.8	0.676				9.8
17/1/2018 16:00	18/1/2018 10:00	18	14.65	14.65	14.65	SEAGOING	12.8	12.8	140	0	SW	5	100			18	11.5	0.639				11.5
18/1/2018 10:00	19/1/2018 9:00	23	14.55	14.55	14.55	SEAGOING	12.3	12.4	146	0.1	W	10	60			23	9.7	0.422				9.7
19/1/2018 9:00	19/1/2018 18:00	9	14.6	14.6	14.6	SEAGOING	11.4	11.8	116	0.4	SW	5	90			9	3.7	0.411				3.7
19/1/2018 18:00	19/1/2018 20:30	2:30	14.6	14.6	14.6	MANOEUVER	0	0	0							2.5	1.6	0.64				1.6
19/1/2018 20:30	20/1/2018 3:30	7	14.6	14.6	14.6	ANCHOR	0	0	0	0	NW	15	10			7	3.3	0.471				3.3
20/1/2018 3:30	20/1/2018 7:00	3:30	14.6	14.6	14.6	MANOEUVER	0	0	0							3.5	1.8	0.514				1.8
20/1/2018 7:00	20/1/2018 9:00	2	14.6	14.6	14.6	BERTH	0	0	0							2	0.8	0.4				0.8
20/1/2018 9:00	22/1/2018 9:00	48	14.6	14.6	14.6	BERTH	0	0	0													
		48	8.3	6.3	7.3		0	0	0	0				2.7	0.2	46	25	0.543	48	31	0.646	56

Table B.8: Case Study No.2 - Noon Reports

UTCDT	Interval	Temperature		Speed GPS [kn]	Speed LOG [kn]	Hull Course [deg]	Current		Wind		Boiler No1			Boiler No2			Op.Mode
		Sea	Air				Speed [kn] Based On Maps	Abs Dir.	Rel. Speed [kn]	Rel. Dir [deg]	Load	Rhrs	Fuel	Load	Rhrs	Fuel	
26/12/2017 12:00		4	3	0	0	0	0	0	2	0							
27/12/2017 9:00	21	4	3	0	0	0	0.05	0	10	60	0	0	HFO	0	0	HFO	0
28/12/2017 9:00	24	4	3	0	0	0	0.05	0	10	120	0	0	HFO	0	0	HFO	0
29/12/2017 9:00	24	5.5	3	0	0	0	0.05	0	10	170	48	23	HFO	0	0	HFO	2
29/12/2017 16:00	7	6.3	3.3	0	0	0	0.05	0	10	250	38	7	HFO	0	0	HFO	2
30/12/2017 9:00	17	7	3.5	12.4	12.3	213	0.1	225	25	10	38	17	HFO	0	0	HFO	2
31/12/2017 9:00	24	7	4	11.9	11.9	255	0.1	225	30	15	25	24	HFO	0	0	HFO	2
1/1/2018 9:00	24	7.5	4.5	12	12	30	0.1	225	30	10	50	6	HFO	0	0	HFO	2
2/1/2018 9:00	24	8.5	6	11.4	11.6	207	0.2	315	30	10	50	5	HFO	0	0	HFO	2
3/1/2018 9:00	24	10	7	11.5	11.6	205	0.2	270	45	5	50	5	HFO	0	0	HFO	2
4/1/2018 9:00	24	11.5	9	10.1	10.4	258	0.3	225	50	5	50	6	HFO	0	0	HFO	2
5/1/2018 9:00	24	12	11	7.9	7.9	209	0.2	225	45	10	79	4	HFO	0	0	HFO	2
6/1/2018 9:00	24	13	10.5	9.6	9.4	209	0.2	0.1	15	90	18	24	HFO	0	0	HFO	2
7/1/2018 9:00	24	14.5	10.5	11.1	10.7	180	0.4	0	15	180	18	24	HFO	0	0	HFO	2
8/1/2018 9:00	24	15	12.5	11.1	10.8	167	0.3	0	10	160	18	24	HFO	0	0	HFO	2
9/1/2018 6:00	21	14.75	13	12.1	12.1	71	0.1	315	20	5	50	8	HFO	0	0	HFO	2
9/1/2018 9:00	3	14.75	13	0	0	0	0.1	315	15	5	0	0	HFO	0	0	HFO	0
9/1/2018 21:00	12	15	13.3	0	0	0	0.1	315	10	10	0	0	HFO	0	0	HFO	0
10/1/2018 9:00	12	15.25	13.5	12.9	12.6	73	0.2	270	5	90	50	9	HFO	0	0	HFO	2
11/1/2018 9:00	24	15.75	14.5	12.6	12.3	85	0.3	0	15	150	50	9	HFO	0	0	HFO	2
12/1/2018 9:00	24	15.75	15.5	12	11.7	104	0.3	270	15	160	50	8	HFO	0	0	HFO	2
13/1/2018 9:00	24	16	15.5	12.6	12.3	107	0.3	225	5	100	50	8	HFO	0	0	HFO	2
14/1/2018 9:00	24	16.25	13.5	11.9	12.1	107	0.2	315	10	60	50	8	HFO	0	0	HFO	2
15/1/2018 9:00	24	16.75	14.5	11.6	11.8	107	0.2	315	10	60	19	23	HFO	0	0	HFO	2
16/1/2018 9:00	24	17	15.5	12.1	12.1	123	0	135	5	30	18	24	HFO	0	0	HFO	2
16/1/2018 10:00	1	17	15.5	12.1	12.1	123	0	135	5	30	27	1	HFO	0	0	HFO	2
17/1/2018 9:00	23	17.25	15.5	0	0	0	0.05	315	10	90	27	23	HFO	0	0	HFO	2
17/1/2018 16:00	7	18.9	16.8	0	0	0	0.05	315	10	90	28	6	HFO	0	0	HFO	2
18/1/2018 9:00	17	20.6	18	12.8	12.8	140	0	225	5	100	28	17	HFO	0	0	HFO	2
19/1/2018 9:00	24	24.7	21.5	12.3	12.4	146	0.1	270	10	60	27	24	HFO	0	0	HFO	2
19/1/2018 18:00	9	25.4	22	11.4	11.8	116	0.4	225	5	90	27	9	HFO	0	0	HFO	2
20/1/2018 9:00	15	26	22.5	0	0	0	0.05	315	15	10	27	15	HFO	0	0	HFO	2

Table B.9: Case Study No.2 – Amended Noon Reports

Days	Date	Average Cargo Temperature		Percentage Error		FO CONS	
		Data	Sim Results			Data	Sim
0	28/12/2017 9:00	58.00	58.00	-		-	-
1	29/12/2017 9:00	59.84	61.14	2.17%		20.9	20.78
2	30/12/2017 9:00	58.54	62.82	7.31%		17.6	17.538
3	31/12/2017 9:00	58.04	62.47	7.63%		11.6	11.616
4	1/1/2018 9:00	57.83	61.26	5.93%		5.2	5.64
5	2/1/2018 9:00	57.20	59.95	4.81%		5.1	4.7
6	3/1/2018 9:00	56.43	58.68	3.99%		5	4.7
7	4/1/2018 9:00	55.73	57.74	3.61%		5.2	5.64
8	5/1/2018 9:00	55.13	57.03	3.45%		6.1	6.0824
9	6/1/2018 9:00	55.05	56.45	2.54%		8.7	8.88
10	7/1/2018 9:00	55.09	56.21	2.03%		8.6	8.88
11	8/1/2018 9:00	55.10	56.2	2.00%		8.6	8.88
12	9/1/2018 9:00	55.13	56.24	2.01%		8.5	8.46
13	10/1/2018 9:00	55.14	56.69	2.81%		8.6	8.46
14	11/1/2018 9:00	55.12	56.86	3.16%		8.5	8.46
15	12/1/2018 9:00	55.08	56.8	3.12%		7.7	7.52
16	13/1/2018 9:00	55.07	56.88	3.29%		7.7	7.52
17	14/1/2018 9:00	55.03	56.98	3.54%		7.7	7.52
18	15/1/2018 9:00	54.98	56.95	3.58%		8.6	8.932
19	16/1/2018 9:00	54.96	57.13	3.95%		8.5	8.88
20	17/1/2018 9:00	54.88	58.58	6.74%		12.7	12.48
21	18/1/2018 9:00	54.94	59.78	8.81%		12.6	12.644
22	19/1/2018 9:00	55.20	61.05	10.60%		12.6	12.48
23	20/1/2018 9:00	54.95	62.37	13.50%		12.7	12.48
				Overall	OOE data points excepted	Total	
				4.79%	3.33%	219	219.18

Table B.10: Case Study No.2 - Model Verification Simulation Results for the entire voyage. Days marked in red represent data points which are out of expectations (OOE data points.)

Days	Date	Average Cargo Temperature		Percentage Error		FO CONS	
		Data	Sim Results			Data	Sim
0	28/12/2017 9:00	58.00	58				
1	29/12/2017 9:00	59.84	61.14				
	29/12/2017 16:00	59.50	59.50				
2	30/12/2017 9:00	58.54	60.76	3.79%		12.44	12.4
3	31/12/2017 9:00	58.04	60.54	4.31%		11.6	11.616
4	1/1/2018 9:00	57.83	59.44	2.78%		5.2	5.64
5	2/1/2018 9:00	57.20	58.24	1.82%		5.1	4.7
6	3/1/2018 9:00	56.43	57.07	1.13%		5	4.7
7	4/1/2018 9:00	55.73	56.23	0.90%		5.2	5.64
8	5/1/2018 9:00	55.13	55.60	0.85%		6.1	6.0824
9	6/1/2018 9:00	55.05	55.11	0.11%		8.7	8.88
10	7/1/2018 9:00	55.09	54.94	0.27%		8.6	8.88
11	8/1/2018 9:00	55.10	54.94	0.29%		8.6	8.88
12	9/1/2018 9:00	55.13	55.11	0.04%		8.5	7.52
13	10/1/2018 9:00	55.14	55.62	0.88%		8.6	8.46
14	11/1/2018 9:00	55.12	55.86	1.34%		8.5	8.46
15	12/1/2018 9:00	55.08	55.86	1.42%		7.7	7.52
16	13/1/2018 9:00	55.07	55.99	1.67%		7.7	7.52
17	14/1/2018 9:00	55.03	56.14	2.02%		7.7	7.52
18	15/1/2018 9:00	54.98	56.15	2.13%		8.6	8.932
19	16/1/2018 9:00	54.96	56.38	2.58%		8.5	8.88
				Overall	OOE exc.	Total	
				1.57%	1.26%	142.34	142.23

Table B.11: Case Study No.2 - Simulation Results excluding the OOE data points at the final days of the voyage

Appendix C

Thermal Resistance Analogy

For the special case of one-dimensional heat transfer with no internal energy generation and with constant properties, an analogy exists between the diffusion of heat and electrical charge. Consider the example of heat transfer through a plane wall, shown in Fig.C.1.
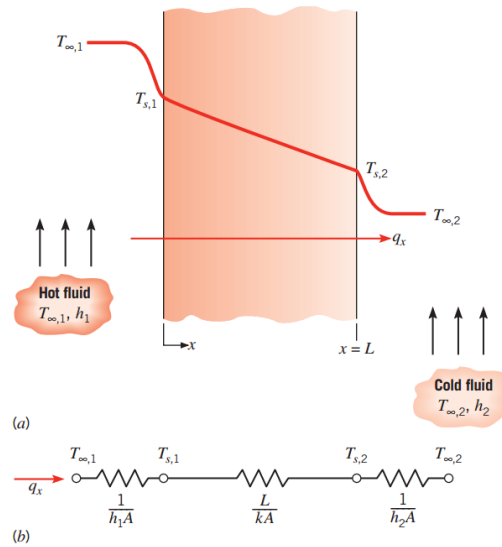

Figure C.1: Heat Transfer through a plane wall, Bergman et al., 2011

According to Fourier's Law for heat conduction, the heat flux q_x'' (W/m^2) is the heat transfer rate in the x-direction per unit area perpendicular to the direction of transfer and is given by the equation

$$q_x'' = -k \frac{dT}{dx}$$

The parameter k is a transport property known as the thermal conductivity (W/mK) and is a characteristic of the wall material. We notice that the heat flux is proportional to the temperature gradient, dT/dx, in the x-direction. The minus sign is a consequence of the fact that heat is transferred in the direction of decreasing temperature. Under steady-state conditions the temperature gradient may be expressed as:

$$\frac{dT}{dx} = \frac{T_{s,2} - T_{s,1}}{L}$$

and the heat flux is then

$$q_x'' = -k\frac{T_{s,2} - T_{s,1}}{L} = k\frac{T_{s,1} - T_{s,2}}{L} = k\frac{\Delta T}{L}$$

Thus the heat rate by conduction, q_x (W), through a plane wall of area A is

$$q_x = kA\frac{T_{s,1} - T_{s,2}}{L} = kA\frac{\Delta T}{L} \tag{C.1}$$

Just as an electrical resistance is associated with the conduction of electricity, a thermal resistance may be associated with the conduction of heat. Defining resistance as the ratio of a driving potential to the corresponding transfer rate, it follows from equation C.1 that the thermal resistance for conduction in a plane wall is

$$R_{t,cond} = \frac{T_{s,1} - T_{s,2}}{q_x} = \frac{L}{kA} \tag{C.2}$$

where in an electric network, Ohm's law provides an electrical resistance of the form

$$R_e = \frac{V_1 - V_2}{I} = \frac{L}{\sigma A} \tag{C.3}$$

The analogy between equations C.2 and C.3 is obvious. A thermal resistance may also be associated with heat transfer by convection at a surface. From Newtons law of cooling,

$$q = hA(T_s - T_\infty)$$

The thermal resistance for convection is then

$$R_{t,conv} = \frac{T_s - T_\infty}{q} = \frac{1}{hA} \tag{C.4}$$

Circuit representations provide a useful tool for both conceptualizing and quantifying heat transfer problems. The equivalent thermal circuit for the plane wall with convection surface conditions is shown in Figure C.1b. The heat transfer rate may be determined from separate consideration of each element in the network. Since q_x is constant throughout the network, it follows that

$$q_x = \frac{T_{\infty,1} - T_{s,1}}{1/h_1 A} = \frac{T_{s,1} - T_{s,2}}{L/kA} = \frac{T_{s,2} - T_{\infty,2}}{1/h_2 A} \tag{C.5}$$

In terms of the overall temperature difference, $T_{\infty,1} - T_{\infty,2}$, and the total thermal resistance, R_{tot}, the heat transfer rate may also be expressed as

$$q_x = \frac{T_{\infty,1} - T_{\infty,2}}{R_{tot}} \tag{C.6}$$

Because the conduction and convection resistances are in series and may be summed, it follows that

$$R_{tot} = \frac{1}{h_1 A} + \frac{L}{kA} + \frac{1}{h_2 A} \tag{C.7}$$

It is evident that all we need to calculate the heat transfer rate is the overall temperature difference and the total thermal resistance. With composite systems, it is often convenient to work with an overall heat transfer coefficient U, which is defined by an expression analogous to Newtons law of cooling. Accordingly,

$$q_x \equiv UA\Delta T \tag{C.8}$$

where ΔT is the overall temperature difference. The overall heat transfer coefficient is related to the total thermal resistance, and from Equations C.6 and C.8 we see that $U = 1/R_{tot}A$. Hence, for any complex arrangement we may write

$$Q_x = \frac{T_{\infty,1} - T_{\infty,2}}{R_{tot}} \tag{C.9}$$

Appendix D

Heat Transfer from Extended Surfaces

The term extended surface is commonly used to depict an important special case involving heat transfer by conduction within a solid and heat transfer by convection (and/or radiation) from the boundaries of the solid. Until now, we have considered heat transfer from the boundaries of a solid to be in the same direction as heat transfer by conduction in the solid. In contrast, for an extended surface, the direction of heat transfer from the boundaries is perpendicular to the principal direction of heat transfer in the solid.

An extended surface typically enhances heat transfer between a solid and an adjoining fluid, as it increases the surface area across which convection occurs. The thermal conductivity of the fin material can have a strong effect on the temperature distribution along the fin and therefore influences the degree to which the heat transfer rate is enhanced. Ideally, the fin material should have a large thermal conductivity to minimize temperature variations from its base to its tip. In the limit of infinite thermal conductivity, the entire fin would be at the temperature of the base surface, thereby providing the maximum possible heat transfer enhancement.

Inside the double hull area, stiffeners are considered to be extended surfaces. The characteristic shape at the tip of each stiffener (angle or tee) will be neglected and all stiffeners will be treated as fins with uniform rectangular cross-sectional area. Also we choose to assume that heat flow is one-dimensional (from the base of the fin to the top, x-direction), even though conduction within the fin is actually two-dimensional. In practice the fin is thin, and temperature changes in the transverse direction are small, compared with the temperature difference between the fin and the environment. Hence, we may assume that the temperature is uniform across the fin thickness and that it is only a function of x. Also we will consider:

- steady-state conditions

- that the thermal conductivity of the extended surface is constant

- that the convection heat transfer coefficient h is uniform over the prime surfaces and the finned surfaces.

As mentioned above, fins were assumed to be straight and have a uniform rectangular cross-sectional area (D.1a). Each fin is attached to a base surface of temperature $T(0) = T_b$ and extends into a fluid of temperature T_∞. If we consider A_s to be the surface area measured from the base to x, then $A_s = Px$, where P is the fin perimeter and A_c is constant.

(a) Straight fin of uniform
cross-section

(b) Fin Array and thermal circuit.
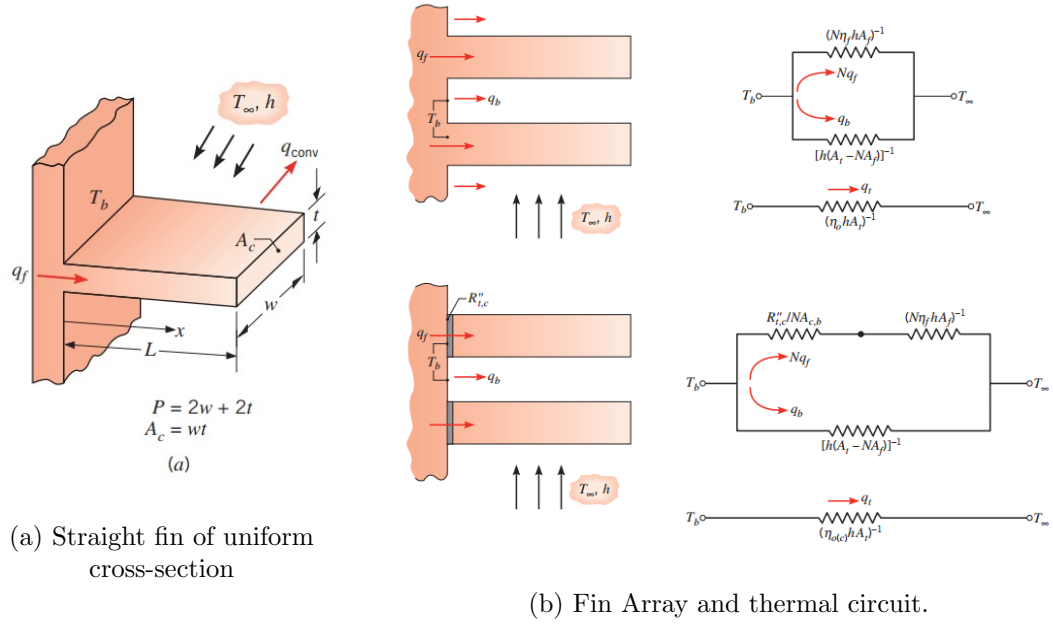
For heat transfer from a straight rectangular fin with an active tip, it has been shown that approximate, yet accurate, predictions may be obtained by using the adiabatic tip result, with a corrected fin length of the form $L_c = L + t/2$ for a rectangular fin. The correction is based on assuming equivalence between heat transfer from the actual fin with tip convection and heat transfer from a longer, hypothetical fin with an adiabatic tip. By making use of the thermal resistance analogy, we can infer an expression for the thermal resistance of a fin array (according to Incropera [2])

$$R_{t,o} = \frac{1}{n_o h A_t} \tag{D.1}$$

where:

- $R_{t,o}$ is an effective resistance

- n_o is the overall surface efficiency and

- A_t is the total surface area

The effective resistance $R_{t,o}$ accounts for parallel heat flow paths by conduction / convection in the fins and by convection from the prime surface. FigureD.1b illustrates the thermal circuits corresponding to the parallel paths and their representation in terms of an effective resistance. If fins are machined as an integral part of the wall from which they extend, there is no contact resistance at their base. However, more commonly, fins are manufactured separately and are attached to the wall by a metallurgical or adhesive joint. In such cases, there is a thermal contact resistance $R_{t,c}$, which may adversely influence overall thermal performance. Although the extended surfaces are currently welded upon the base plate, we will assume that $R_{t,c} = 0$ and heat transfer by conduction is made as if they were integrated to the plate.

The overall surface efficiency n_o characterizes an array of fins and the base surface to which they are attached and it is the fraction of the total heat rate (q_t) from the surface area A_t to the maximum possible heat rate that would result if the entire fin surface, as well as the exposed base, were maintained at the base temperature T_b. Thus

$$n_o = \frac{q_t}{q_{max}} = \frac{q_t}{h A_t T_b} \tag{D.2}$$

If there are N fins in the array, each of surface area A_f, the total surface area A_t would be equal to the summation of the finned surfaces and of the exposed portion of the base, here designated as A_b (often termed as the prime surface). The total rate of heat transfer by convection from the fins and the prime (unfinned) surface may be expressed as

$$q_t = Nn_f hA_f T_b + hA_b T_b = h[Nn_f A_f + (A_t - NA_f)]T_b \Leftrightarrow$$

$$q_t = hA_t[1 - \frac{NA_f}{A_t}(1 - n_f)]T_b$$

(D.3)

Consequently we can proceed from equationsD.2 and D.3 that the overall surface coefficient is equal to:

$$n_o = [1 - \frac{NA_f}{A_t}(1 - n_f)]$$

(D.4)

For a straight fin of uniform cross section and an adiabatic tip, the fin efficiency n_f

$$n_f = \frac{tanhmL}{mL}$$

(D.5)

where :

$$m = \sqrt{\frac{hP}{kA_c}}$$

(D.6)

Appendix E

Equivalent Thermal Circuits
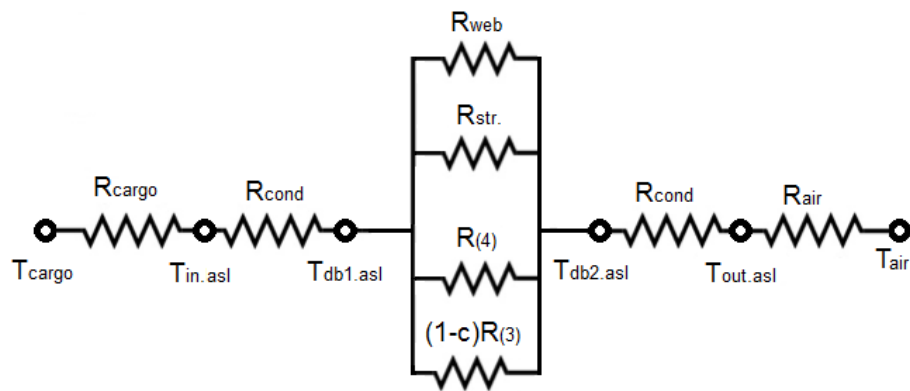
Figure E.1: Thermal circuit for heat transfer above sealevel
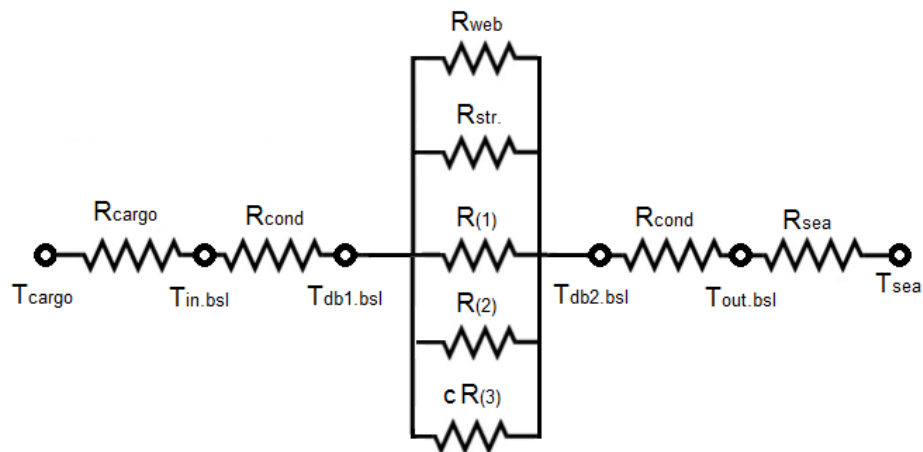
Figure E.2: Thermal circuit for heat transfer below sealevel
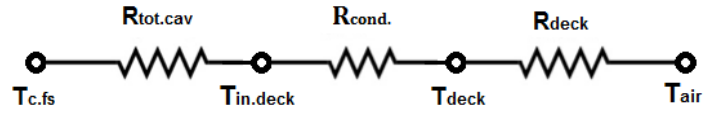
Figure E.3: Thermal circuit for heat losses towards ship's deck
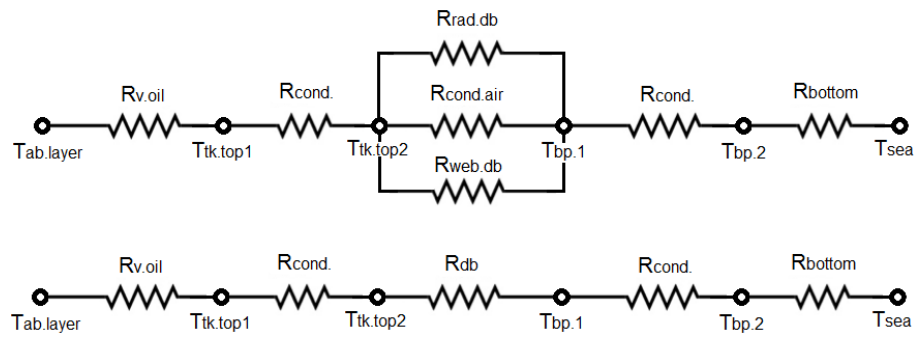
Figure E.4: Prime and equivalent thermal circuit for heat losses towards the ship's bottom
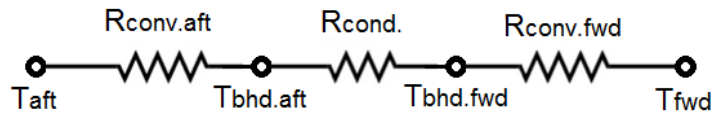
Figure E.5: Thermal circuit for adjacent tanks
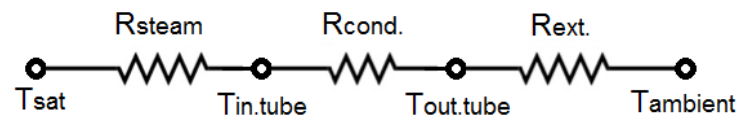
Figure E.6: Thermal circuit for pipe

Appendix F

Pressure Drop Along Pipeline

Pressure Drop of Two Phase Flow in Straight Pipe

The pressure drop in the annular flow is calculated by [38]:

$$\frac{dP}{dz} = \left(\frac{dP}{dz}\right)_f + \left(\frac{dP}{dz}\right)_m + \left(\frac{dP}{dz}\right)_g \tag{F.1}$$

where the three terms refer to friction, momentum and, if the flow is not horizontal, gravity, which are calculated from the following relations:

$$\left(\frac{dP}{dz}\right)_f = -0.09(1 + 2.85X_{tt}^{0.523})^2 \frac{\mu_g^{0.2}(Gx)^{1.8}}{\rho_g D^{1.2}} \tag{F.2}$$

$$\left(\frac{dP}{dz}\right)_m = -\frac{G^2}{\rho_g}\frac{dx}{dz}\left[2x \ + \ (1-2x)(\frac{\rho_g}{\rho_l})^{1/3} \ + \ (1-2x)(\frac{\rho_g}{\rho_l})^{2/3} - (2-2x)(\frac{\rho_g}{\rho_l})\right] \tag{F.3}$$

$$\left(\frac{dP}{dz}\right)_g = gsin\theta\big[\alpha\rho_g + (1-\alpha)\rho_l\big] \tag{F.4}$$

$$\frac{1}{\alpha} = 1 + \frac{1-x}{x}\left(\frac{\rho_g}{\rho_l}\right)^{2/3} \tag{F.5}$$

where α is the void fraction and θ the angle of the tube from the horizontal. For a horizontal tube, $sin\theta$ and $(dP/dz)_g$ are both zero. Note that this pressure drop may be large enough to produce a drop in T_{sat}.

Pressure Drop of Two Phase Flow due to Fittings and Valves

Furthermore, an added factor to the total pressure drop along each pipeline is the existence of fittings such as bends and/or pipe reductions, as well as the valves used to control the steam mass flow rate in each tank. The latter is caused due to obstructions and sudden or gradual changes in the cross-section of the flow path. For two-phase flow, we made use of the general method of equivalent lengths as described in Crane Co. [40]. That was because it is the most convenient method to use with general application in two phase flow systems, without any restrictions. In addition to this, steam condensation estimation methods already have a high level of inaccuracy, so we aim to acquire a brief evaluation of the pressure drop caused by the liquid-vapor mixture. Equivalent-length method expresses the flow resistance of valves and fittings in terms of length of the same

size of pipe. The total summation of the actual run of pipe plus the equivalent lengths for the valves and fittings, results in the length used during the calculations of pressure losses. Tables in pages 120-122 of the appendix show equivalent lengths for various valves and fittings arrangements.

Pressure Drop of Condensate Flow (single phase)

When a liquid flows through a pipe, the pressure drops. This is caused by the viscous forces within the liquid and by the turbulence that occur along the internal walls of the pipe, caused by the roughness of the pipe material. This resistance is usually known as pipe friction and is measured on meters head, thus the term head loss is used to express the resistance to flow. The Bernoulli theorem is a means of expressing the application of the law of energy conservation to nonviscous, incompressible fluids which do not exchange shaft work with their surroundings. In real flow systems, Bernoulli equation must be supplemented by a term that expresses any energy alterations. Thus, an energy balance equations may be written for two points in a fluid,

$$\frac{u_1{}^2}{2g} + \frac{p_1}{\rho_1 g} + z_1 = \frac{u_2{}^2}{2g} + \frac{p_2}{\rho_2 g} + z_2 + H_L \tag{F.6}$$

where (H_L) is the pipe friction loss from point 1 to point 2.

The general equation for pressure drop, known as Darcy-Weisbach formula is expressed in metres of fluid (m), but it can be rewritten to express pressure drop in newtons per square meter (Pa) by substitution of proper units as follows:

$$h_L = f \frac{L}{D} \frac{v^2}{2g} \Leftrightarrow \Delta P_f = f \frac{L}{D} \frac{\rho v^2}{2} \tag{F.7}$$

The Darcy equation is valid for laminar or turbulent flow of any liquid inside a pipe, with the exception of extreme velocities, which create cavitations as the downstream pressure drops to the vapour pressure of the liquid. In equation Eq.F.7, f is a dimensionless coefficient, called the friction factor and can be obtained from the Moody diagram (see appendix) or from the following correlations proposed by Petukhov [61] and Haaland [62] respectively.

For fully developed laminar flow,

$$f = \frac{64}{Re_D} \tag{F.8}$$

while for fully developed turvulent flow, the correlations are more complicted and based on experimental results

$$f = (0.790 \, lnRe_D - 1.64)^{-2} \tag{F.9}$$

$$f = \left(-1.8 log \left[\frac{6.9}{Re} + (\frac{\epsilon/D}{3.7})^{1.11} \right] \right)^{-2} \tag{F.10}$$

where ϵ is the absolute roughness of the pipe. For drawn brass pipes, absolute roughness is equal to $\epsilon = 0.0015 mm$.

Friction loss in pipe is sensitive to changes in diameter and roughness of pipe. For a given rate of flow and a fixed friction factor, the pressure drop per meter of pipe varies inversely with the fifth power of the diameter. Therefore, a 2% reduction of diameter causes an 11% increase in pressure drop. The roughness of the pipe may be expected to increase with use (due to corrosion or incrustation) however in this thesis we are going

to ignore that kind of phenomena, and neglect the effects of ageing and use on the pipe friction.

Pressure Drop of Condensate Flow due to Fittings

Pressure losses which occur in piping systems due to bends, elbows, joints, valves and so forth are called form losses. When a fluid is flowing steadily in a long straight pipe of uniform diameter, the flow pattern, as indicated by the velocity distribution across the pipe diameter, will develop a certain characteristic form. Any impediment in the pipe which changes the direction of the stream will alter the characteristic flow pattern and create turbulence, causing an energy loss greater than that normally accompanying flow in straight pipe. Because valves and fittings in a pipeline disturb the flow pattern, they produce an additional pressure drop.

Velocity in a pipe is obtained at the expense of static head, and decrase in static head due to velocity is $h_L = v^2/2g$, which is defined as the "velocity head" or "dynamic head". Flow through a valve or fitting in a pipe line also causes a reduction in velocity head. The resistance coefficient K in the equation

$$h_L = K\frac{v^2}{2g} \tag{F.11}$$

therefore, is defined as the number of velocity heads lost due to a valve or fitting. The resistance coefficient K is considered as being independent of friction factor or Reynolds number, and may be treated as a constant for any given obstruction in a piping system, under all conditions of flow. The same loss as that of equation Eq.F.11 is expressed by the Darcy equation Eq.F.7 in straight pipe. It follows that form losses may also be expressed as

$$f\frac{L}{D}\frac{v^2}{2g} = K\frac{u^2}{2g} \Leftrightarrow K = f\frac{L}{D} \tag{F.12}$$

where the ratio L/D is the equivalent length, in pipe diameters of straight pipe, that will cause the same pressure drop as the obstruction under the same flow conditions. Since the resistance coefficient K is constant for all conditions of flow, the value L/D for any given valve or fitting must necessarily vary inversely with the change in friction factor for different flow conditions.

In a bend, the total resistance or head loss h_t is conventionally assumed to consist of

1. the loss due to curvature, h_c

2. the excess loss in the downstream tangent, h_p

3. the loss due to length, h_L thus

$$h_t = h_p + h_c + h_L \tag{F.13}$$

If:

$$h_b = h_p + h_c$$

then

$$h_t = h_b + h_L$$

Similarly to equation F.12, the quantity h_b can be expressed as a function of velocity head, but now the resistance coefficient K is called the bend coefficient, K_b. Hence

$$h_b = K_b \frac{v^2}{2g} \tag{F.14}$$

According to Beij [41], K_b is strongly related to the relative radius of a bend, which is the ratio of the radius of the bend axis to the internal diameter of the pipe (r/d). The loss due to continuous bends greater than 90 degrees, such as pipe coils, is less than the summation of losses in the total number of 90 degree bends contained in the coil, considered seperately, because the head loss h_p occurs only once in the coil. In the absence of experimental data, it is assumed that $h_p = h_c$. On this basis, the total value of K for a pipe coil made up of continuous 90 degree bends can be determined

$$K_B = (n-1)(0.25 \ f_T \ \pi \frac{r}{d} + 0.5K_1) + K_1 \tag{F.15}$$

where subscript 1 defines the value of K for one 90 degree bend and subscript T refers to flow in zone of complete turbulence. The resistance coefficient K method is more complex, but it may be more accurate than the equivalent-lengths method.

Appendix G

Boiler's Performance Curve
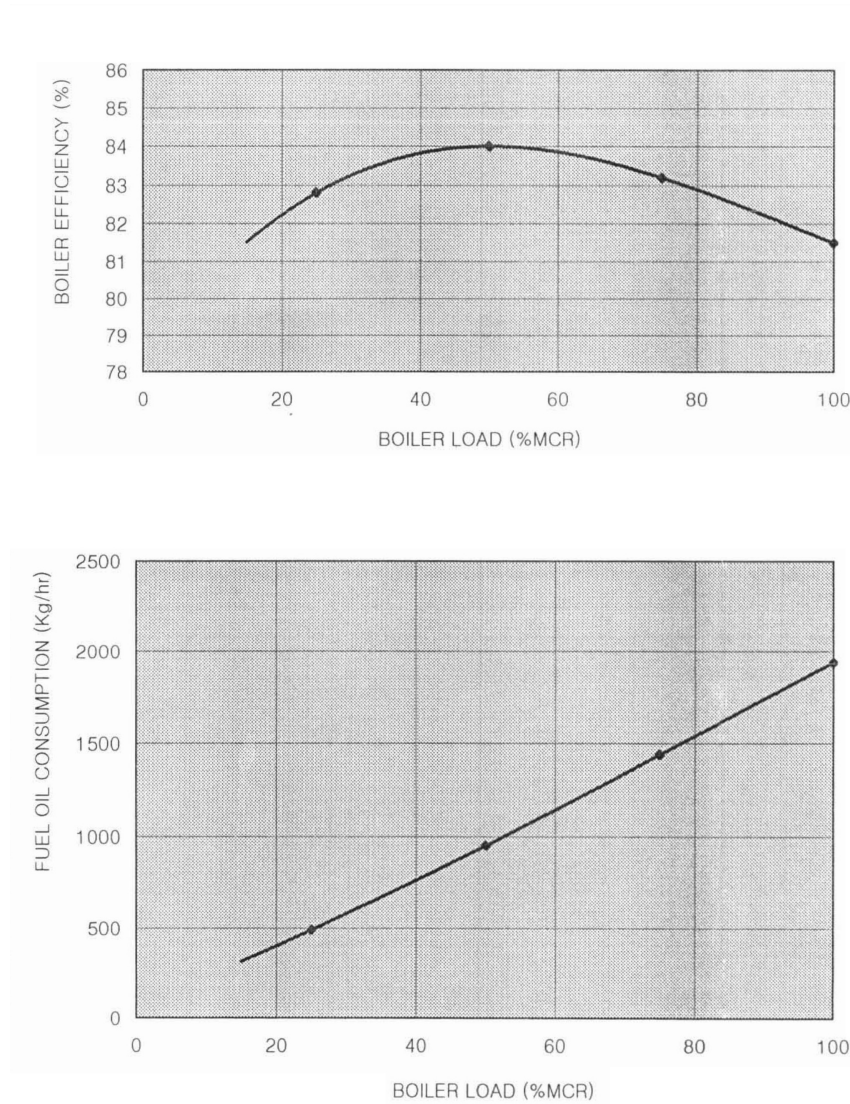
Figure G.1: Boiler's efficiency and fuel consumption as a function of the boiler's load given by manufacturer.

Appendix H

Resistance Coefficients K - Equivalent Lengths by Crane Co.

## Relative Roughness of Pipe Materials and Friction Factors

For Complete Turbulence

Pipe Diameter, in inches

Pipe Diameter, in millimetres — d
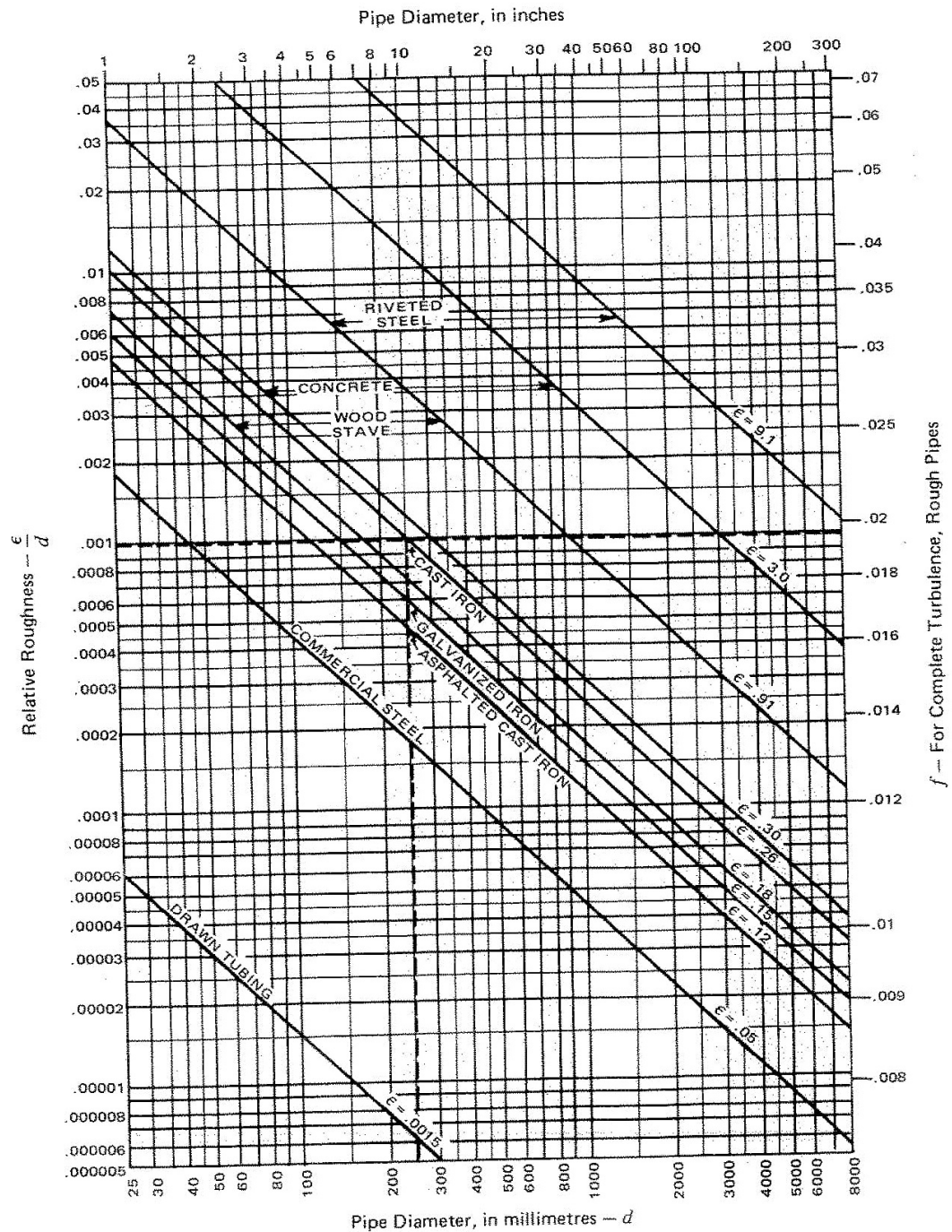
(Absolute Roughness is in millimetres)

Adapted from data extracted from Bibliography reference 18

Problem: Determine absolute and relative roughness, and friction factor, for fully turbulent flow in a cast iron pipe, 250 mm int. diam.

Solution: Absolute roughness (ϵ) = 0.26 . . . . . Relative roughness (ϵ/d) = 0.001 . . . . . Friction factor at fully turbulent flow (f) = 0.0196.

Friction Factors for Any Type of Commercial Pipe

VALUES OF (vd) FOR WATER AT 15°C (VELOCITY IN m/s × DIAMETER IN mm)
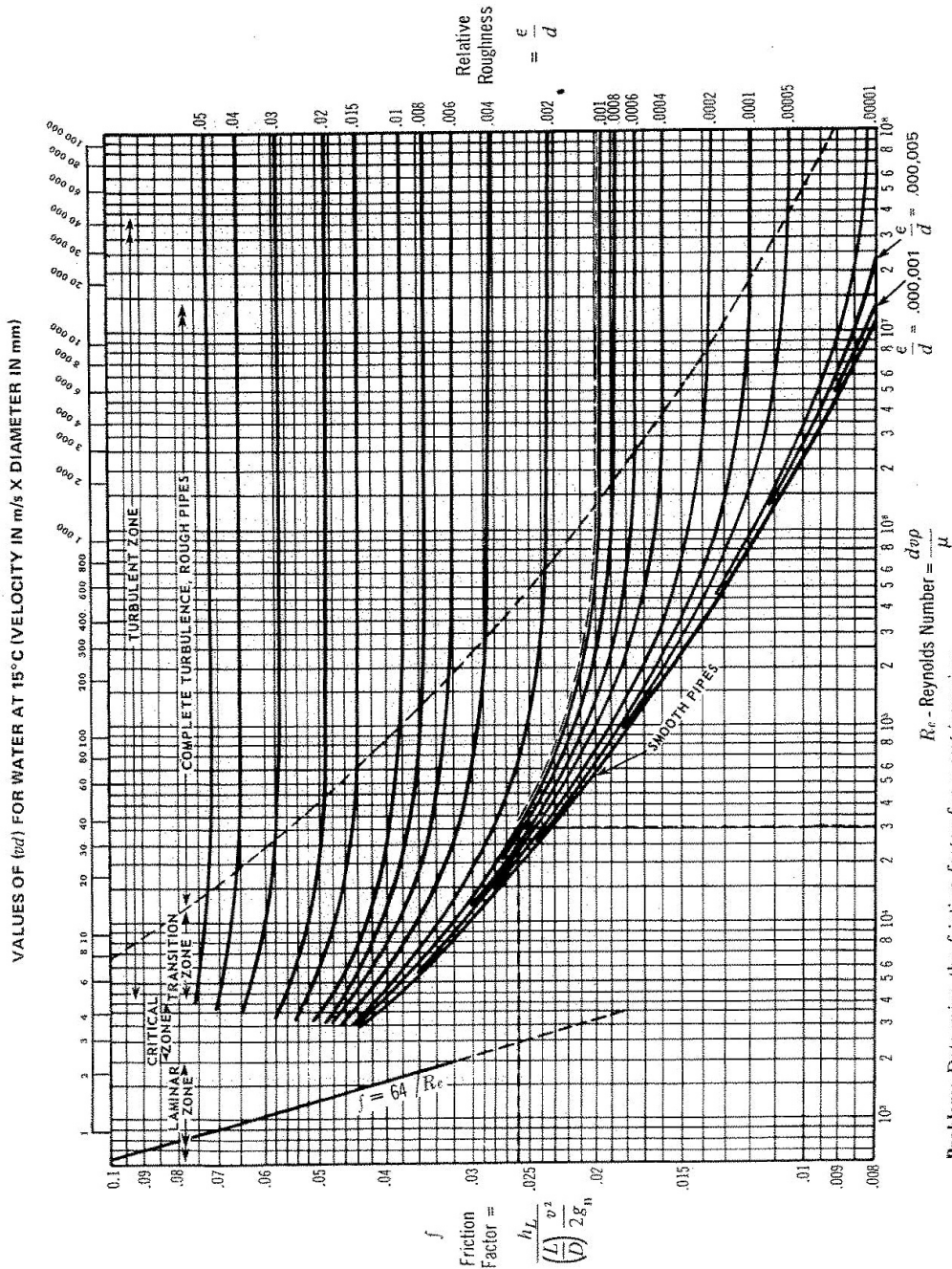
Problem: Determine the friction factor for a cast iron pipe 250 mm int. diam. at a Reynolds number flow of 30,000.

Solution: The relative roughness (see page A-23) is 0.001. Then, the friction factor (f) equals 0.026.

For other forms of the R_e equation, see page 3-2.

Adapted from data extracted from Bibliography reference 18.

Representative Resistance Coefficients (K) for Valves and Fittings

PIPE FRICTION DATA FOR CLEAN COMMERCIAL STEEL PIPE WITH FLOW IN ZONE OF COMPLETE TURBULENCE

Nominal Size	mm	15	20	25	32	40	50	65, 80	100	125	150	200, 250	300-400	450-600
	in.	½	¾	1	1¼	1½	2	2½, 3	4	5	6	8, 10	12-16	18-24
Friction Factor (f_T)		.027	.025	.023	.022	.021	.019	.018	.017	.016	.015	.014	.013	.012

FORMULAS FOR CALCULATING "K" FACTORS* FOR VALVES AND FITTINGS WITH REDUCED PORT
(Ref. pages 2-11 and 3-4)

Formula 1

$$K = \frac{0.8 \left(\sin \frac{\theta}{2} \right) (1 - \beta^2)}{\beta^4} = \frac{K_1}{\beta^4}$$

Formula 2

$$K_2 = \frac{0.5 (1 - \beta^2) \sqrt{\sin \frac{\theta}{2}}}{\beta^4} = \frac{K_1}{\beta^4}$$

Formula 3

$$K_2 = \frac{2.6 \left(\sin \frac{\theta}{2} \right) (1 - \beta^2)^2}{\beta^4} = \frac{K_1}{\beta^4}$$

Formula 4

$$K_2 = \frac{(1 - \beta^2)^2}{\beta^4} = \frac{K_1}{\beta^4}$$

Formula 5

$$K_2 = \frac{K_1}{\beta^4} + \text{Formula 1} + \text{Formula 3}$$

$$K_2 = \frac{K_1 + \sin \frac{\theta}{2} [0.8 (1 - \beta^2) + 2.6 (1 - \beta^2)^2]}{\beta^4}$$

Formula 6

$$K_2 = \frac{K_1}{\beta^4} + \text{Formula 2} + \text{Formula 4}$$

$$K_2 = \frac{K_1 + 0.5 \sqrt{\sin \frac{\theta}{2}} (1 - \beta^2) + (1 - \beta^2)^2}{\beta^4}$$

$$K_2 = \frac{K_1}{\beta^4} + \beta (\text{Formula 2} + \text{Formula 4}) \text{ when } \theta = 180°$$

$$K_2 = \frac{K_1 + \beta [0.5 (1 - \beta^2) + (1 - \beta^2)^2]}{\beta^4}$$
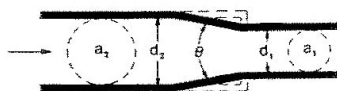
$$\beta = \frac{d_1}{d_2}$$

$$\beta^2 = \left(\frac{d_1}{d_2} \right)^2 = \frac{a_1}{a_2}$$

Subscript 1 defines dimensions and coefficients with reference to the smaller diameter.
Subscript 2 refers to the larger diameter.

*Use K furnished by valve or fitting supplier when available

SUDDEN AND GRADUAL CONTRACTION

If: $\theta \lesssim 45°$ . . . . K_2 = Formula 1
$45° < \theta \lesssim 180°$ . . . . K_2 = Formula 2

SUDDEN AND GRADUAL ENLARGEMENT

If: $\theta \lesssim 45°$ . . . . K_2 = Formula 3
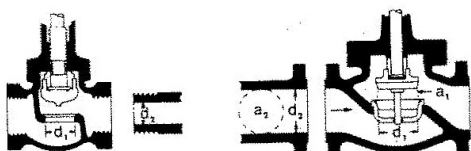$45° < \theta \lesssim 180°$ . . . . K_2 = Formula 4

Representative Resistance Coefficients (K) for Valves and Fittings
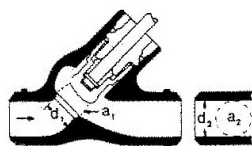
GATE VALVES
Wedge Disc, Double Disc, or Plug Type
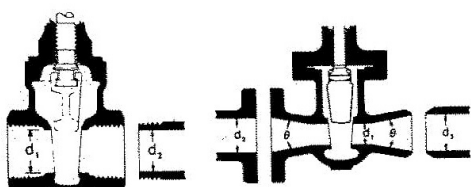
If: $\beta = 1, \theta = 0$ .... $K_1 = 8 f_T$

$\beta < 1$ and $\theta \lesssim 45°$ .... K_2 = Formula 5

$\beta < 1$ and $45° < \theta \lesssim 180°$ .... K_2 = Formula 6

SWING CHECK VALVES
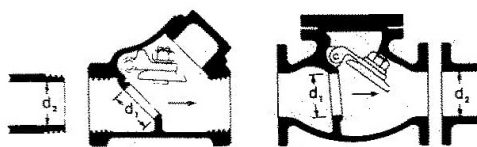
$K = 100 f_T$ $\qquad$ $K = 50 f_T$

Minimum pipe velocity (mps) for full disc lift

$= 45 \sqrt{\overline{V}}$ $\qquad$ $= 75 \sqrt{\overline{V}}$ except

U/L listed $= 120 \sqrt{\overline{V}}$

GLOBE AND ANGLE VALVES
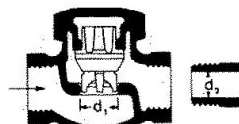
If: $\beta = 1$ $\quad$ $K_1 = 340 f_t$

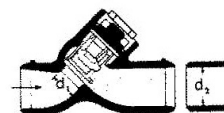If: $\beta = 1 \dots K_1 = 55 f_T$
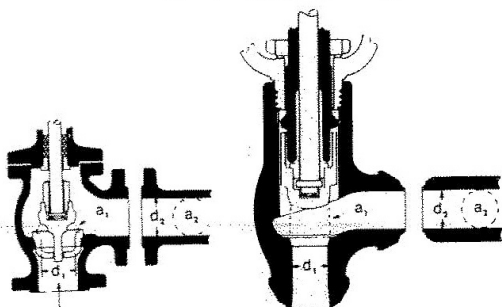
If: $\beta = 1 \dots K_1 = 150 f_T$ $\quad$ If: $\beta = 1 \dots K_1 = 55 f_T$

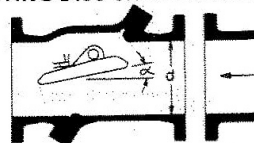All globe and angle valves,
whether reduced seat or throttled,

If: $\beta < 1 \dots K_2$ = Formula 7

LIFT CHECK VALVES

If: $\beta = 1 \dots K_1 = 600 f_T$

$\beta < 1 \dots K_2$ = Formula 7

Minimum pipe velocity (mps) for full disc lift

$= 50 \beta^2 \sqrt{\overline{V}}$

If: $\beta = 1 \dots K_1 = 55 f_T$

$\beta < 1 \dots K_2$ = Formula 7

Minimum pipe velocity (mps) for full disc lift

$= 170 \beta^2 \sqrt{\overline{V}}$

TILTING DISC CHECK VALVES

Sizes	$\alpha = 5°$	$\alpha = 15°$
50 mm (2") to 200 mm (8") $K=$	$40 f_T$	$120 f_T$
250 mm (10") to 350 mm (14") $K=$	$30 f_T$	$90 f_T$
400 mm (16") to 1200 mm (48") $K=$	$20 f_T$	$60 f_T$
Minimum pipe velocity (mps) for full disc lift =	$100 \sqrt{\overline{V}}$	$40 \sqrt{\overline{V}}$

Note. mps = metres per second
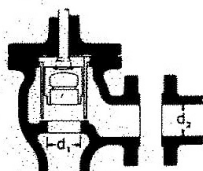
"K" FACTOR TABLE – SHEET 3 of 4

Representative Resistance Coefficients (K) for Valves and Fittings

(for formulas and friction data, see page A-26)
("K" is based on use of schedule pipe as listed on page 2-10)

STOP-CHECK VALVES
(Globe and Angle Types)
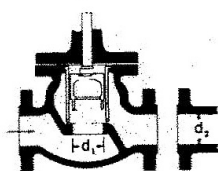
If:

$\beta = 1 \ldots K_1 = 400 f_T$ $\beta = 1 \ldots K_1 = 200 f_T$
$\beta < 1 \ldots K_2 = $ Formula 7 $\beta < 1 \ldots K_2 = $ Formula 7

Minimum pipe velocity (mps) for full disc lift

$= 70 \beta^2 \sqrt{\bar{V}}$ $= 95 \beta^2 \sqrt{\bar{V}}$

If:

$\beta = 1 \ldots K_1 = 300 f_T$ $\beta = 1 \ldots K_1 = 350 f_T$
$\beta < 1 \ldots K_2 = $ Formula 7 $\beta < 1 \ldots K_2 = $ Formula 7

Minimum pipe velocity (mps) for full disc lift

$= 75 \beta^2 \sqrt{\bar{V}}$

$\beta = 1 \ldots K_1 = 55 f_T$ $\beta = 1 \ldots K_1 = 55 f_T$
$\beta < 1 \ldots K_2 = $ Formula 7 $\beta < 1 \ldots K_2 = $ Formula 7

Minimum pipe velocity (mps) for full disc lift

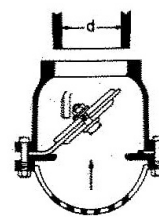$= 170 \beta^2 \sqrt{\bar{V}}$
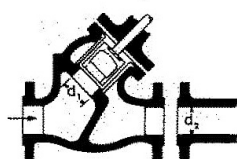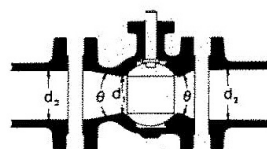
FOOT VALVES WITH STRAINER

Poppet Disc   **Hinged Disc**

$K = 420 f_T$ $K = 75 f_T$

Minimum pipe velocity (mps) for full disc lift   Minimum pipe velocity (mps) for full disc lift

$= 20 \sqrt{\bar{V}}$ $= 45 \sqrt{\bar{V}}$
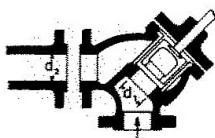
BALL VALVES

If: $\beta = 1, \theta = 0 \ldots \ldots \ldots \ldots \ldots K_1 = 3 f_T$
$\beta < 1$ and $\theta \lessapprox 45° \ldots \ldots \ldots K_2 = $ Formula 5
$\beta < 1$ and $45° < \theta \lessapprox 180° \ldots \ldots K_2 = $ Formula 6
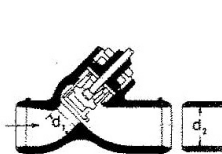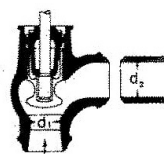
BUTTERFLY VALVES
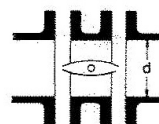
Sizes 50 mm (2") to 200 mm (8") $\ldots \ldots K = 45 f_T$
Sizes 250 mm (10") to 350 mm (14") $\ldots K = 35 f_T$
Sizes 400 mm (16") to 600 mm (24") $\ldots K = 25 f_T$

Representative Resistance Coefficients (K) for Valves and Fittings

PLUG VALVES AND COCKS

Straight-Way

3-Way

View X—X

If: $\beta = 1$, $K_1 = 18 f_T$

If: $\beta = 1$, $K_1 = 30 f_T$

If: $\beta = 1$, $K_1 = 90 f_T$

If: $\beta < 1$ K_2 = Formula 6

STANDARD ELBOWS

90°

45°

$K = 30 f_T$

$K = 16 f_T$

MITRE BENDS

α	K
0°	$2 f_T$
15°	$4 f_T$
30°	$8 f_T$
45°	$15 f_T$
60°	$25 f_T$
75°	$40 f_T$
90°	$60 f_T$

STANDARD TEES

Flow thru run . . . . $K = 20 f_T$

Flow thru branch . . . . . . $K = 60 f_T$

90° PIPE BENDS AND FLANGED OR BUTT-WELDING 90° ELBOWS

r/d	K	r/d	K
1	$20 f_T$	8	$24 f_T$
1.5	$14 f_T$	10	$30 f_T$
2	$12 f_T$	12	$34 f_T$
3	$12 f_T$	14	$38 f_T$
4	$14 f_T$	16	$42 f_T$
6	$17 f_T$	20	$50 f_T$

The resistance coefficient, K_B, for pipe bends other than 90° may be determined as follows:

$$K_B = (n - 1) \left(0.25 \, \pi f_T \frac{r}{d} + 0.5 \, K \right) + K$$

n = number of 90° bends
K = resistance coefficient for one 90° bend (per table)

PIPE ENTRANCE

Inward Projecting

Flush

r/d	K
0.00*	0.5
0.02	0.28
0.04	0.24
0.06	0.15
0.10	0.09
0.15 & up	0.04

*Sharp-edged

$K = 0.78$

For K, see table

CLOSE PATTERN RETURN BENDS

$K = 50 f_T$

PIPE EXIT

Projecting

Sharp-Edged

Rounded

$K = 1.0$

$K = 1.0$

$K = 1.0$
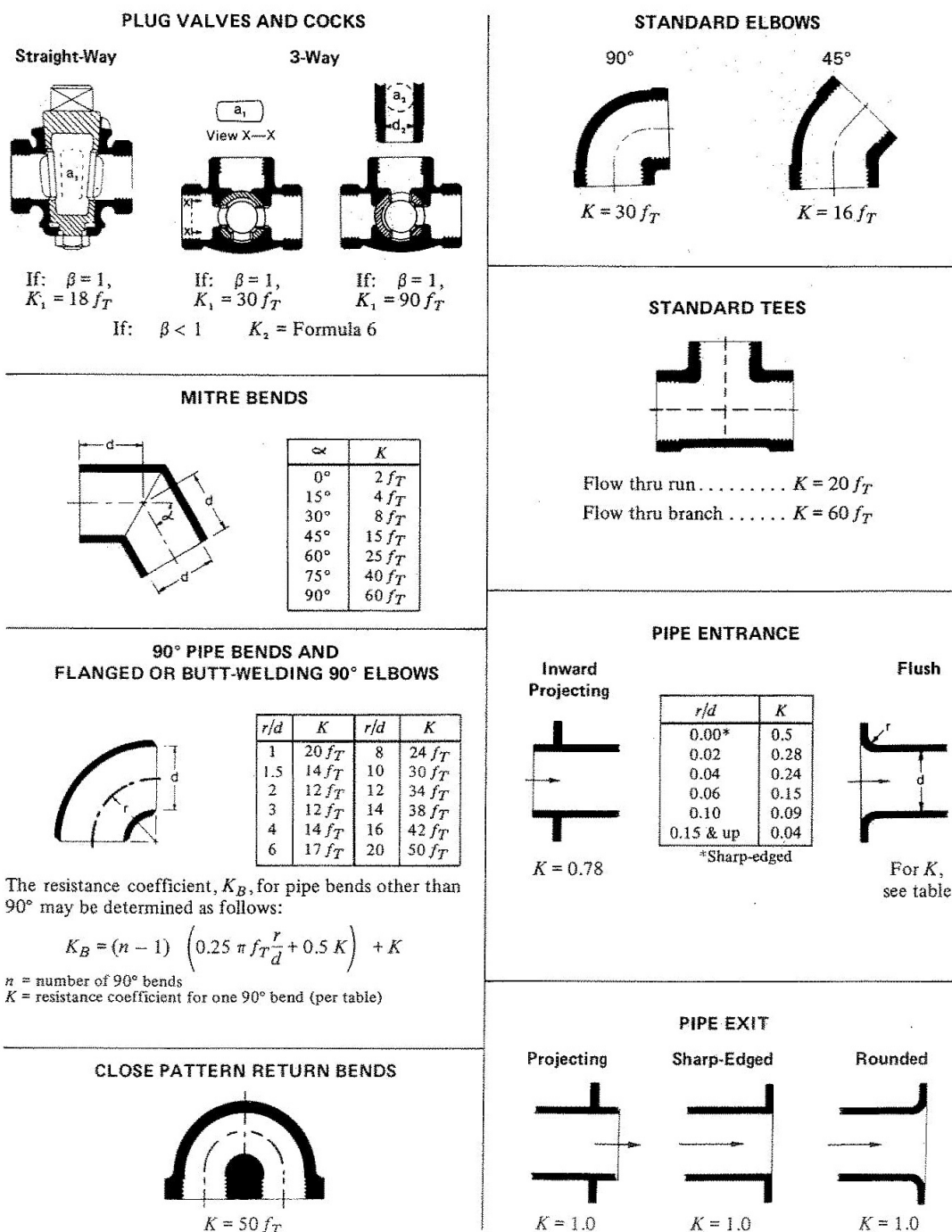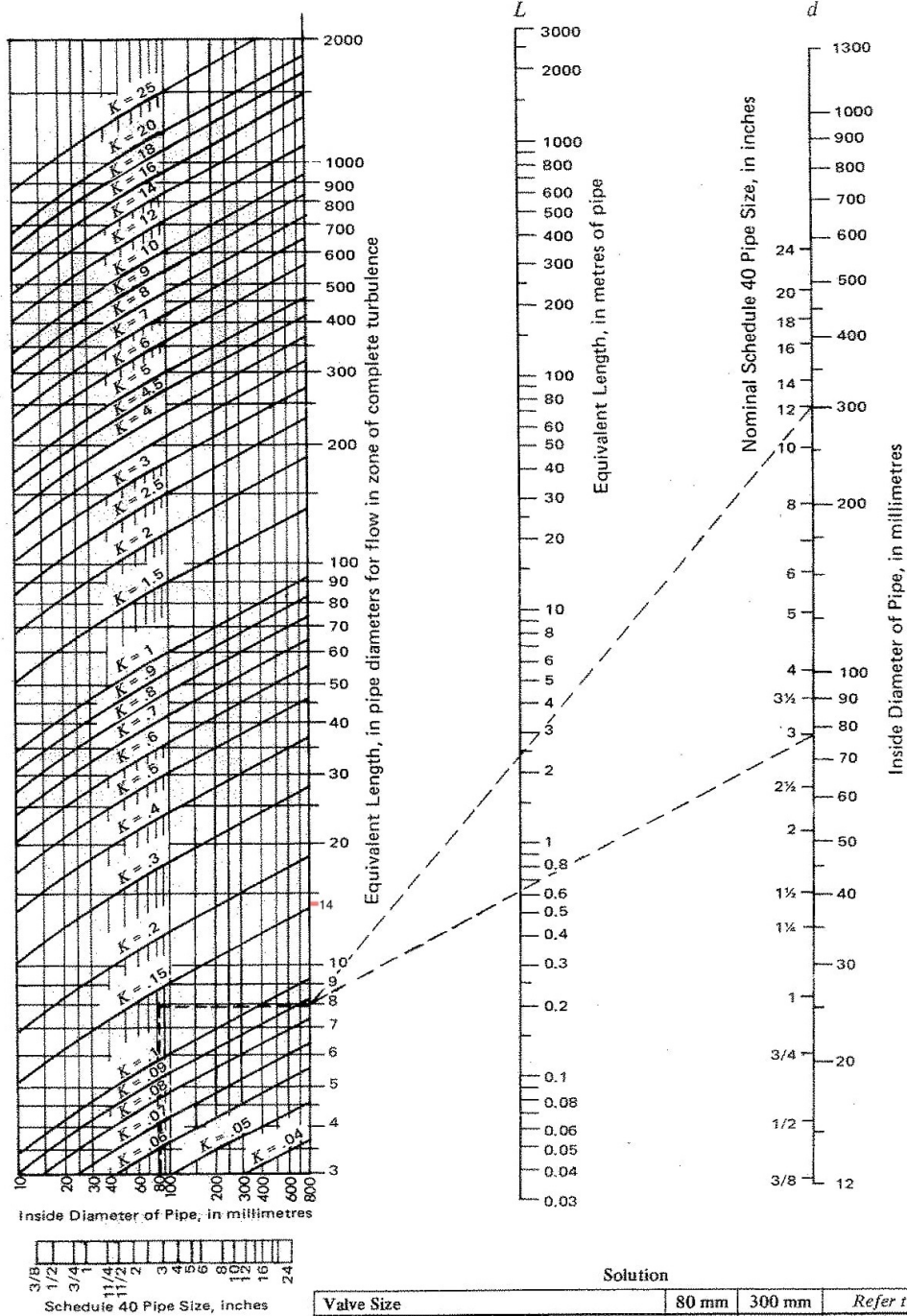
Figure H.1: Representative Resistance Coefficients (K) for Valves and Fittings

Equivalent Lengths L and L/D and Resistance Coefficient K

Inside Diameter of Pipe, in millimetres

Schedule 40 Pipe Size, inches

Problem: Find the equivalent length in pipe diameters and metres of Schedule 40 clean commercial steel pipe, and the resistance factor K for 80 mm and 300 mm fully opened gate valves, ANSI Class 300, with flow in zone of complete turbulence.

Solution

Valve Size	80 mm	300 mm	Refer to
Equivalent length, pipe diameters	8	8	Page A-27
Equivalent length, metres of Sched. 40 pipe	0.62	2.43	Dotted lines
Resist Factor K, based on Sched. 40 pipe	0.14	0.10	on chart

Valve Losses in Equivalent Meters of Pipe

Nominal pipe or tube size, DN	Globe[a]	60° − Y	45° − Y	Angle[a]	Gate[b]	Swing check[c]	Lift check
10	5.2	2.4	1.8	1.8	0.2	1.5	
15	5.5	2.7	2.1	2.1	0.2	1.8	Globe
20	6.7	3.4	2.1	2.1	0.3	2.2	and
25	8.8	4.6	3.7	3.7	0.3	3.0	vertical
32	12	6.1	4.6	4.6	0.5	4.3	lift
40	13	7.3	5.5	5.5	0.5	4.9	same as
50	17	9.1	7.3	7.3	0.73	6.1	globe
65	21	11	8.8	8.8	0.9	7.6	valve[d]
80	26	13	11	11	1.0	9.1	
90	30	15	13	13	1.2	10	
100	37	18	14	14	1.4	12	
125	43	22	18	18	1.8	15	
150	52	27	21	21	2.1	18	
200	62	35	26	26	2.7	24	Angle
250	85	44	32	32	3.7	30	lift
300	98	50	40	40	4.0	37	same as
350	110	56	47	47	4.6	41	angle
400	125	64	55	55	5.2	46	valve
450	140	73	61	61	5.8	50	
500	160	84	72	72	6.7	61	
600	186	98	81	81	7.6	73	

Note: Losses are for valves in fully open position and with screwed, welded, flanged, or flared connections.

[a] These losses do not apply to valves with needlepoint seats.

[b] Regular and short pattern plug cock valves, when fully open, have same loss as gate valve. For valve losses of short pattern plug cocks above 150 mm, check with manufacturer.

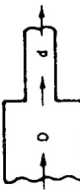[c] Losses also apply to the in-line, ball-type check valve.

[d] For *Y* pattern globe lift check valve with seat approximately equal to the nominal pipe diameter, use values of 60° wye valve for loss.

Fitting Losses in Equivalent Meters of Pipe (Screwed, Welded, Flanged, Flared, and Brazed Connections)

Nominal pipe or tube size, DN	Smooth bend elbows						Smooth bend tees			
	90° Std[a]	90° Long-rad.[b]	90° Street[a]	45° Std[a]	45° Street[a]	180° Std[a]	Flow-through branch	Straight-through flow		
								No reduction	Reduced 1/4	Reduced 1/2
10	0.4	0.3	0.7	0.2	0.3	0.7	0.8	0.3	0.4	0.4
15	0.5	0.3	0.8	0.2	0.4	0.8	0.9	0.3	0.4	0.5
20	0.6	0.4	1.0	0.3	0.5	1.0	1.2	0.4	0.6	0.6
25	0.8	0.5	1.2	0.4	0.6	1.2	1.5	0.5	0.7	0.8
32	1.0	0.7	1.7	0.5	0.9	1.7	2.1	0.7	0.9	1.0
40	1.2	0.8	1.9	0.6	1.0	1.9	2.4	0.8	1.1	1.2
50	1.5	1.0	2.5	0.8	1.4	2.5	3.0	1.0	1.4	1.5
65	1.8	1.2	3.0	1.0	1.6	3.0	3.7	1.2	1.7	1.8
80	2.3	1.5	3.7	1.2	2.0	3.7	4.6	1.5	2.1	2.3
90	2.7	1.8	4.6	1.4	2.2	4.6	5.5	1.8	2.4	2.7
100	3.0	2.0	5.2	1.6	2.6	5.2	6.4	2.0	2.7	3.0
125	4.0	2.5	6.4	2.0	3.4	6.4	7.6	2.5	3.7	4.0
150	4.9	3.0	7.6	2.4	4.0	7.6	9	3.0	4.3	4.9
200	6.1	4.0	—	3.0	—	10	12	4.0	5.5	6.1
250	7.6	4.9	—	4.0	—	13	15	4.9	7.0	7.6
300	9.1	5.8	—	4.9	—	15	18	5.8	7.9	9.1
350	10	7.0	—	5.5	—	17	21	7.0	9.1	10
400	12	7.9	—	6.1	—	19	24	7.9	11	12
450	13	8.8	—	7.0	—	21	26	8.8	12	13
500	15	10	—	7.9	—	25	30	10	13	15
600	18	12	—	9.1	—	29	35	12	15	18

[a] R/D approximately equal to 1.
[b] R/D approximately equal to 1.5.

Special Fitting Losses in Equivalent Meters of Pipe

Nominal pipe or tube size, DN	Sudden enlargement, d/D			Sudden contraction, d/D			Sharp edge		Pipe projection	
	¼	½	¾	¼	½	¾	Entrance	Exit	Entrance	Exit
10	0.4	0.2	0.1	0.2	0.2	0.1	0.5	0.2	0.5	0.3
15	0.5	0.3	0.1	0.3	0.3	0.1	0.5	0.3	0.5	0.5
20	0.8	0.5	0.2	0.4	0.3	0.2	0.9	0.4	0.9	0.7
25	1.0	0.6	0.2	0.5	0.4	0.2	1.1	0.5	1.1	0.8
32	1.4	0.9	0.3	0.7	0.5	0.3	1.6	0.8	1.6	1.3
40	1.8	1.1	0.4	0.9	0.7	0.4	2.0	1.0	2.0	1.5
50	2.4	1.5	0.5	1.2	0.9	0.5	2.7	1.3	2.7	2.1
65	3.0	1.9	0.6	1.5	1.2	0.6	3.7	1.7	3.7	2.7
80	4.0	2.4	0.8	2.0	1.5	0.8	4.3	2.2	4.3	3.8
90	4.6	2.8	0.9	2.3	1.8	0.9	5.2	2.6	5.2	4.0
100	5.2	3.4	1.2	2.7	2.1	1.2	6.1	3.0	6.1	4.9
125	7.3	4.6	1.5	3.7	2.7	1.5	8.2	4.3	8.2	6.1
150	8.8	6.7	1.8	4.6	3.4	1.8	10	5.8	10	7.6
200	—	7.6	2.6	—	4.6	2.6	14	7.3	14	10
250	—	9.8	3.4	—	6.1	3.4	18	8.8	18	14
300	—	12.4	4.0	—	7.6	4.0	22	11	22	17
350	—	—	4.9	—	—	4.9	26	14	26	20
400	—	—	5.5	—	—	5.5	29	15	29	23
450	—	—	6.1	—	—	6.1	35	18	35	27
500	—	—	—	—	—	—	43	21	43	33
600	—	—	—	—	—	—	50	25	50	40

Note: Enter table for losses at smallest diameter *d*.

Bibliography

[1] IMO. "Marpol Annex VI for Emission Control Areas". International Maritime Organisation, May 2005, .

[2] T.L.Bergman, F.P. Incropera, A.S.Lavine, D.P.Dewitt, Fundamentals of Heat and Mass Transfer, John Wiley & Sons (2011)

[3] Yunus A.Cengel, Heat Transfer - A Practical Approach, McGraw Hill (2011)

[4] E.R.G. Eckert, R.M. Drake, Analysis of Heat and Mass Transfer, Forced convection in turbulent flow, pp.215

[5] E.R.G. Eckert, R.M. Drake, Analysis of Heat and Mass Transfer, Free Convection, pp.324

[6] S.A.Mavrakos, Calculations of the heating coils area inside an oil tanker, Msc thesis, Faculty of Naval Architecture & Marine Engineering, National Technical University of Athens,1976

[7] Saunders, Heat Losses from Oil Tanker Cargoes.

[8] Ostrach, S., An Analysis of Laminar Free Convection Flow and Heat Transfer About a Flat Plate Parallel to the Direction of the Generating Body Force, National Advisory Committee for Aeronautics, Report 1111, 1953.

[9] Churchill, S. W., and H. H. S. Chu, Int. J. Heat Mass Transfer, 18, 1323, 1975.

[10] Churchill, S. W., and H. H. S. Chu, Int. J. Heat Mass Transfer, 18, 1049, 1975

[11] Sparrow, E. M., and J. L. Gregg, Trans. ASME, 78, 435,1956.

[12] Sparrow, E. M., and J. L. Gregg, Trans. ASME, 78, 1823,1956.

[13] A.E.Gill, The boundary layer regime for convection in a rectangular cavity, J.Fluid Mech.26,515(1966)

[14] O.G. Martynenko, P.P. Khramtsov, Natural Convection in Enclosures Free-Convective Heat Transfer, pp 279-343 Springer, Berlin, Heidelberg(2005), doi.org/10.1007/3-540-28498-2_4

[15] K.H. Winters, Hopf bifurcation in the double-glazing problem with conducting boundaries, J. Heat Transfer 109 (1987) 894898.

[16] R.A.W.M. Henkes, Natural-Convection Boundary Layers, Ph.D. thesis, Faculty of Applied Physics at the Delft University of Technology, 1995.

[17] A. Rincn-Casado, F.J. Snchez de la Flor, E. Chacn Vera, J. Snchez Ramos (2017) New natural convection heat transfer correlations in enclosures for building performance simulation, Engineering Applications of Computational Fluid Mechanics, 11:1, 340-356, DOI: 10.1080/19942060.2017.1300107

[18] Trias, F. X., Gorobets, A., Soria, M., & Oliva, A. (2010). Direct numerical simulation of a differentially heated cavity of aspect ratio 4 with Rayleigh numbers up to 10^11 Part II:Heat transfer and Flow Dynamics. International Journal of Heat and Mass Transfer, 53, 674683. doi:10.1016/j.ijheatmasstransfer.2009.10.026

[19] Pivac, Ivan; Magazinovi, Gojko Numerical analysis of tank heating coil heat transfer process // Towards Green Marine Technology and Transport / Guedes Soares, Carlos ; Dejhalla, Roko ; Pavleti, Duko (ur.). London: Taylor & Francis Group, 2015. str. 603-608

[20] Bejan, A. (1979). A synthesis of analytical results for natural convection heat transfer across rectangular enclosures. International Journal of Heat and Mass Transfer, 23, 723726. doi:10.1016/0017-9310(80)90017-4

[21] Berkovsky, B. M., Polevikov, V. K. (1977). Numerical study of problems on high-intensive free convection. In Heat Transfer and Turbulent Buoyant Convection (Eds.), Proceedings of International Turbulent Buoyant Convection Seminar, 443455. Washington.

[22] Zekeriya Altac, Nihal Ugurlubilek (2016),Assessment of turbulence models in natural convection from two- and three-dimensional rectangular enclosures,J.of Thermal Sciences,107,237-246

[23] Anil Kumar Sharma, K. Velusamy, C. Balaji, S.P. Venkateshan, Conjugate turbulent natural convection with surface radiation in air filled rectangular enclosures, Int.Journal of Heat and Mass Transfer 50 (2007) pp.625639

[24] Morgan, V. T., The Overall Convective Heat Transfer from Smooth Circular Cylinders, in T. F. Irvine and J. P. Hartnett, Eds., Advances in Heat Transfer, Vol. 11, Academic Press, New York, 1975, pp. 199264.

[25] Catton, I., Natural Convection in Enclosures, Proc. 6th Int. Heat Transfer Conf., Toronto, Canada, 1978, Vol. 6,pp. 1331.

[26] K. G. T. Hollands, T. E. Unny, G. D. Raithby, and L. Konicek. Free Convective Heat Transfer Across Inclined Air Layers. Journal of Heat Transfer 98 (1976), pp. 189193.

[27] S. M. ElSherbiny, G. D. Raithby, K. G. T. Hollands, "Heat Transfer by Natural Convection Across Vertical and Inclined Air Layers", Int. Journal of Heat Transfer Vol.104(1) (1982), pp.103-110 doi:10.1115/1.3245035.

[28] A.Bejan, Convective Heat Transfer, third edition, Wiley, New York, 2003, pp. 222-223.

[29] Hewitt,G.F.,1998, "Multiphase Fluid Flow and Pressure Drop", Heat Exchanger Design Handbook, Vol.2, Begell House, New York, NY.

[30] Thome,J.R.,2004, Engineering Data Book III, Wolverine Tube, Inc. Huntsville, AL

[31] Globe, S., and D. Dropkin, J. Heat Transfer, 81C,24, 1959

[32] M.Monteiro,V.Svet,D.Sandilands,S.Tsysar,"Experimental Investigations of Various Methods of Sludge Measurements in Storage Oil Tanks",Advances in Remote Sensing, Vol.04,(2015) pp. 119-137

[33] Rohsenow W. M.,Hartnett J. P. and Ganic E.N., *Handbook of Heat Transfer Fundamentals*, McGraw Hill, (1985) Ch.11, pp 20-23

[34] Dobson, M. K., and J. C. Chato, Condensation in Smooth Horizontal Tubes, J. Heat Transfer, Vol.120, pp.193-213, 1998.

[35] M.Altman, F. W. Staub, and R. H. Norris, Proc. 3d Nat. Heat Transfer Conf. ASME/AIChE,Storrs,Conn., Preprint No. 115, August 1959

[36] W. W. Akers, O.K. Crosser, and H.A. Deans, Proc.2d Nat. Heat Transfer Conf. ASME/AIChE,Storrs,Conn., Preprint No.1, August 1959

[37] S. Bae, J.S. Maulbetsch, and W.M. Rohsenow, *Refrigerant Forced Convection Condensation Inside Horizontal Tubes*, ASHRAE Trans., 1971

[38] D. P. Travis, W.M. Rohsenow and A.B. Baron, *Forced Convection Condensation Inside Tubes : A Heat Transfer Equation for Condenser Design*, ASHRAE Trans., 1972

[39] M. L. Nayyar, Piping Handbook, 7th edition, McGraw Hill inc., 2000

[40] *Flow of Fluids through Valves, Fittings and Pipe*, Technical Papaer No.410M, Crane Co.,New York, 1982

[41] K. H. Beij, Pressure Losses for Fluid Flow in 90 Degree Pipe Bends, J. of Research of the National Bureau of Standards, Vol.21, July 1938

[42] S. W. Churchill and M. Bernstein. A correlating equation for forced convection from gases and liquids to a circular cylinder in cross-flow. J.Heat Mass Transfer, 18 : 387-396, 1975

[43] K.G. Nayar, M.H. Sharqawy, L.D. Banchik and J.H. Lienhard V, Thermophysical properties of seawater: A review and new correlations that include pressure dependence, Desalination, 390 (2016), 1-24. doi:10.1016/j.desal.2016.02.024.

[44] M.H. Sharqawy, J.H. Lienhard, S.M. Zubair, Thermophysical properties of seawater: a review of existing correlations and data, Desalination and Water Treatment, 16 (2010) 354-380. doi:10.5004/dwt.2010.1079.

[45] Hilpert, R., Forsch. Geb. Ingenieurwes., 4, 215, 1933.

[46] Zukauskas, A., Heat Transfer from Tubes in Cross Flow, in J. P. Hartnett and T. F. Irvine, Jr., Eds., Advances in Heat Transfer, Vol. 8, Academic Press, New York, 1972.

[47] G. M. Hebbard, W. L. Badger, Steam Film Heat Transfer Coefficients for Vertical Tubes, J. Industrial and Engineering Chemistry, Vol.26, No.4, April 1934

[48] M. M. Shah, A general Correlation for Heat Transfer During Film Condensation Inside Pipes, Int. J. Heat and Mass Transfer, Vol.22, pp.547-556, Pergamon Press Ltd. 1979

[49] W. Nusselt, Die oberflachenkondensation des wasserdampfes, Z. Ver. Dt. Ing. 60 (1916) 541546, 569575.

[50] Gnielinski, V., Int. Chem. Eng., 16, 359, 1976

[51] Czeslaw O. Popiel (2008) Free Convection Heat Transfer from Vertical Slender Cylinders: A Review, Heat Transfer Engineering, 29:6, 521-536, DOI: 10.1080/01457630801891557

[52] A. Bejan and J.L. Lage. The Prandtl number effect on the transition in natural convection along a vertical surface. J. Heat Transfer, Trans. ASME, 112:787-790, 1990.

[53] McAdams, W.H., Heat Transmission, 3rd ed., McGrow-Hill, New York, 1954.

[54] Harjit Singh, Philip C. Eames. A review of natural convective heat transfer correlations in rectangular cross-section cavities and their potential applications to compound parabolic concentrating (CPC) solar collector cavities. Applied Thermal Engineering, Elsevier, 2011, 31 (14-15), pp.2186.

[55] A. K. Sharma, K. Velusamy, C.Balaji, S. P. Venkateshan, Conjugate turbulent natural convection with surface radiation in air filled rectangular enclosures, Journal of Heat and Mass Transfer, Vol.50, pp.625-639, (2007)

[56] Eigenson, L.S., Les Lois Gouvernantla Transmission de la Chaleur aux Gaz Biatomiques par les Parois Descylindres Verticaux dans le Cas de Convection Naturelle, Dokl. Akad. Nauk SSSR, vol. 26, pp. 440444, 1940

[57] Le Fevre, E.J., and Ede, A.J., 1956, Laminar Free Convection from the Outer Surface of a Vertical Cylinder, Proceedings of the 9th International Congress of Applied Mechanics, Brussels, Vol. 4, pp. 175-183.

[58] Cess, R. D. , The effect of radiation upon forced-convection heat transfer, Appl.Sci. Res., 10(A), 430-438, 1961

[59] M. K. Goel and S. N. Gupta, The effect of neighbouring tubes on heat transfer coefficient for newtonian and non-newtonian fluids flowing across tube bank, Int. J. Mech. Eng. & Rob., Vol.4, No.1, January 2015

[60] A.H.S. Dehaghani, M.H. Badizad, Experimental study of Iraniani heavy crude oil viscosity reduction by diluting with heptane, methanol, toluene, gas condensate and naptha, Petroleum Journal, Vol.2, Issue 4, December 2016, pp. 415-424.

[61] Petukhov, B. S., in T. F. Irvine and J. P. Hartnett, Eds., Advances in Heat Transfer, Vol. 6, Academic Press, New York, 1970.

[62] S. E. Haaland. Simple and Explicit Formulas for the Friction Factor in Turbulent Pipe Flow. Journal of Fluids Engineering (March 1983), pp. 8990

[63] E.M. Sparrow, G.T. Geiger, Local and average heat transfer characteristics for a disk situated perpendicular to

[64] Tandon, T.N., Varma, H.K., and Gupta, C.P., 1982, A New Flow Regime Map for Condensation inside Horizontal Tubes, ASME Journal of Heat Transfer, Vol. 104, pp. 763-768. a uniform-flow, J. Heat Transfer 107 (2) (1985) 321326.

[65] R. Wibergh, N. Lior, Heat transfer from a cylinder in axial turbulent flows, J. Heat and Mass Transfer 48 (2005) 1505-1517.

[66] S. Akagi, H. Kato, 1987, "Numerical analysis of mixed convection heat transfer of a high viscosity fluid in a rectangular tank with rolling motion", Int. Journal Heat Mass Transfer, Vol.30, No.11, pp.2423-2432

[67] Faghri, A., Zhang, Y. and Howell, J.R. (2010) Advanced Heat and Mass Transfer. Global Digital Press, Columbia, 52-55.

[68] P. J. Robinson and J. A. Davis, Laboratory Determination of Water Surface Emissivity, Vol.11, 1972

[69] Steven Earle,*Physical Geology*,BC Open Textbook Project, Gabriola Island, 2015

[70] Davies,T. W., 2011, February 2, Thermal Conductivity Values, Retrieved from http://www.thermopedia.com

[71] McQuillan,F.J., Culham,J.R., Yovanovich, M.M., "Properties Of Dry Air at One Atmosphere", UW/MHTL 8406 G-01, Microelectronics Heat Transfer Lab, Waterloo University, Waterloo, Ontario, June 1984

[72] Dixon, J.C., "The Shock Absorber Handbook, Second Edition, John Wiley & Sons LTD, pp. 375-378, 2007

[73] Reid, R.C., Sherwood, T.K., (1966), "The Properties of Gases and Liquids, McGraw-Hill.

[74] Stephan, K., Laesecke, A., "The thermal Conductivity of Fluid Air", Journal of Physical and Chemical Reference Data, Vol.14, No.1, pp.227-234

[75] Briggs D.K.H. 'Thermal Conductivity of liquids', Industrial and Engineering Chemistry, Vol.49, pp. 418-421 (1956)

[76] Edwards,D.K., Liley,P.E., Maddox,R.N., Matavosian,R., Pugh,S.F., Schunck,M., Schwier, K., and Shulman, Z.P. (1983). Heat Exchanger Design Handbook, Vol.5. Washington, DC: Hemisphere Publishing Corporation

[77] Kesler,M. G. and Lee, B. I., "Improve Prediction of Enthalpy of Fractions", Hydrocarbons Processing, Vol. 55, No.3, 1976, pp. 153-158

[78] Daubert, T. E. and Danner, R. E, Eds., API TechnicalData Book–Petroleum Refining, 6th ed., American Petroleum Institute (API), Washington, DC, 1997.

[79] The International Association for the Properties of Water and Steam IAPWS, "Revised Release on the IAPWS Industrial Formulation 1997 for the Thermodynamic Properties of Water and Steam", Lucerne, Switzerland, August 2007

[80] Zannikos, F., Lois,E., Karonis,D., "Fuel and Lubricant Oil Technology", NTUA Publications, Athens, 2014.

[81] Cragoe, C.S., "Thermal Conductivity For Petroleum Fractions and Light Hydrocarbon Mixtures Below a Reduced Temperature, T_R, of 0.85", National Bureau of Standards, Miscellaneous Publication No. 97, (1929)